A gut-derived metabolite alters brain activity and anxiety behavior in mice

Brittany D. Needham[1*], Masanori Funabashi[2,3], Mark D. Adame[1], Zhuo Wang[4], Joseph C. Boktor[1], Jillian Haney[5], Wei-Li Wu[1,6,7], Claire Rabut[8], Mark S. Ladinsky[1], Son-Jong Hwang[8], Yumei Guo[4], Qiyun Zhu[9,10], Jessica A. Griffiths[1], Rob Knight[9,11,12], Pamela J. Bjorkman[1], Mikhail G. Shapiro[8], Daniel H. Geschwind[5], Daniel P. Holschneider[4,13,14], Michael A. Fischbach[2], Sarkis K. Mazmanian[1*]

[1]Division of Biology and Biological Engineering, California Institute of Technology, Pasadena, CA, 91125, USA.
[2]Department of Bioengineering and ChEM-H, Stanford University, Stanford, CA 94305, USA.
[3]Translational Research Department, Daiichi Sankyo RD Novare Co., Ltd., Tokyo Japan.
[4]Dept. of Psychiatry and the Behavioral Sciences, Keck School of Medicine, University of Southern California, Los Angeles, CA, 90089, USA.
[5]Department of Neurology, University of California Los Angeles, Los Angeles, CA, USA.
[6]Department of Physiology, College of Medicine, National Cheng Kung University, Tainan, Taiwan.
[7]Institute of Basic Medical Sciences, College of Medicine, National Cheng Kung University, Tainan, Taiwan.
[8]Division of Chemistry and Chemical Engineering, California Institute of Technology, Pasadena, CA, 91125, USA.
[9]Department of Pediatrics, University of California San Diego, La Jolla, CA, USA.
[10]School of Life Sciences, Arizona State University, Tempe, AZ 85281, USA.
[11]Department of Computer Science and Engineering, University of California San Diego, La Jolla, CA, USA;
[12]Center for Microbiome Innovation, University of California San Diego, La Jolla, CA, USA.
[13]Dept. of Neurology, Keck School of Medicine, University of Southern California, Los Angeles, CA, 90089, USA.
[14]Viterbi School of Engineering, Dept. of Biomedical Engineering, University of Southern California, Los Angeles, CA, 90033, USA.

Integration of sensory and molecular inputs from the environment shapes animal behavior. A major site of exposure to environmental molecules is the gastrointestinal tract, where dietary components are chemically transformed by the microbiota[1] and gut-derived metabolites are disseminated to all organs, including the brain[2]. In mice, the gut microbiota impacts behavior[3], modulates neurotransmitter production in the gut and brain[4,5], and influences brain development and myelination patterns[6,7]. Mechanisms mediating gut-brain interactions remain poorly defined, though broadly involve humoral or neuronal connections. We previously reported that levels of the microbial metabolite 4-ethylphenyl sulfate (4EPS) were elevated in a mouse model of atypical neurodevelopment[8]. Herein, we identified biosynthetic genes from the gut microbiome that mediate conversion of dietary tyrosine to 4-ethylphenol (4EP), and bioengineered gut bacteria to selectively produce 4EPS in mice. 4EPS entered the brain and was associated with changes in region-specific activity and functional connectivity. Gene expression signatures revealed altered oligodendrocyte function in the brain, and 4EPS impaired oligodendrocyte maturation in mice as well as decreased oligodendrocyte-neuron interactions in *ex vivo* brain cultures. Mice colonized with 4EP-producing bacteria exhibited reduced myelination of neuronal axons. Altered myelination dynamics in the brain have been associated with behavioral outcomes[7,9–14,13,14]. Accordingly, we observed that mice exposed to 4EPS displayed anxiety-like behaviors, and pharmacologic treatments that promote oligodendrocyte differentiation prevented the behavioral effects of 4EPS. These findings reveal that a gut-derived molecule influences complex behaviors in mice via effects on oligodendrocyte function and myelin patterning in the brain.

A microbial biosynthetic pathway for 4EP

Previously, the metabolite 4EPS was measured at higher relative abundance in a mouse model of atypical neurodevelopment, and systemic delivery of synthetic 4EPS to naïve mice altered behavior in the open-field test[8]. We recently reported that 4EPS is elevated in the plasma of individuals with autism spectrum disorder (ASD)[15], and show here it is increased in the blood of the CNTNAP2 model of ASD (Extended Data Fig. 1f). The gut microbiome is predicted to harbor genes that convert tyrosine, the source of several mammalian neurotransmitters, to 4-ethylphenol (4EP), which could then be sulfated[16] to 4EPS by the host (Fig. 1a). Consistent with this notion, germ-free (GF) mice devoid of a microbiota contain virtually no detectable levels of 4EPS (Extended Data Fig. 1f)[8]. Some rare bacterial species in the Firmicutes phylum produce 4EP using *p*-coumaric acid as a substrate[17,18], and precursors of *p*-coumaric acid include tyrosine or plant-based molecules that can be metabolized by the gut microbiota to 4EP. Indeed, both a high-tyrosine fish-based diet and a soy-based diet resulted in measurable 4EPS levels in conventionally colonized mice (Extended Data Fig. 1g). By screening candidate gut bacterial isolates, we discovered that *Bacteroides ovatus* produces *p*-coumaric acid from tyrosine (Fig. 1b). Using the basic alignment search tool (BLAST), we identified a tyrosine ammonia lyase in *B. ovatus* (BACOVA_01194) that upon deletion, abrogated *p*-coumaric acid production (Fig. 1b).

We co-colonized GF mice with *B. ovatus* and *Lactobacillus plantarum,* the latter of which can subsequently convert *p*-coumaric acid to 4EP[18]; however, the resulting 4EPS levels in urine were low (Extended Data Fig. 1f, h). To improve the efficiency of 4EP production, we carried out several rounds of strain engineering (see Methods). Briefly, an extra copy of the first two genes in the pathway, BACOVA_01194 and the phenolic acid decarboxylase (*pad*), were inserted into *B. ovatus* as a single, highly expressed operon (Fig. 1c). The engineered *B. ovatus* strain MFA05 robustly converts tyrosine to the intermediate, 4-vinylphenol (Fig. 1c, Extended Data Fig. 1a-e), and in co-culture with *L. plantarum*, 4-vinylphenol is quantitatively metabolized to 4EP (Fig. 1d). In contrast, when the *B. ovatus* Δ1194 mutant was co-cultured with *L. plantarum*, no 4EP was detected (Fig. 1d). We find homologs of each gene in ~25 genomes of sequenced human gut microbes, indicating common pathways may be intact in the human microbiome (Extended Data Fig. 1i).

Gut-derived 4EPS in the circulation and brain

We colonized separate groups of GF mice with either of the engineered strain pairs represented in Fig. 1d, generating 4EP+ or 4EP- animals. As expected, 4EP was detected in feces (Fig. 1e), and its host-sulfated derivative, 4EPS, was detected in the serum and urine of 4EP+ colonized mice (Fig. 1f, Extended Data Fig. 1j). 4EP was undetectable in the serum of 4EP+ mice, suggesting efficient sulfation to 4EPS (Extended Data Fig. 1j). Conversely, 4EP- mice do not have measurable 4EP or 4EPS levels (Fig. 1e-f, Extended Data Fig. 1j). 4EPS was detectable in brains of 4EP+ mice treated with probenecid, which inhibits organic anion transporters that mediate efflux of small molecules through the blood brain barrier, suggesting accumulation of 4EPS in the brain (Fig. 1g, Extended Data Fig. 1k-m). We observed sulfation of 4EP to 4EPS by the sulfotransferase SULT1A1 and others during *in vitro* biochemical reactions (Extended Data Fig. 2a-b). SULT1A1 is found in intestinal, liver, and brain tissues of mice (Extended Data Fig. 2c-d), though the site(s) of 4EP sulfation remains unknown.

4EP and 4EPS are phenolic molecules that may have toxic or inflammatory properties[19]. However, we observed no differences between 4EP+ and 4EP- groups in body weight or ambulatory activity (i.e., locomotion) (Extended Data Fig. 2f-g). No evidence of intestinal dysfunction was detected in 4EP+ mice when assessing epithelial permeability (Extended Data Fig. 2h), fecal output (Extended Data Fig. 2i), or gross histopathology (Extended Data Fig. 2j). Bacterial colonization levels and ultrastructural localization of bacteria were similar between groups of mice (Extended Data Fig. 2k-m). We did not observe pro-inflammatory cytokine responses in colonic tissue or serum (Extended Data Fig. 3a-b), and only modest changes in peripheral immune cell proportions (Extended Data Fig. 3c-d). Cytokine levels trended toward an anti-inflammatory profile in the brain with no signatures of microglial activation in 4EP+ mice (Extended Data Fig. 3e-g). Collectively, these studies establish a simplified animal model that reproduces the natural route of exposure to a gut microbial metabolite associated with altered behaviors (Extended Data Fig 2e).

4EPS-dependent brain activity patterns

While 4EP or 4EPS --designated here as 4EP(S)-- may have effects on various organs, we focused our study on the brain. Initially, to capture brain-wide differences between 4EP+ and 4EP- mice, we performed functional ultrasound imaging (fUSi), an *in vivo* method that measures resting state cerebral blood volume variation to assess functional connectivity (Extended Data Fig. 4a). We observed altered (mostly increased) correlation of signaling patterns within 4EP+ mice compared to 4EP- mice (Fig. 2a). These changes were primarily observed in subregions of the hippocampus, thalamus, amygdala, hypothalamus, piriform, and cortex (Fig. 2b, Extended Data Fig. 4b), indicating that elevated 4EPS is associated with aberrant functional connectivity between various brain regions in mice.

To compare neural activity across the brain, we mapped glucose uptake where a systemically injected radiolabeled tracer [(^{14}C]-2-deoxyglucose, 2DG) is rapidly incorporated into active brain regions. Changes in brain activity were evaluated by autoradiography of brain sections comparing 4EP+ to 4EP- mice. 4EP(S) was associated with increased glucose uptake in subregions of the hypothalamus (anterior area; lateral; and paraventricular nucleus), amygdala (anterior, basolateral, central, cortical), and the bed nucleus of the stria terminalis (BNST), as well as in the paraventricular nucleus of the thalamus (PVT) (Fig. 2c,d). We also mapped uptake during a behavioral task (open-field exploration) where we observed overlap in increased activity in some regions (amygdala, hypothalamus, BNST, PVT), with differences in the spatial extent of these changes between stimuli conditions (Extended Data Fig. 4c-e). The regions highlighted by this analysis are important for a range of functions, including mediating appropriate responses to innate and learned fear stimuli[20–23] and anxiety responses[24,25]. We conclude that gut exposure to 4EP in mice results in altered functional connectivity and activity in multiple brain regions, including several associated with the limbic system.

Altered oligodendrocyte maturation

To resolve molecular effects of 4EP(S) on the brain, we performed mRNA sequencing (QuantSeq) of six brain regions from 4EP+ and 4EP- mice, including the PVT, basolateral amygdala, hypothalamus, BNST, medial prefrontal cortex (mPFC), and ventral hippocampus, resulting in tight clustering of transcriptomic profiles by brain region (Extended Data Fig. 5a). 4EP(S) predominantly affected global gene expression in the PVT, and the BNST and basolateral

amygdala to a lesser extent (Fig. 3a, Extended Data Fig. 5b, e). Differentially expressed genes were aggregated into functional categories using annotated Gene Ontology (GO) terms, disclosing that the Notch signaling pathway was elevated in the PVT of 4EP+ mice, while GO terms associated with dendrite and neuronal projection development were decreased (Extended Data Fig. 5c-d). Cell-specific enrichment analysis revealed decreased expression of genes specific to neurons, newly formed oligodendrocytes, and mature oligodendrocytes in the PVT of 4EP+ mice compared to 4EP- mice (Fig. 3b), suggesting that a potential decrease in development, abundance, and/or activity of these cell types is associated with exposure to 4EP(S). Increased proliferation of immature oligodendrocytes and decreased differentiation into mature oligodendrocytes has been associated with elevated Notch signaling[26,27]. Mature oligodendrocytes insulate neuronal projections with myelin, a fatty sheath that promotes conduction of action potentials along axons[28]. Accordingly, many genes that are hallmarks of mature oligodendrocytes such as the myelin oligodendrocyte glycoprotein (*Mog*) and *Opalin* genes were downregulated in the PVT of 4EP+ mice, while several genes associated with non-myelinating, oligodendrocyte progenitor cells (OPCs) were elevated (Fig. 3c, Ext. Data Fig. 5f, Supplementary Information). Using seed analysis of the 2DG-uptake data[29], we observed fewer significant correlations between the PVT and the rest of the brain in the 4EP+ group (168,042 voxels) compared to the 4EP- group (271,392 voxels), an effect that is largely driven by the reduced number of positive correlations in the 4EP+ compared to the 4EP- group (61,572 vs 141,493 voxels) (Fig. 3d, Extended Data Fig. 5g).

We tested the hypothesis that 4EP(S) impacts oligodendrocyte maturation. Immunostaining in the PVT revealed increased expression of neural/glial antigen 2 (NG2) in 4EP+ mice, indicative of immature, oligodendrocyte precursor cells, along with decreased levels of a mature oligodendrocyte marker stained by a CC1 antibody (Fig. 3e-f, Extended Data Fig. 5h-o). Analysis by flow cytometry and Western blot corroborated a skewing toward immature oligodendrocytes in 4EP+ mice (Fig. 3g, h, Extended Data Fig. 6a-c). Levels of NeuN, a pan-neuronal marker, and OLIG2, a pan-oligodendrocyte marker, were unchanged (Extended Data Fig. 5k-n), indicating effects on oligodendrocyte maturation by 4EP(S) rather than a change in the total number of cells within this lineage. These data suggest that 4EP(S) exposure leads to reduced oligodendrocyte maturation.

Similar phenotypes were observed in organotypic brain slices cultured in the presence of 4EPS. 4EPS-treated *ex vivo* brain tissue showed increased levels of the early oligodendrocyte marker NG2 relative to the mature marker CC1 (Fig. 3i, Extended Data Fig. 6d), and reduced colocalization of myelin with neuronal axons (Fig. 3j-k, Extended Data Fig. 6e). Further, functional markers of mature oligodendrocytes (MOG and myelin basic protein, MBP), were lower in 4EPS-treated samples, while transcription of the gene for NG2 (*Cspg4*) was increased (Fig. 3l, Extended Data Fig. 6f-g). While 4EPS enters the brain and has direct effects on brain tissue, we cannot exclude peripheral influences.

Reduced neuronal myelination in 4EP+ mice

We employed electron microscope tomography (ET) to examine the ultrastructure of myelin in the dense and organized axonal tracts of the corpus callosum to facilitate myelin quantification. We observed a striking increase in the ratio of unmyelinated to myelinated axons in the brains of 4EP+ mice compared to 4EP- mice (Fig. 4a, d), and a decrease in normalized (indicated by an increased g-ratio) and actual myelin thickness in 4EP+ mice (Fig. 4b-d, Extended Data Fig. 7a-e). Thus, consistent with the decrease in mature oligodendrocytes, 4EP(S) exposure reduces myelination frequency and efficiency in the brain.

Diffusion tensor imaging (DTI), a magnetic resonance imaging modality that assesses diffusion along myelinated tracts in the brain, was used to investigate the structural connectivity of myelin between the PVT and the rest of the brain. We found lower fractional anisotropy (FA), an indication of more dispersive rather than linear/restricted diffusion, in 4EP+ compared to 4EP- mice (Fig. 4e, Extended Data Fig. 7f). A similar defect in myelination was observed in whole brains and trended in the corpus callosum (Extended Data Fig. 7g-i). The significance of altered myelin dynamics and brain connectivity is an emerging concept in behavioral neuroscience[10–12,30,31].

4EP(S) increases anxiety-like behavior

Our previous study[8] and the 4EP(S)-dependent changes in the limbic system observed here prompted us to investigate whether 4EP production in the gut can modulate complex behaviors

in mice. 4EP(S) promoted robust anxiety-like behavior in several testing paradigms: 1) the elevated plus maze (EPM) where 4EP+ mice spend less time in the terminus of the open arms, 2) open-field exploration where mice ventured less into the more exposed zone of the arena, and 3) the light/dark box where 4EP+ mice spent more time in the dark (Fig. 4f, g, Extended Data Fig. 8a-c). 4EP+ mice also displayed increased marble burying, reflecting features of anxiety and/or stereotypic behaviors, but no increase in self-grooming (Fig. 4h, Extended Data Fig. 8d). Beyond anxiety-like behaviors, 4EP+ mice exhibited modestly altered social communication with increased anogenital sniffing in the direct social interaction assay (Extended Data Fig. 8e). In the adult ultrasonic vocalization (USV) test, male 4EP+ mice emit significantly fewer auditory communications to a novel age-matched female (Extended Data Fig. 8f). Interestingly, there were no significant differences in cognition or motor function between groups (via novel object recognition, Y-maze alternation, beam traversal, pole descent, or wire hang tests) (Extended Data Fig. 8g-k), further suggesting the effects of 4EP(S) are selective for emotional behaviors. Our reductionist model system employs an artificial microbiome to study the effects of a gut microbial metabolite (Extended Data Fig. 8l). Importantly however, oral administration of 4EP(S) to elevate levels in conventionally colonized mice also increased anxiety-like behaviors and reduced oligodendrocyte maturation (Extended Data Fig. 9a-j). 4EP- mice behaved similarly to conventionally colonized controls (Extended Data Fig. 9k,l), indicating the behavioral effects of 4EP(S) are not specific to gnotobiotic mice.

Finally, we sought to determine whether the 4EP(S)-mediated effects on oligodendrocytes contribute to altered behaviors. Administration of clemastine fumarate, a drug that promotes oligodendrocyte maturation[32], increased mature oligodendrocyte ratios in 4EP+ mice as measured by CC1 and NG2 staining of brain sections (Fig. 4i,j, Extended Data Fig. 10a). Notably, enhancing maturation of oligodendrocytes prevented behavioral changes in 4EP+ mice, including alterations in EPM, open field, and the marble burying tests (Fig. 4k-m, Extended Data Fig. 10c,e,f). We observed similar improvements in anxiety-like behaviors with another myelination-inducing drug, miconazole (Extended Data Fig. 10b,d, g-i). We conclude that 4EP(S) impacts anxiety-like behaviors in mice in a manner that includes effects on oligodendrocyte maturation.

Discussion

Herein, we discovered a biosynthetic pathway for production of the gut microbial metabolite 4EP. While this pathway can utilize tyrosine as a precursor, we show that other dietary sources can also be metabolized by the gut microbiota into 4EP, and expect that in humans, diverse dietary and microbial community structures may impact circulating metabolite levels. Additionally, we show that 4EP is sulfated and 4EPS enters the brains of mice, is associated with altered activation and connectivity of specific brain regions, and disrupts the maturation of oligodendrocytes and myelination patterns in the brain. Environmental cues are known to have regional effects on oligodendrocyte-neural interactions, influencing brain circuits that govern particular behaviors[6,7]. While other brain regions are likely involved in the 4EP(S) response, as we detect broad changes to activation patterns, the PVT receives sensory and cognitive input, integrates these cues locally, and exports finely tuned signals to cortical and subcortical areas resulting in applied behavioral responses[33]. Indeed, we show gut exposure to 4EP alters several emotional, but not non-emotional, behaviors in mice. Future work will focus on uncovering how 4EPS leads to changes in oligodendrocyte maturation and myelination, defining brain regions that are causally affected, and exploring how myelination changes impact behavior. Our data do not resolve if 4EPS is the neuroactive metabolite, versus 4EP or unknown breakdown products. Identification of gut-derived microbial metabolites that enter the brain and affect brain activity defines a novel environmental influencer of anxiety-like behaviors.

Gut bacteria can synthesize classical neurotransmitters such as dopamine, norepinephrine, serotonin and gamma-aminobutyric acid, and the production of novel classes of neuroactive metabolites by the microbiome has been postulated[34]. Molecules with phenolic structures similar to 4EP(S) are dysregulated in several preclinical models of behavior[8,35,36] as well as in certain neuropsychiatric disorders[37–41]. Intriguingly, a metabolite of tyrosine closely related to 4EP, *p*-cresol, has been suggested to influence oligodendrocyte function and affect social and depression-like behaviors in mice[6,42]. Increased 4EPS is associated with abnormal repetitive behavior in non-human primates[36], and plasma levels of 4EPS are significantly increased in a subset of individuals with ASD[15]. Additionally, relative abundances of several related metabolites such as 2-ethylphenylsulfate, 4-allylphenyl sulfate, and 4-methylbenzenesulfonate are altered in this same cohort[15]. We propose the hypothesis that 4EP(S) represents the

archetypical example of a neuroactive microbial molecule that impacts brain activity and complex behaviors in animals, conceptually akin to mammalian neurotransmitters that regulate nervous system function.

Figure Legends:

Fig. 1 | Discovery of a 4EP biosynthetic pathway, strain engineering of gut bacteria, and colonization of mice to produce 4EPS. a, Proposed biosynthetic pathway of 4EP in gut bacteria via tyrosine ammonia lyase (AL), phenolic acid decarboxylase (PAD), and vinyl phenol reductase (VPR) enzymes, and subsequent sulfation to 4EPS by host sulfotransferase (SULT1A1). The genes identified and cloned for bacterial strain engineering can convert tyrosine to 4EP via two chemical intermediates. **b and c,** 4EP precursors, *p*-coumaric acid and 4-vinylphenol from *in vitro* cultures of *Bacteroides ovatus* strains provided tyrosine as substrate. **b,** Conversion, or lack thereof, of tyrosine to *p*-coumaric acid by BACOVA_01194 gene (AL/1194 in figure) and deletion mutant (MFA01), respectively. **c,** The BACOVA_01194 gene (AL/1194 in figure) was introduced separately (MFA02), in addition to the *pad* gene (MFA04), or both genes as a single, highly expressed operon (MFA05). Standards are shown at top. Further details in Extended Data Figure 1, Methods, and Supplementary Information Tables 1-3. **d**, 4EP levels from *in vitro* cultures (provided with tyrosine) of 4EP- strain pair (*B. ovatus* Δ1194 (MFA01) and *Lactobacillus plantarum*) or the highest 4-vinylphenol producing engineered strain, *B. ovatus* 1194/PAD (MFA05) with *L. plantarum* (4EP+ strain pair). A standard is shown at the top. **e**, Levels of 4EP in feces (μg/mg) of mice colonized with bacterial strains lacking (4EP-) and producing (4EP+) 4EP (n=5). **f**, Levels of 4EPS in urine of mice colonized with 4EP- or 4EP+ (n=9) bacterial strains. Additional urine data, Extended Data Fig. 1k. **g**, Brain levels of 4EPS (after injection with probenecid) in mice colonized with 4EP- (n=4) and 4EP+ (n=6) bacterial strains. Additional controls, Extended Data Fig. 1f. At least two biologically independent trials were performed for each experiment. Abbreviations: N.D., not detectable. Data in panels e-g represent mean ± SEM.

Fig. 2 | Functional brain connectivity and regional activation is altered in response to colonization by 4EP-producing bacteria. a, fUSi mean connectivity matrices correlating signal in brain regions[43] for each group, 4EP+ and 4EP- (n=7), and each coronal plane, bregma -0.9mm, -1.6mm, and -2mm. Pearson correlation coefficient (r) is indicated by color according to the legend on right. Location of regions of interest (ROI) is categorized below, with further details found in Ext. Data Fig. 4a,b and Supplementary Information Table 4. **b,** Region pairs with significantly different connectivity in 4EP+ compared to 4EP- groups. Regions pairs are indicated by identical color of *p*-value (according to legend), and further indicated by dotted lines where necessary. Landmark brain regions are labeled in black, and specific ROIs are defined in Extended Data Fig. 4b and Supplementary Information Table 4. Analysis was performed using a paired t-test of each of the connectivity matrices with a Bonferroni correction to control for multiple comparisons. **c-d**, Color-coded overlays over representative coronal (c) and sagittal (d) sections of the mouse brain template showing significant differences in regional cerebral glucose uptake 4EP+ mice compared to 4EP- mice (n=11) (t-test, $p \leq 0.05$, extent threshold > 200 contiguous voxels, with both conditions met to be deemed significant; red/blue: increase/decrease in glucose uptake in 4EP+ compared to 4EP- mice). Two independent cohorts of mice from multiple litters were used for each experiment in the figure. Abbreviations: AM, amygdala; TH, thalamus; HY, hypothalamus; CC, corpus callosum; HPC, hippocampus; CTX, cortex; GP, globus pallidus; LS, lateral septum; PVT, paraventricular nucleus of the thalamus; BNST, bed nucleus of the stria terminalis; RT/VPL: reticular/ventral posterolateral thalamic nuclei; Cb: cerebellar vermis; Pn: pontine reticular nucleus.

Fig. 3 | Reduced oligodendrocyte maturation in 4EP+ mice. a, Number of differential genes in brain regions (n=5) of baseline mice; QuantSeq, one-way ANOVA Tukey test. **b**, Cell-specific enrichment analysis; *p*-values<0.05 in white. **c**, Representative subset of differential OPC and MO genes, one-way ANOVA Tukey with boxes showing 25-75th percentiles, median, and min/max points (n=5). **d**, Whole brain correlation to PVT seed using 2DG uptake data (n=11). PVT (red cross-section) is indicated. One-tailed multiple linear regression with minimum threshold of 200 contiguous voxels with $p<0.05$ was performed. **e**, Representative images of brain sections from 4EP- and 4EP+ mice; NG2 (red) and CC1 (green). Scale 100µm. **f**, Maturity quotient of oligodendrocytes in the PVT (n=8 cumulative totals used from biologically independent mice). $p=0.004$. **g**, Quantitative flow cytometry of PVT cells comparing the MOG+ quadrant 4 population over the NG2+ quadrant 1 population (n=4 pools of 5 PVTs). $p=0.03$. **h**, Representative flow plots. **i-l,** Organotypic brain slices treated with 10µM 4EPS. Each datapoint represents separate biological replicates. **i,** Maturity quotient of oligodendrocytes; using total cumulative counts from 3-5 images per replicate (vehicle, n=9; 4EPS, n=10). $p=0.003$. **j,** Percent colocalization of neurofilament (NF) and proteolipid protein (PLP) antibody stain (n=6). $p=0.01$. **k,** Representative images of panel j. Scale 20µm. **l,** Western blot for MBP of slices (n=6). $p=0.04$. Abbreviations: PVT, paraventricular nucleus of thalamus; BNST, bed nucleus of stria terminalis; BLA, basolateral amygdala; mPFC, medial prefrontal cortex; HY, hypothalamus; vHPC, ventral hippocampus; Astro, astrocyte; OPC, oligodendrocyte precursor cell; NFO, newly formed oligodendrocytes; MO, mature oligodendrocytes; Micro, microglia; Endo, endothelia; CC1, adenomatous polyposis coli; NG2, neural/glial antigen 2; MBP, myelin basic protein. Biologically independent mice from multiple randomized litters examined over one (a-c) or two respective experiments (d-l). Data represent mean ± SEM. Panels e-l analyzed by two-tailed Welch's t-test. *$p \leq 0.05$; **$p \leq 0.01$.

Fig. 4 | 4EP(S) alters myelination and anxiety-like behavior. a, Percent of unmyelinated axons (n=3; 4 images scored from each biological replicate). $p=0.005$. **b**, G-ratio (r/R) of all axons (4EP-, 56; 4EP+, 70 axons)(n=4; 4 images scored from each biological replicate). $p=0.0001$. **c**, Width of myelin; (4EP-, 56; 4EP+, 70 axons) (n=4; 4 images scored from each biological replicate). $p=0.003$. **d**, Representative electron tomography images. Several myelinated and unmyelinated axons marked by blue and orange arrows, respectively. **e,** Fractional anisotropy (FA) measured by diffusion tensor imaging (DTI) (n=4). $p=0.04$. **f**, Elevated plus maze: time spent in the terminus (outer one-third) of the open arms (4EP+ n=21; 4EP- n=24). $p=0.003$. **g**, Open field test (4EP+ n=21; 4EP- n=24). $p=0.002$. **h**, Number of marbles buried (4EP+ n=24; 4EP- n=23). $p=0.02$. **i**, Maturity quotient of oligodendrocytes in the PVT of 4EP- and 4EP+ mice ±clemastine fumarate (Cumulative totals used from individual mice: 4EP- control=7, treated=10; 4EP+ control=6, treated=6)(Cont 4EP-vs 4EP+ $p=0.03$; 4EP+Cont vs Treatment $p=0.01$). **j**, Representative images of brain sections from mice ±clemastine fumarate, stained for CC1 (green) and NG2 (red). **k-m**, Behavioral tests of mice (independent of cohorts used previously) ±clemastine fumarate. **k**, EPM (4EP- control n=13, treated n=13; 4EP+ control n=12, treated n=14)(4EP+Cont vs Treatment $p=0.05$). **l**, Open field test (4EP- control =15, treated n=17; 4EP+ control n=17, treated n=17) $p=0.04$. **m**, Number of marbles buried(4EP- control =15, treated n=17; 4EP+ control n=17, treated n=17)(Cont 4EP-vs 4EP+ $p=0.009$; 4EP+Cont vs Treatment $p=0.03$). Abbreviations: FA, fractional anisotropy;

NG2; neural/glial antigen 2; CC1, adenomatous polyposis coli. Biologically independent mice from multiple randomized litters examined over two respective experiments used for all experiments. Data represent mean ± SEM analyzed by two-tailed Welch‘s t-test (a-h) or two-way ANOVA with Dunnett multiple comparison to the 4EP+control group (i-m). *$p \leq 0.05$; **$p \leq 0.01$; ***$p \leq 0.001$.

References

1. Sharon, G. *et al.* Specialized metabolites from the microbiome in health and disease. *Cell Metab.* **20**, 719–730 (2014).
2. Swann, J. R. *et al.* Application of 1H NMR spectroscopy to the metabolic phenotyping of rodent brain extracts: A metabonomic study of gut microbial influence on host brain metabolism. *J Pharm Biomed Anal* **143**, 141–146 (2017).
3. Vuong, H. E., Yano, J. M., Fung, T. C. & Hsiao, E. Y. The Microbiome and Host Behavior. *Annu. Rev. Neurosci.* **40**, 21–49 (2017).
4. Needham, B. D., Kaddurah-Daouk, R. & Mazmanian, S. K. Gut microbial molecules in behavioural and neurodegenerative conditions. *Nature Reviews Neuroscience* 1–15 (2020) doi:10.1038/s41583-020-00381-0.
5. Huang, F. & Wu, X. Brain Neurotransmitter Modulation by Gut Microbiota in Anxiety and Depression. *Front Cell Dev Biol* **9**, 649103 (2021).
6. Gacias, M. *et al.* Microbiota-driven transcriptional changes in prefrontal cortex override genetic differences in social behavior. *eLife* **5**, e13442 (2016).
7. Hoban, A. E. *et al.* Regulation of prefrontal cortex myelination by the microbiota. *Transl Psychiatry* **6**, e774 (2016).
8. Hsiao, E. Y. *et al.* Microbiota Modulate Behavioral and Physiological Abnormalities Associated with Neurodevelopmental Disorders. *Cell* **155**, 1451–1463 (2013).
9. Berer, K. *et al.* Commensal microbiota and myelin autoantigen cooperate to trigger autoimmune demyelination. *Nature* **479**, 538–541 (2011).
10. Pan, S., Mayoral, S. R., Choi, H. S., Chan, J. R. & Kheirbek, M. A. Preservation of a remote fear memory requires new myelin formation. *Nature Neuroscience* **23**, 487–499 (2020).
11. Maheras, K. J. *et al.* Absence of Claudin 11 in CNS Myelin Perturbs Behavior and Neurotransmitter Levels in Mice. *Sci Rep* **8**, 3798 (2018).
12. Bonnefil, V. *et al.* Region-specific myelin differences define behavioral consequences of chronic social defeat stress in mice. *Elife* **8**, (2019).
13. Galvez-Contreras, A. Y., Zarate-Lopez, D., Torres-Chavez, A. L. & Gonzalez-Perez, O. Role of Oligodendrocytes and Myelin in the Pathophysiology of Autism Spectrum Disorder. *Brain Sci* **10**, (2020).
14. Cassoli, J. S. *et al.* Disturbed macro-connectivity in schizophrenia linked to oligodendrocyte dysfunction: from structural findings to molecules. *npj Schizophrenia* **1**, 1–10 (2015).
15. Needham, B. D. *et al.* Plasma and Fecal Metabolite Profiles in Autism Spectrum Disorder. *Biol Psychiatry* (2020) doi:10.1016/j.biopsych.2020.09.025.
16. Gamage, N. *et al.* Human Sulfotransferases and Their Role in Chemical Metabolism. *Toxicol Sci* **90**, 5–22 (2006).
17. Chamkha, M., Garcia, J. L. & Labat, M. Metabolism of cinnamic acids by some Clostridiales and emendation of the descriptions of Clostridium aerotolerans, Clostridium celerecrescens and Clostridium xylanolyticum. *Int J Syst Evol Microbiol* **51**, 2105–2111 (2001).

18. Santamaría, L., Reverón, I., Felipe, F. L. de, Rivas, B. de las & Muñoz, R. Ethylphenol Formation by Lactobacillus plantarum: Identification of the Enzyme Involved in the Reduction of Vinylphenols. *Appl. Environ. Microbiol.* **84**, (2018).

19. Agency for Toxic Substances and Disease Registry (ATSDR). Toxicological profile for Cresols. https://wwwn.cdc.gov/TSP/ToxProfiles/ToxProfiles.aspx?id=946&tid=196 (2008).

20. Penzo, M. A. *et al.* The paraventricular thalamus controls a central amygdala fear circuit. *Nature* **519**, 455–459 (2015).

21. Ahrens, S. *et al.* A Central Extended Amygdala Circuit That Modulates Anxiety. *J. Neurosci.* **38**, 5567–5583 (2018).

22. Duval, E. R., Javanbakht, A. & Liberzon, I. Neural circuits in anxiety and stress disorders: a focused review. *Ther Clin Risk Manag* **11**, 115–126 (2015).

23. Robinson, O. J., Pike, A. C., Cornwell, B. & Grillon, C. The translational neural circuitry of anxiety. *J Neurol Neurosurg Psychiatry* **90**, 1353–1360 (2019).

24. Barson, J. R., Mack, N. R. & Gao, W.-J. The Paraventricular Nucleus of the Thalamus Is an Important Node in the Emotional Processing Network. *Front. Behav. Neurosci.* **14**, (2020).

25. Kirouac, G. J. The Paraventricular Nucleus of the Thalamus as an Integrating and Relay Node in the Brain Anxiety Network. *Front Behav Neurosci* **15**, (2021).

26. Park, H.-C. & Appel, B. Delta-Notch signaling regulates oligodendrocyte specification. *Development* **130**, 3747–3755 (2003).

27. Wang, S. *et al.* Notch Receptor Activation Inhibits Oligodendrocyte Differentiation. *Neuron* **21**, 63–75 (1998).

28. Williamson, J. M. & Lyons, D. A. Myelin Dynamics Throughout Life: An Ever-Changing Landscape? *Front. Cell. Neurosci.* **12**, (2018).

29. Holschneider, D. P., Wang, Z. & Pang, R. D. Functional connectivity-based parcellation and connectome of cortical midline structures in the mouse: a perfusion autoradiography study. *Front Neuroinform* **8**, (2014).

30. Kaller, M. S., Lazari, A., Blanco-Duque, C., Sampaio-Baptista, C. & Johansen-Berg, H. Myelin plasticity and behaviour — connecting the dots. *Curr Opin Neurobiol* **47**, 86–92 (2017).

31. Barak, B. *et al.* Neuronal deletion of Gtf2i , associated with Williams syndrome, causes behavioral and myelin alterations rescuable by a remyelinating drug. *Nature Neuroscience* **22**, 700–708 (2019).

32. Xie, D. *et al.* Clemastine improves hypomyelination in rats with hypoxic–ischemic brain injury by reducing microglia-derived IL-1β via P38 signaling pathway. *Journal of Neuroinflammation* **17**, 57 (2020).

33. Kirouac, G. J. Placing the paraventricular nucleus of the thalamus within the brain circuits that control behavior. *Neurosci Biobehav Rev* **56**, 315–329 (2015).

34. Sharon, G., Sampson, T. R., Geschwind, D. H. & Mazmanian, S. K. The Central Nervous System and the Gut Microbiome. *Cell* **167**, 915–932 (2016).

35. Tian, P., Wang, G., Zhao, J., Zhang, H. & Chen, W. Bifidobacterium with the role of 5-hydroxytryptophan synthesis regulation alleviates the symptom of depression and related microbiota dysbiosis. *The Journal of Nutritional Biochemistry* **66**, 43–51 (2019).

36. Koyama, H. *et al.* Effects of housing conditions on behaviors and biochemical parameters in juvenile cynomolgus monkeys (Macaca fascicularis). *Exp. Anim.* **68**, 195–211 (2019).

37. Tian, J.-S. *et al.* A GC-MS urinary quantitative metabolomics analysis in depressed patients treated with TCM formula of Xiaoyaosan. *J. Chromatogr. B Analyt. Technol. Biomed. Life Sci.* **1026**, 227–235 (2016).

38. Sankowski, B. *et al.* Higher cerebrospinal fluid to plasma ratio of p-cresol sulfate and indoxyl sulfate in patients with Parkinson‘s disease. *Clin. Chim. Acta* **501**, 165–173 (2020).

39. Gabriele, S. *et al.* Urinary p-cresol is elevated in young French children with autism spectrum disorder: a replication study. *Biomarkers* **19**, 463–470 (2014).

40. Neul, J. L. *et al.* Metabolic Signatures Differentiate Rett Syndrome From Unaffected Siblings. *Front Integr Neurosci* **14**, (2020).

41. Takesada, M., Miyamoto, E., Kakimoto, Y., Sano, I. & Kaneko, Z. Phenolic and Indole Amines in the Urine of Schizophrenics. *Nature* **207**, 1199–1200 (1965).

42. Sun, C.-Y. *et al.* p-Cresol Sulfate Caused Behavior Disorders and Neurodegeneration in Mice with Unilateral Nephrectomy Involving Oxidative Stress and Neuroinflammation. *Int J Mol Sci* **21**, (2020).

43. Paxinos, G. & PhD, K. B. J. F., MA. *The Mouse Brain in Stereotaxic Coordinates*. (Elsevier Science, 2007).

44. Holdeman, Lillian V. & Moore, W.E.C. *Anaerobe laboratory manual (4th ed).* (Virginia Polytechnic Institute and State University, 1977).

Materials and Methods

Bacterial strains and culture conditions

All bacterial strains and plasmids used in this study are shown in Supplementary Information Tables 1 and 2. *B. ovatus* was cultured in brain heart infusion (BHI) agar medium supplemented with 10% horse blood, TYG (tryptone-yeast extract-glucose) broth or minimal medium (MM) at 37 ˚C in an anaerobic chamber from Coy Laboratories[44,45]. Tyrosine was supplied as a substrate during investigation of 4EP production. *L. plantarum* was cultured anaerobically in MRS media (BD) at 37˚C. *Escherichia coli* strains were cultured aerobically in LB broth. When appropriate, the growth medium was supplemented with 100 µg/ml carbenicillin, 25 µg/ml erythromycin, 2 µg/ml tetracycline, 200 µg/ml gentamicin and 200µg/ml 5-fluoro-2‘-deoxyuridine (FUdR).

Disruption of BACOVA_01194 in *B. ovatus*

Using NCBI BLAST alignment tools, we predicted that BACOVA_01194 was an ammonia lyase that could metabolize tyrosine. For all PCR amplification steps we used PrimeSTAR Max DNA polymerase (Takara Bio, Mountain View, CA) according to the manufacturer‘s instructions. Primer sequences are shown in Extended Data Table 3. We used a previously reported double-crossover recombination method to construct *B. ovatus* Δ1194[46]. Briefly, ~1 kb DNA fragments corresponding to the upstream and downstream regions of the target gene were PCR amplified and then digested with restriction endonucleases. The digested fragments were then ligated into the suicide plasmid pExchange-*tdk* using T4 DNA ligase (New England Biolabs, Ipswich, MA). The resulting plasmid was transformed into *Escherichia coli* S17-1 λ *pir* by electroporation and transformants were confirmed by PCR amplification of the junction regions. An *E. coli* clone harboring the plasmid was cultivated and plasmid DNA was isolated, purified, and verified by DNA sequencing.

For conjugation into *B. ovatus, B. ovatus* Δ*tdk* and *E. coli* S17-1 λ *pir* harboring the plasmid were cultivated and the cells were harvested by centrifugation. The cell pellets were washed with PBS to remove residual antibiotics and combined in TYG medium. The suspension was plated on BHI-blood agar medium without any antibiotics and cultivated aerobically at 37 ˚C for 1 day. The bacterial biomass was recovered by scraping and re-suspended in TYG medium. The suspension was then plated on BHI-blood agar medium supplemented with erythromycin and gentamicin and single-crossover integrants were selected. These strains cultured in TYG medium overnight and plated on BHI-blood agar medium supplemented with FUdR. The deletion mutant was screened by PCR amplification and verified by DNA sequencing.

B. ovatus strain engineering

When a culture of *L. plantarum* was supplemented with 4-vinylphenol, it was converted quantitatively to 4-ethylphenol; in contrast, when the culture was supplemented with *p*-coumarate, the conversion to 4-vinylphenol was slow. This suggested that the decarboxylation step might be rate-limiting for 4-ethylphenol biosynthesis in binary culture. To address this challenge, we introduced the *pad* gene from *L. plantarum* into *B. ovatus* in order to enable *B. ovatus* to produce 4-vinylphenol directly from tyrosine. However, the resulting strain did not produce 4-vinylphenol. We next introduced a second copy of the BACOVA_01194 gene into *B. ovatus* along with *pad* in case the intermediate p-coumarate was limiting, but this strain failed to produce 4-vinylphenol. To address the possibility that the *pad* gene from *L. plantarum* does not function robustly in *B. ovatus*, *pad* from *Bacillus subtilis* was introduced into *B. ovatus*; the

engineered strain produced 4-vinylphenol robustly from tyrosine. To boost the level of 4-vinylphenol, a second copy of BACOVA_01194 was introduced into *B. ovatus* along with *pad* from *B. subtilis* using a second integration vector with a different antibiotic marker. This strain produced 4-vinylphenol more robustly. We then combined the second copy of BACOVA_01194 and *pad* into a single artificial operon driven by a strong phage promoter and introduced this construct into *B. ovatus*. Interestingly, this strain produced a much higher level of 4-vinylphenol and it was used throughout the manuscript for co-cultivation and colonization. Vector maps and sequences of primers used for *B. ovatus* engineering are shown in Extended Data Fig. 1 and Supplementary Information Table 3, respectively. The artificial operon was constructed in the following way: A phage promoter along with 5‘ and 3‘ flanking sequences from the target vector, pNBU2, and one of the target genes was amplified by PCR. The target gene with 5‘ and 3‘ flanking sequences containing sequences of the phage promoter and the pNBU2 vector were also amplified. These two PCR fragments were assembled by overlap PCR. The BO_01194 and *pad* genes were each assembled by one more round of overlap PCR. The fragment containing the target gene and the phage promoter was cloned into the fragment of pNBU2 vector using Gibson Assembly. The assembled plasmids were transformed into *Escherichia coli* S17-1 λ *pir* competent cells by electroporation and transformants were confirmed by PCR amplification of the junction regions. The positive clone harboring assembled plasmid was cultivated and the plasmid was isolated, purified, and confirmed by DNA sequencing. To conjugate the plasmid into *B. ovatus, B. ovatus* Δ*tdk* and *E. coli* S17-1 λ *pir* harboring the plasmid were cultivated and the cells were harvested. The cell pellets were washed with PBS to remove residual antibiotics and combined them in TYG medium. The suspension was plated on BHI-blood agar medium without any antibiotics and grown aerobically at 37 ˚C for 1 day. The bacterial biomass was recovered by scraping and re-suspended in TYG medium. The suspension was then plated on BHI-blood agar medium supplemented with erythromycin and gentamicin and antibiotic resistant strains were selected followed by PCR amplification of the junction regions.

Extraction of bacterial culture metabolites

For metabolite analysis, *B. ovatus* was cultured in TYG medium overnight and the cells were harvested and washed with MM. The cell pellet was re-suspended in MM containing 0.5 mg/ml tyrosine to a density of OD_{600} = 1.0 and incubated anaerobically for 1 day. The culture was extracted with acetone (20% v/v) and centrifuged. The supernatant was analyzed by LC/MS as described below. For LC-MS analysis of co-culture experiments, *B. ovatus* and *L. plantarum* were cultivated anaerobically in TYG and MRS, respectively overnight and the cells were harvested and washed with MM. The cell pellet was re-suspended in MM containing 0.5 mg/ml tyrosine to a density of OD_{600} = 1.0 and combined in the same culture tube. After 1-day incubation, samples for HPLC analysis were prepared as described above.

LC/MS analysis of bacterial culture metabolites

Metabolite extracts were analyzed using an Agilent 1260 LC system coupled to an Agilent 6120 quadrupole mass spectrometer with a 3 µm, 4.6 x 75 mm Unison UK-C18 column (Imtakt, Portland, OR). Water with 10mM ammonium acetate and 0.1% formic acid (A) and acetonitrile with 0.1% formic acid (B) was used as the mobile phase at a flow rate of 1.0 ml/min with the following 20 min gradient: 0-5 min, 0% B; 5-17 min, 0-90% B; 17-20 min, 95% B. P-coumaric acid and 4-VP were detected at 280nm and these retention times were ~10.3 min and ~12.6 min,

respectively. Retention time of 4-EP was ~7.6 min. Standards of p-coumaric acid and 4-ethyl phenol were purchased (Sigma, St. Louis, MO).

Gene sequence alignment

Sequences of the genes used for strain engineering were aligned against the reference genomes in the WoL database, which were pre-annotated using UniRef release 2019_07. The annotation files are publicly available at: https://biocore.github.io/wol/download. The alignment used DIAMOND v0.9.25 with all default parameters (`diamond blastx-d/path/to/db-qinput.fa-o output.txt`). The output files were then processed using Woltka (https://github.com/qiyunzhu/woltka), which generated the taxonomic and functional (UniRef) profile of the three genes against the entire WoL genome catalog.

Mouse Husbandry

All animal husbandry and experiments were approved by the Caltech Institutional Animal Care and Use Committee. Throughout the study, animals were maintained in autoclaved microisolator cages with autoclaved bedding (Aspen Chip Bedding, Northeastern Products Corp, Warrensburg, NY), water, and chow (Laboratory Autoclavable Rodent Diet - 5010, LabDiet; St. Louis, MO, USA). Diets used in Extended Data Fig. 1g were purchased from Envigo Teklad (Madison, WI), carbohydrate, and fat content. The soy protein has ~300ppm total isoflavones. The tyrosine levels are 4.6g/kg in soy diet and 17.1g/kg in fish diet. 8-wk, SPF C57BL/6J male mice (Jackson Laboratory, Bar Harbor, ME), were provided these special diets for 2 weeks ad libitum prior to urine collection for metabolite analysis as described below.

Mice were maintained at an ambient temperature of 71-75F, 30% - 70% humidity, at a cycle of 13 hours light & 11 hours dark.

Experimental Design of Mouse Experiments

Germ-free (GF) C57BL/6J male weanlings (3 weeks of age) from the Mazmanian laboratory colony were colonized by gavage of 100ul of 1:1 mixture of 10^9 CFU/ml *B. ovatus* (+/- 4EP pathway genes) and wild type *L. plantarum*. This process was continually performed, yielding a steady schedule of cohorts for continued study throughout this work. Size of animal groups was determined by the largest number of pups that could be born within the space of the germ-free isolators. Weekly tests to confirm gnotobiotic status were performed and 4EPS levels were confirmed in urine regularly. All experiments in the study were repeated on at least two independent cohorts. Preliminary behavioral analysis identified a stronger phenotype in males (Extended Data Fig. 10j-l), so they were used for the remainder of the study in effort to limit animal use.

16S sequencing was performed by Laragen (Culver City, CA) and analysis was done with a 16S V6 library. Paired-end fastq files were processing using Qiime2[47]. Briefly, sequences were quality control processed with dada2[48], truncating reads to 150 bp. Taxonomic classification was then conducted using the greengenes database. Analysis was conducted on samples rarefied to 24,000 reads.

In the conventionally colonized (SPF) experiment, male weanlings (3 weeks of age) were provided 250mM 4EP and 4EPS in drinking water (or vehicle). In these experiments, oral

administration continued until endpoint. 4EPS was synthesized as previously described[8], and 4EP was purchased from Sigma, (St. Louis, MO). When appropriate, beginning at 4-5 weeks of age, sterile clemastine fumarate (0.03mg/ml) or DMSO vehicle (Sigma, St. Louis, MO) was added to drinking water and water was changed every other day, or miconazole solution (40mg/kg) or 3% DMSO vehicle was gavaged once daily. In all cases, behavior testing started at 6 weeks of age.

Extraction of urine, feces, serum and brain metabolites

Urine was collected by placing autoclaved aluminum foil under the mouse while briefly scruffing it, and then pipetting the urine from the foil. The urine was diluted 5-fold with aqueous acetonitrile (50% v/v) and centrifuged. The supernatant was analyzed by LC/MS to detect 4EPS. 4EPS for a standard was prepared as previously described[8]. Ethyl acetate was added to the supernatant to create a 1:1:1 mixture (v/v) of water, acetonitrile, and ethyl acetate. After mixing and centrifugation, the organic layer was analyzed by GC/MS to detect 4EP.

Fecal pellets were collected by placing the mouse briefly into a sterile plastic beaker. A 5x volume of 50% acetonitrile/water was added and the pellets were homogenized by bead beating, followed by centrifugation. The supernatant was analyzed by LC/MS to detect 4EPS. To detect 4EP, samples were extracted with ethyl acetate as described above.

Blood was collected by cardiac puncture followed by separation using Sarstedt Serum-Gel microtubes (Thermo Fisher Scientific, Waltham, MA) according to the manufacturer‘s specifications.

Brain tissue was collected by cardiac perfusion as described for immunohistochemistry but with PBS instead of PFA, then dissected. A 2x volume of 50% acetonitrile/water was added and the tissue was homogenized by bead beating, followed by centrifugation. The supernatant was directly injected for analysis by LC/MS to detect 4EPS.

LC/MS analysis of metabolites from urine, serum, and brain

Samples were analyzed using an Agilent 1290 LC system coupled to an Agilent 6530 QTOF with a 3 μm, 4.6 x 75 mm Unison UK-C18 column using the same method described above. All data were collected in negative ion mode. 4EPS was detected as [M-H]- (calculated m/z is 201.0227) and retention time was ~7.9 min. 4EPS prepared previously was used as a standard[8].

GC/MS analysis of metabolites from feces

Samples were analyzed with a split ratio of 10:1 using an Agilent 7890 GC coupled to an Agilent 5977 MSD with a HP-5MS fused silica capillary column (30m x 250 μm x 0.25 μm). The injector temperature was set at 250˚C and high purity helium gas was used as carrier at a constant flow rate of 1.0 ml/min. The column temperature was initially kept on 40˚C for 2 min, then increased to 100˚C at a rate of 40˚C/min, then went up to 105˚C at a rate of 2˚C/min and then raised to 320˚C at a rate of 30˚C/min, held for 3 min, giving 16.367 min in total. Retention time of 4-EP (calculated m/z is 122.07) was ~7.6 min.

Creatinine measurement

Concentration of creatinine was measured using Colorimetric Creatinine Assay Kit (Abcam, Cambridge, UK) according to the manufacturer's instructions.

Brain Levels of 4EPS

Probenecid (Invitrogen, Carlsbad, CA), an organic anion transporter (OAT) inhibitor that works on OAT1 and OAT3 was injected intraperitoneally (i.p.) into mice (120mg/kg). After 1-hour, whole brains were removed, homogenized, and analyzed as described above by LCMS. For SPF animals, 30 minutes after the probenecid injection, either an i.p. injection of 100ul of 8mM 4EPS or an oral gavage of 160mg/kg 4EP (Sigma, St. Louis, MO) was administered, then brains were harvested after 30 additional minutes or along 30-minute time points. For mice colonized with 4EP- and 4EP+ strains, mice were perfused with PBS before tissue collection to ensure any metabolite detected was not simply due to levels in the blood.

qPCR

RNA was extracted using the RNeasy Mini Kit (Qiagen, Hilden, Germany) and cDNA was transcribed using the iScript cDNA Synthesis Kit (Thermo Fisher Scientific, Waltham, MA). qPCR was performed with the SYBR master mix (Thermo Fisher Scientific, Waltham, MA) using the primers found in Supplementary Information Table 5.

In vitro assays of 4EP sulfation

Recombinant sulfotransferases (sult1b1, 1c2, 1e1, 2a1, and 1a1) and the Universal Sulfotransferase Activity Kit (R&D Systems, Minneapolis, MN) were used according to manufacturer's recommendations. Following analysis by plate reader, samples were analyzed by LCMS as described above to confirm that the sulfated product was indeed 4EPS. Cytosolic fractions from 50-200ug tissue containing endogenous sulfotransferases were extracted and tested for SULT activity on 4EP as previously described[49,50] and analyzed by LCMS as described above.

Intestinal Permeability

The FITC-dextran intestinal permeability assay was performed as described previously[51] on 4EP- and 4EP+ mice at nine weeks.

Hematoxylin and eosin (H&E) staining

Gut tissue was dissected immediately after sacrifice at nine weeks of age and fixed in neutral 10% formalin, paraffin embedded, sectioned, and stained with hematoxylin and eosin (H&E) by Pacific Pathology, Inc, San Diego, CA.

Cytokine Analysis

Tissue samples collected at nine weeks of age were homogenized by bead beating in lysing matrix D tubes (MP Biomedicals, Irvine, CA) in RIPA buffer (Millipore, Burlington, MA) containing protease inhibitor tablets (Roche, Basel, Switzerland) followed by protein quantification and normalization using the Pierce BCA Protein Assay Kit (Thermo Fisher Scientific, Waltham, MA). Blood samples were collected by cardiac puncture followed by serum isolation in clotting tubes (Sarstedt, Newton, NC). Using the Bio-Plex Pro Mouse Cytokine 23-plex assay (Bio-Rad, Hercules, CA) according to manufacturer's recommendations, cytokine and chemokine levels were determined using a Bio-Plex 200 Systems instrument. Undetected values

were rare, and in those cases were imputed with the lowest detected value from that cytokine. One-way ANOVA with multiple comparisons was performed and significance is indicated with asterisks (*<0.05, **<0.01, ***<0.001).

Microglial enrichment for qPCR

Brain samples were collected and single cell suspensions were generated as described in flow cytometry section below. Microglial-enriched populations were obtained using CD11b microbeads (Miltenyi Biotec, San Diego, CA).

Animal protocol for functional ultrasound imaging (fUSi) session

14 mice were imaged in total: 7 mice for the 4EP- group and 7 for the 4EP+ group. Images were acquired through intact skull and skin after hair removal using a commercial depilatory cream (Nair^{TM} , Church&Dwigth, USA) without any contrast agent injection. During handling (shaving, positionning) mice were anaesthetized with isoflurane (2%) administered in a mixture of 30% O_2 and 70% N_2. During the resting state experiment, animals were sedated using dexmedetomidine (Tocris Bioscience, Minneapolis, MN). A bolus of 0.10 mg/kg was injected subcutaneously, and isoflurane was discontinued after 5 minutes. Mice were head fixed on a stereotaxic frame to minimize brain motion during imaging. After a 90 min. imaging session, animals were euthanized by cervical dislocation.

Functional ultrasound imaging

Functional ultrasound imaging (fUSi) visualizes neural activity by mapping local changes in cerebral blood volume (CBV). CBV variations are tightly linked to neuronal activity through the neurovascular coupling[52] and are evaluated by calculated power doppler variations in the brain[53]. fUSi was performed transcranially as described in[54] using a 15 MHz ultrasonic ultralight probe prototype (15 MHz, 64 elements, 0.110 mm pitch, Vermon, Tours, France) connected to a Verasonics Vantage ultrasound system (Verasonics Inc., Redmond, WA, USA) driven by custom Matlab® (MathWorks, USA) transmission scripts (https://github.com/brittanyneedham/Needham_Nature2022)[55]. Each Power Doppler image was obtained from the temporal integration of 220 compounded frames acquired at 500 Hz frame rate, using 5 tilted plane waves separated by 3° (-6°, -3°, 0°, 3°, 6°) acquired at a 2500 Hz pulse repetition frequency (PRF). Power Doppler images were then repeated every second (1Hz image framerate). Each block of 220 images was processed using a SVD clutter filter[56] to separate tissue signal from blood signal to obtain a final Power Doppler image exhibiting cerebral blood volume (CBV) in the whole imaging plane. Three coronal planes per mice were scanned at a rate of 15min imaging time per plane, respectively Bregma -0.9mm, Bregma -1.6mm, and Bregma -2mm.

Functional ultrasound data processing and statistics

Power Doppler data were collected continuously during the imaging session and connectivity process was applied afterwards. We followed the functional connectivity process on fUSi data described in Osmanski, et. al[57]. For each coronal plane, for each acquisition, and each mouse: first, a low-pass filter (cutting-frequency: 0.2 Hz) was performed on the Power Doppler temporal signals for each individual pixel of the image to remove high frequency signals while preserving the resting-state frequency band. The signal was then detrended with a polynomial fit of order 4 to remove low frequencies which could bias the correlation value. Finally, the normal score of

the temporal filtered signals were calculated to make possible correlation calculation. In order to build functional connectivity matrices, we determined within each coronal plane regions of interest (ROIs) defined from the Paxinos Atlas[43] (See Extended Data Fig. 2a for ROIs mapping in each plane). The Pearson correlation of the filtered signals of each pair of ROIs' within a same plane were then calculated and the corresponding correlation values were stored in the cells where regions intersect in the connectivity matrix. Fig.2 shows the mean connectivity matrices from each coronal plane (Bregma-0.9mm, Bregma-1.6mm and Bregma-2mm) of each studied group (4EP- and 4EP+). Within the same coronal plane, cells of the connectivity matrices from the 4EP- and 4EP+ groups were statistically analyzed individually using a paired t-test. Multiple comparison correction was ensured with a Bonferroni correction[58]. Region pairs that showed significant differences between groups are shown in Fig. 2c.

ROIs distribution graphs of each coronal plane are provided. Coronal plane B-0.9mm: ROIs #1 to #8 are located in the left cortex, ROI#9 is the left hippocampus, ROIs#11 to #21 are located in the thalamus, ROI#22 is the right hippocampus, ROIs#23 to #30 are located in the right cortex and finally ROIs#31 to #48 are subthalamic regions. Coronal plane B-1.6mm: ROIs #1 to #20 are located in the cortex, ROIs#21 #22 are the left and right hippocampi, ROIs#23 to #38 are located in the thalamus and ROIs#39 to #42 are subthalamic regions. Coronal plane B-2mm: ROIs #1 to #9 are located in the left cortex, ROI#10 is the left hippocampus, ROIs#11 to #22 are located in the thalamus, ROI#23 is the right hippocampus, ROIs#24 to #32 are located in the right cortex and finally ROIs#33 to #50 are subthalamic regions.

Autoradiography Brain Mapping

The autoradiographic 2DG uptake method is a well-established, time-tested approach to functional brain mapping based on a tight coupling between neural activity and metabolism. It is particularly suitable in awake, free-moving animals, and complements the fUSi approach. Male mice colonized as described above were housed in pairs from weaning. Mapping of cerebral glucose metabolism was performed as described previously[59,60] in four groups: 4EP+/Home cage (n = 11), 4EP+/Open field (n = 11), 4EP-/Home cage (n = 10), 4EP-/Open field (n = 11). The experiment was performed in two cohorts with balanced group assignment in each cohort. At 7 weeks mice were habituated to handling for 5 minutes each day for 3 days prior to 2DG mapping. They were brought in their home cages to the experimental suite 16 hours prior to mapping and were fasted of food overnight with water ad libitum. A pair of mice from the same home cage were administered i.p. [^{14}C]-2-deoxy-D-glucose (Cat # MC355, radiochemical purity > 97%, specific activity 45 - 60 mCi/mmol, Moravek Inc., Brea, CA, USA) at 0.3 µCi/g bodyweight in 0.5 ml normal saline. Animals were placed back in their home cage for five minutes. One mouse was then placed into the Open Field arena and allowed to explore the arena for 45 minutes to allow uptake of the tracer, while the other remained in the home cage. At the end of exposure, following cervical dislocation, brains were extracted and flash frozen in methylbutane over dry ice (~ -55^{o}C) and later serially sectioned into 20-µm slices in a cryostat at -20^{o}C (Mikron HM550 OMP, Thermofisher Scientific, Waltham, MA, USA). Slices were heat dried on glass slides and exposed to Kodak Biomax MR diagnostic film (Eastman Kodak, Rochester, NY, USA) for 3 days at room temperature. Autoradiographs were then digitized on an 8-bit gray scale using a voltage stabilized light box (Northern Lights Illuminator, InterFocus Ltd., England) and a Retiga 4000R charge-coupled device monochrome camera (Qimaging, Canada).

Relative regional cerebral glucose uptake (rCGU) was measured and analyzed on a whole-brain basis using Statistical Parametric Mapping (SPM, version 5, Wellcome Centre for Neuroimaging, University College London, London, UK) as previously described[59,61]. Here briefly, each three-dimensional (3D) brain was reconstructed from 68 digitized autoradiographs (voxel size: 40 × 140 × 40 μm) using TurboReg, an automated pixel-based registration algorithm implemented in ImageJ (version 1.35, http://rsbweb.nih.gov/ij/). This algorithm registered each section sequentially to the previous section using a nonwarping geometric model that included rotations, rigid-body transformation, and nearest-neighbor interpolation. One "artifact free" mouse brain was selected as reference, and all brains were spatially normalized to the reference in SPM. Spatial normalization consisted of applying a 12-parameter affine transformation followed by a nonlinear spatial normalization using 3D discrete cosine transforms. All normalized brains were then averaged to create a final mouse brain template. Each original 3D-reconstructed brain was then spatially normalized to the template. Normalized brains were smoothed with a Gaussian kernel (full width at half maximum = 3x voxel dimension in the coronal plane). Voxels for each brain failing to reach a specified threshold in optical density (70% of the mean voxel value) were masked out to eliminate the background and ventricular spaces without masking gray or white matter. Differences in the absolute amount of radiotracer uptake in the brain were normalized in SPM for each animal by scaling the voxel optical densities such that the whole-brain mean for each brain was the same (proportional scaling). For each condition (open field and home cage exposure), one-tailed t-tests were performed voxel-by-voxel comparing 4EP+ and 4EP- animals. Threshold for significance was set at $P < 0.05$ at the voxel level and an extent threshold of 200 contiguous voxels to eliminate false positive statistically significant results. Color-coded functional overlays showing statistically significant changes in rCGU were displayed over coronal sections of the template brain in MRIcro (version 1.40, https://people.cas.sc.edu/rorden/mricro/mricro.html). This combination reflected a balanced approach to control both type I and type II errors. The minimum cluster criterion was applied to avoid basing our results on significance at a single or small number of suprathreshold voxels. Brain regions were identified according to a mouse brain atlas([43] and atlas.brain-map.org).

A seed correlation approach was applied to assess 4EP-related differences in the functional connectivity of the PVT. A structural region of interest (ROI) was hand drawn in MRIcro over the template brain according to the mouse brain atlas for the PVT between bregma -1.0 and -1.6mm. Mean optical density of the seed ROI was extracted for each animal using the MarsBaR toolbox for SPM (version 0.42, http://marsbar.sourceforge.net). Correlation analysis was performed in SPM for each home cage group. *T* statistics were calculated using a linear regression model with the seed value as the only covariate (regressor). Threshold for significance of directional correlation was set at $p < 0.05$ (one-tailed *t*-test) at the voxel level and an extent threshold of 200 contiguous voxels to serve as a proxy for multiple comparison correction, which is standard for the field. Regions showing statistically significant correlations (positive or negative) in rCGU with the seed are considered functionally connected with the seed. Color-coded functional overlays were displayed in the template brain after 3D rendering in MRIcro to allow visual comparison of overall level of functional connectivity.

Brain sample collection for immunohistochemistry

Mice were perfused via the cardiovascular system with PBS followed by 4% paraformaldehyde (Electron Microscopy Sciences, Hatfield, PA). Brains were removed and post-fixed in 4%

paraformaldehyde 1 day at 4°C. The brains were kept in PBS with 0.02% sodium azide at 4°C until sectioning. For sectioning, the brains were embedded in 4% UltraPure low melting point agarose (Thermo Fisher Scientific, Waltham, MA) and were coronally sectioned by vibratome (VT1000S; Leica Microsystems, Wetzlar, Germany) at a thickness of 50 µm. Brain sections of 50 µm were collected and stained every 0.15 mm. The brain sections were stored as free-floating in PBS with 0.02% sodium azide at 4°C until staining.

The free-floating sections were incubated with primary antibody in blocking solution (10% horse serum, 0.3% triton X-100, and 0.02% sodium azide in PBS) overnight at room temperature. The next day, sections were incubated with fluorescence-conjugated secondary antibody for 1.5-2 hours at room temperature. Between each step and after secondary antibody staining, sections were thoroughly washed with PBS or PBS with 0.1% triton-X-100 at least three times for 10 minutes each. The stained free-floating sections were then mounted onto the Superfrost Plus microscope slides (Fisher Scientific, Hampton, NH) in PBS. Excess PBS from adhered sections were carefully removed. Slides were dried at room temperature for 2-5 minutes. 150-200 µl of ProLong Diamond, anti-fade mountant with DAPI (Thermo Fisher Scientific, Waltham, MA) was applied to the slides before placing the coverslip. The slides were left to set overnight before imaging.

Primary antibodies used for imaging throughout and their dilutions were: mouse anti-NeuN (1:1000; MAB377; Millipore Sigma, Burlington, MA), goat anti-Olig2 (1:500; AF2418; R&D Systems, Minneapolis, MN); mouse anti-CC1 (1:250; NB600-1021; Novus Biologicals, Littleton, CO); rabbit anti-NG2 (1:300; AB5320; Millipore Sigma, Burlington, MA); chicken anti-MBP (1:250; CH22112; Neuromics, Edina, MN); mouse anti-neurofilament (1:250; 837802; Biolegend, San Diego, CA), rabbit anti-PLP (ab183493, Abcam, Cambridge, UK). The fluorescent-conjugated secondary antibodies were donkey anti-goat (1:1000; A-32814, A-21082, A11057; ThermoFisher Scientific, Waltham, MA), donkey anti-rabbit (1:1000; A-21206, A-10042, A-31573; ThermoFisher Scientific, Waltham, MA), and donkey anti-mouse (1:1000; A-21202, A-10037, A-31571; ThermoFisher Scientific, Waltham, MA), and donkey anti-chicken (1:1000; A-11041; A-11039; A-21449, Thermo Fisher Scientific, Waltham, MA).

Microscopic imaging and image analysis

Imaging was performed using the Zeiss LSM 800 inverted confocal laser scanning microscope (Carl Zeiss, Oberkochen, Germany) with Zen software (Carl Zeiss, Oberkochen, Germany). Confocal images were obtained by Z-stacks covering the entire Z-axis range of the sections. The interval for each focal plane was 2 µm intervals. The images were then projected in the visualization plane with maximum intensity voxels (3D pixel) by maximum intensity projection using Zen software. Positively stained cells were quantified using a manual cell counter in ImageJ software (NIH). All images were minimally processed with brightness and contrast adjustment. The adjustment was applied equally across the entire image and consistent in the corresponding controls. Regions of interest were selected by a segmented line based on the anatomical features of each region. The final number of positive cells reported is averaged from 4 images.

Coordinates for imaging relative to Bregma (bilateral) were: BLA -1.06 to -2.06mm; BNST: +0.38 to +0.26mm; PVN and AH: -0.70 to -0.94mm; mPFC: +1.10mm; PVT: -0.70 to -1.58mm;

LHB and MBH: -1.06 to -1.34mm; SM: -0.46 to -1.34mm; ACA: 0.26mm; CC: 0.26mm; LS: ; MS: 0.26mm; ME: -0.82mm.

QuantSeq

Following cervical dislocation, brains were extracted and placed in iced PBS for five minutes. The brains were placed upside down into a brain matrix (SA-2175; Roboz, Gaithersburg, MD) and sliced by single edge blades (Personna, Verona, VA). Brain slices were left on the blades and placed on ice to maintain RNA integrity. Specific brain regions were isolated by gross dissection or brain punches by using 1.0 mM Biopsy Punches (Miltex, VWR, Radnor, PA) and were immediately frozen in RNAlater (Qiagen, Hilden, Germany) until RNA collection following manufacturers recommendations using the Split RNA extraction kit (Lexogen, Greenland, NH).

Coordinates for mPFC brain slices spanned from anterior to posterior (AP) +1.94 mm to +1.10 mm relative to bregma. The gross anatomy of the mPFC was based on the morphology of corpus callosum and the appearance of lateral septum. Coordinates for BNST brain slices spanned from anterior to posterior (AP) +0.62 mm to +0.14 mm relative to bregma (bilateral). The gross anatomy of the BNST was based on the features of caudate putamen, lateral ventricle, and anterior commissure. Coordinates for PVT brain slices spanned from anterior to posterior (AP) -0.94 mm to -1.58 mm relative to bregma. The gross anatomy of the PVT was based on the appearance of dorsal hippocampus. Coordinates for the hypothalamus spanned from anterior to posterior (AP) −0.58 mm to −2.92 mm relative to bregma. The gross anatomy of the hypothalamus was based on the medioventral part of the brain and covered numerous hypothalamic subregions. Coordinates for BLA brain slices spanned from anterior to posterior (AP) −1.06 mm to −2.06 mm relative to bregma (bilateral). The gross anatomy of the BLA was based on the terminal of external capsule branches nearby the piriform cortex. Coordinates for vHPC brain slices spanned from anterior to posterior (AP) −2.06 mm to −4.04 mm relative to bregma (bilateral). All coordinates and diagrams were based on the Paxinos and Franklin atlas[43].

Isolated brain tissue was immediately frozen in RNAlater (Qiagen, Hilden, Germany) until RNA collection following manufacturers recommendations using the Split RNA extraction kit (Lexogen, Greenland, NH). Quality control, library prep, and sequencing was performed by the Penn State College of Medicine's genome sciences facility as follows. The cDNA libraries were prepared using the QuantSeq 3‘mRNA-Seq Library Prep Kit FWD for Illumina (Lexogen, Greenland, NH) as per the manufacturer‘s instructions. Briefly, total RNA was reverse transcribed using oligo (dT) primers. The second cDNA strand was synthesized by random priming, in a manner that DNA polymerase is efficiently stopped when reaching the next hybridized random primer, so only the fragment closed to the 3‘ end gets captured for later indexed adapter ligation and PCR amplification. The processed libraries were assessed for its size distribution and concentration using BioAnalyzer High Sensitivity DNA Kit (Agilent Technologies, Santa Clara, CA- Cat. No. 5067-4626 and -4627). Pooled libraries were diluted to 2 nM in EB buffer (Qiagen, Hilden, Germany, Cat. No. 19086) and then denatured using the Illumina protocol. The libraries were pooled and diluted to 2 nM using 10 mM Tris-HCl, pH 8.5 and then denatured using the Illumina protocol. The denatured libraries were diluted to 10 pM by pre-chilled hybridization buffer and loaded a TruSeq SR v3 flow cell on an Illumina HiSeq 2500 and run for 50 cycles using a single-read recipe according to the manufacturer's instructions.

Single-end 50 bp reads were obtained. De-multiplexed sequencing reads were generated using Illumina bcl2fastq (version 2.18.0.12).

After the quality and polyA trimming by BBDuk (Version 37.90; http://jgi.doe.gov/data-and-tools/bb-tools/) and alignment by STAR (Version 2.5.2b)[62], read counts were calculated from BAM files using Salmon (Version 0.7.2)[63]. The Ensembl genome was used with GENCODE annotation (GRCm38, M11). Quality statistics were also gathered from genome aligned BAM files using Picard (Version 2.5.0) to use in downstream differential gene expression analysis. Genes were filtered such that only genes with a CPM (counts per million) > 0.1 in at least 10% of samples were retained. Normalized expression data was obtained through taking log2(CPM + 0.001). Then, six outliers were removed such that 114 samples were carried forward for differential gene expression analysis. Two of these outliers contained less than one million reads, and four samples were removed based on the principal components plot of the normalized expression data (these samples did not cluster with other samples from the same brain region).

A linear regression was then conducted to test for differential gene expression in four groups (4EP+PostEPM, 4EP+ Baseline, 4EP- PostEPM, 4EP- Baseline) separately within each brain region. The first five sequencing principal components (derived from the Picard sequencing statistics) were used as covariates in the linear regression to account for technical effects in the gene expression data. A one-way ANOVA test was then used to identify genes with any difference across our four test groups. This was followed by a post-hoc Tukey HSD test, which was performed on the genes with a significant p-adjusted (FDR) value less than 0.05 for the group ANOVA. Three specific comparisons were then made with the groups using the significantly differentially expressed genes from the post-hoc Tukey test ($p<0.05$): 1) 4EP differences in the PostEPM, but not in homecage, baseline condition. 2) 4EP differences at baseline, but not in the PostEPM. 3) Baseline and PostEPM differences with 4EP. To gain a functional understanding of genes in these comparisons, cell type enrichment was done with the pSI package[64] in R using cell type markers from Zhang et al.[65], and gene ontology enrichment was done with Go-Elite[66] and Metascape (metascape.org).

For visualization of the normalized gene expression data without the influence of technical factors, the effects of the five sequencing principal components were removed with a linear regression, such that only the model intercept, residual, behavior, metabolite, and regional gene expression effects remained. This ‗regressed' dataset was used to generate principal components for sample visualization. Metascape (metascape.org) was used to determine enriched gene ontology terms in brain regions with sufficient differentially regulated genes, with p-value < 0.01 and biological processes as output.

Flow Cytometry

Spleens or brain tissue dissections of the PVT, hypothalamus, cerebellum or cortex were collected. Single cell suspensions were generated by passing the tissue through a 100um cell strainer (Corning, Corning, NY) with syringe plunger and rinsed with HBSS (Corning, Corning, NY) containing 10% FBS (Gibco, Life Technologies, Thermo Fisher Scientific, Waltham, MA). Red blood cell lysis was performed (Sigma, St. Louis, MO), diluted with HBSS 10% FBS, and tissue suspension was spun at 350xg for 5 minutes at 4°C. For brain regions, papain digestion in 1ml (200U papain, 0.1mg/ml DNase I) was performed for 20 minutes at 37°C, samples were

triturated gently through a 1000ul pipette tip, and then passed through a 40uM filter. Samples were then mixed with 5-10 mls of 25% percoll in HBSS and spun at 1000xg for 25 minutes in a swinging rotor. Myelin debris layer was aspirated from the top, cell pellet was washed in HBSS 10% FBS and then resuspended in HBSS buffer containing Fc block (Anti-Mo CD16/CD32, Ebioscience, San Diego, CA; Invitrogen, Carlsbad, CA) for 20 minutes at 4°C. Further staining was done as previously described for flow cytometry. Primary stains and antibodies included: Aqua Dead cell stain (Thermo Fisher Scientific, Waltham, MA), anti-NG2 (1:400; Alexa488; Ebioscience, San Diego, CA) and anti-MOG (1:100; biotinylated, Novus Biologicals, Littleton, CO), anti-CX3Cr1 (1:500, PE-Cy7, Biolegend, San Diego, CA), anti-CD45.2 (1:500, PerCP-Cy5.5, Tonbo, San Diego, CA), anti-CD11b (1:500, PE, Biolegend San Diego, CA), anti-CD19 (1:500, FITC, Biolegend, San Diego, CA), anti-CD3e (1:500, PE, Thermofisher, Waltham, MA), anti-CD4 (1:500, APC, Biolegend, San Diego, CA), anti-TCRb (1:500, PerCP-Cy5.5, Tonbo, San Diego, CA), anti-CD8a (1:500, APC-Cy7, Thermofisher, Waltham, MA) and were incubated with cells for 30 minutes at 4°C. After washing, secondary streptavidin antibody (1:1000, SAV Alexa 647, 405237, Biolegend, San Diego, CA), was incubated with cells for 30 minutes at 4°C. After washing, cells were fixed with 2% PFA for 20 minutes, washed, and analyzed on a 4 laser (Violet, Blue, Yellow, and Red) CytoFLEX S Flow Cytometer in the Caltech Flow Cytometry Core Facility and analyzed in Flowjo v10.6.2.

MRI mouse brain scanning and Data analysis

Brain samples were collected by cardiac perfusion as described above for immunohistochemistry. Intact, defleshed skulls were collected and fixed in 4% PFA overnight, followed by incubation for 14 days at 4C in gadoteridol (Prohance®, Bracco Diagnostics Inc., Princeton NJ) and 0.01% sodium azide in PBS as previously described[67]. Samples were scanned immersed in Krytox perfluoropolymer vacuum oil (Sigma, St. Louis, MO), supported by cotton wool, in 15 ml conical tubes.

All MRI scans were performed using a Bruker Avance Neo 7T/30 scanner and a Bruker gradient and shim unit (B-GA12SHP insert for BGA20) supported by a Bruker PV360 software package. A Bruker quadrature volume coil (B-GA12s HP) and a mouse brain 2x2 receive-only four element array coil were used for ^{1}H RF pulse transmission and signal receiving, respectively, at its operating frequency of 300.33 MHz. A Bruker standard DWSE (diffusion weighted spin echo) sequence was used to collect images with b value of 4000 s/mm^2, gradient duration=5.6 ms, gradient separation=12.54 ms, repetition time TR=200 ms, echo time TE=23.34 ms, and using 60 gradient different directions. T_1 and T_2 weighted images were also collected using standard Bruker sequences (T1_FLASH_3D, T2_TurboRARE). Image resolution was fixed for all scanning at a field of view (FoV)= 14 mm and a resolution of 175 μm at each dimension. All GQI based tractographic images were acquired after data analysis that was performed using DSI Studio software package ([68]). The total surface area (TSA), dfi_FA, MD, AD, and RD of tracts were calculated using built-in functions of the DSI studio after individual ROI (i.e, PVT) was first calculated using the implemented routine under CIVM mouse atlas (Duke radiology, https://www.civm.duhs.duke.edu/). The GQI based diffusion data reconstruction was performed with a diffusion sampling length ratio of 1.2. A deterministic fiber tracking algorithm96 was used. In track calculations, a seeding region was placed at whole brain and the change threshold was set to 20% uniformly and the angular threshold was randomly selected. The tracking anisotropy threshold was varied from 0.06-0.1, depending on ROIs employed (Extended Data

Figure 7). The step size was randomly selected from 0.5 voxel to 1.5 voxels. Various Min and Max track lengths were tested, but we have not seen any significant difference among track parameter values, and data reported here are limited for tracks within 5 mm < L<10 mm range. A total of 20000 tracts were calculated.

Electron Microscopy

Mice were anesthetized using 150 ul Euthasol and perfused with 30 ml of 37°C PBS followed by 40-50 ml 37°C 4% PFA at 6ml/minute flow rate. Brains and intestinal tissue were harvested and continuously hydrated with cold (4°C) fixative solution of 3% glutaraldehyde, 1% paraformaldehyde, 5% sucrose in 0.1M sodium cacodylate trihydrate throughout the dissection process. Fixed brains were rapidly dissected out and fitted into. 1.0mm brain matrix (Roboz SA-2175, Gaithersburg, MD) where two gross cuts were made at +0.75mm and -0.25mm relative to bregma. Brain tissue anterior to +0.75mm and posterior to -0.25mm was discarded. The remaining tissue block was cut at positions ±0.5mm lateral to the midline and the flanking tissues discarded. Remaining tissue dorsal and ventral to the visible corpus callosum was excised and discarded. Fixed intestines were rapidly dissected out and cuts were made to harvest the proximal colon. The 2 mm^3 of intestinal tissue or 1 mm^3 brain tissue containing the corpus callosum were immediately stored in the cold fixative solution until proceeding to the next step.

Corpus collosum tissue was placed into petri dishes with 0.1M cacodylate buffer and cut into ~1mm^2 x 0.5 mm thick slices using a microsurgical scalpel. These were placed individually into brass high-pressure freezing planchettes (Ted Pella, Inc., Redding, CA) with cacodylate buffer containing 10% Ficoll (an extracellular cryoprotectant). Samples were ultra-rapidly frozen with an HPM-010 high pressure freezing machine and transferred to liquid nitrogen. Planchettes containing vitrified tissue were transferred under liquid nitrogen to cryotubes (Nunc, Roskilde, Denmark) prefilled with 2% OsO_4, 0.05% uranyl acetate in acetone. Samples were placed in a AFS-2 freeze-substitution machine (Leica Microsystems, Wetzlar, Germany), processed at -90°C for 72 h, warmed to -20°C over 12 h, further processed at that temperature for 24 h, then rinsed with acetone and flat-embedded in Epon-Araldite resin (Electron Microscopy Sciences, Port Washington, PA) between Teflon-coated glass slides. Resin was polymerized at 60° for 48 h.

Embedded tissue blocks were observed by phase-contrast microscopy to select well-preserved and optimally oriented regions, then extracted with a scalpel and glued to plastic sectioning stubs. Semi-thick (300-400 nm) serial sections were cut with an EM UC-6 ultramicrotome (Leica Microsystems, Wetzlar, Germany) using a diamond knife (Diatome U.S., Hatfield, PA). Sections were collected onto Formvar-coated copper/rhodium slot grids and stained with 3% uranyl acetate and lead citrate. Colloidal gold particles (10 nm) were placed on both surfaces of the grids to serve as fiducial markers for tomographic image alignment.

Tomography

Grids were placed in a dual-axis tomography holder (Model 2040, E.A. Fischione Instruments, Inc., Export, PA) and imaged with a TF-30ST transmission electron microscope (Thermo Fisher Scientific, Waltham, MA) at 300KeV. For tomography, grids were tilted +/-64° and images acquired at 1° increments. The grid was then rotated 90° and a similar tilt-series was taken about the orthogonal axis. Tilt-series were acquired automatically using the SerialEM software package[68] and recorded with a CCD camera (US1000, Gatan, Inc., Pleasanton, CA).

Tomographic datasets were processed and analyzed with the IMOD software package[69,70] on MacPro and iMacPro computers (Apple, Inc.).

Western Blots

Western blots were performed on the PVT using brain punches collected using 1.0mM Biopsy Punches (Miltex, VWR, Radnor, PA), or on *ex vivo* organotypic brain slices. Tissue samples were homogenized by bead beating in lysing matrix D tubes (MP Biomedicals, Irvine, CA) in RIPA buffer (Millipore Sigma, Burlington, MA) containing Protease Inhibitor tablets (Roche, Basel, Switzerland) followed by protein quantification and normalization using the Pierce BCA Protein Assay Kit (Thermo Fisher Scientific, Waltham, MA). Proteins were separated by SDS page using 4-20% tris-glycine Wedgewell gels (Invitrogen, Carlsbad, CA) and blotted onto 0.45um PVDF membrane (Millipore Sigma, Burlington, MA). B-actin loading controls were used, and images were taken of the same blot under specific excitation wavelengths for the various protein visualization. Antibody titrations were 1:500 for primary antibodies and 1:5,000 for fluorescent conjugated secondary antibodies. Antibodies included: mouse anti-MOG (CL2858, Thermo Fisher Scientific, Waltham, MA), chicken anti-MBP (CH22112, Neuromics, Edina, MN), rabbit anti-ß-actin (13E5, Cell Signaling, Danvers, MA), 2° anti-chicken-488 (ab150173, abcam, Cambridge, UK); 2° anti-mouse-488 (ab150113, abcam, Cambridge, UK); 2° anti-rabbit-647 (A31573, Thermo Fisher Scientific, Waltham, MA).

Organotypic brain slice culturing

Brains from P8 mice were sectioned by Vibratome into 300µm sections in HBSS with 3mM HEPES while bubbling in carbogen gas. Sections were cultured at 37°C with 5% CO_2 on 12-well transwell membrane plates in 50% DMEM/HEPES (Gibco, Gaithersburg MD) containing 25% heat inactivated horse serum (Gibco), 25% Hank‘s solution (Gibco), 2mM sodium bicarbonate (Merck, Rahway, NJ), 6.5 mg/ml glucose, 2mM glutamine, 1x pen/strep (Gibco), pH 7.2. Samples were visually observed for general signs of health (adherence, spread on membrane) and viability tested by standard lactate dehydrogenase and alamarblue assays as previously described[71]. After 10 days culture in the presence of 10uM 4EPS or vehicle (PBS), samples were taken for downstream western blot and qPCR as described above. For immunohistochemistry, samples were fixed in 4% paraformaldehyde for 3 hours at 4°C and stained for neurofilament and PLP as described above. Colocalization was quantified using IMARIS software (South Windsor, CT).

Analysis of myelination and calculation of g-ratio

Tomograms containing cross-sectional images of myelinated and unmyelinated axons were visualized in three dimensions using IMOD and analyzed using the 3dmod image processing program. Myelinated and unmyelinated axons were differentiated by eye and counted accordingly. To calculate g-ratio (ratio of axon radius to its outer, myelinated radius), the edge of the axon and the edge of the outer myelin sheath were traced using the Object tool. Traces were analyzed for area, yielding one inner and one outer area per myelinated axon. Radii were determined using the formula r_{axon}=square root of (A_{axon}/π) for the bare axon, and $r_{axon+myelin}$=square root of ($A_{axon+myelin}/\pi$) for the myelinated axon. Final g-ratios were calculated as $r_{axon}/r_{axon+myelin}$. Every axon apparent in the tomogram was included in all analyses of myelination.

Behavior Testing

Behavior testing was performed as previously described[8,51,72–76]. All mice were tested by a blinded researcher starting at six weeks of age, in the following order: EPM, light/dark box, open-field testing, marble burying, grooming, social behavior, and USV (male-female context). Separate cohorts of mice were used to test cognitive and motor function. These cohorts were tested in elevated plus maze to confirm phenotype followed by novel object recognition and Y-maze or beam traversal, pole descent, and wire hang. Mice were allowed to settle for at least two days after cage changing before they were tested, and tests were performed 2-3 days apart to allow mice to rest between tests. Mice were acclimated to the behavior testing room for one hour prior to testing. Mice were tested during the light phase of the light cycle.

Elevated Plus Maze (EPM)

EPM was performed in a maze with 25cm by 5cm arms and a 5cm by 5cm center, recorded using an overhead camera, and tracked and analyzed using the EthoVision XT 4 software package (Noldus Information Technology; Leesburg, VA, USA). Prior to testing, the maze was disinfected using Rescue disinfectant (Virox technologies, Oakville, ON, Canada) then allowed to evaporate. Mice were then introduced to the arena and allowed to explore for 5 min while being tracked. The number of entries into and the time spent in open and closed arms as well as the outer third of the open arms (the terminus) were analyzed. If a mouse fell or jumped from the apparatus during the test it was removed from the dataset.

Light/Dark Box

The light/dark box test was performed in a 50x30cm^2 arena with a 30x30 cm^2 open section and a black, lidded section sized 20x30 cm^2 with an open doorway for free passage from light to dark areas. Prior to testing, the arena was disinfected using Rescue disinfectant (Virox technologies, Oakville, ON, Canada) then allowed to evaporate. Mice were placed into the dark box and lid replaced, and then recorded using an overhead camera, and tracked and analyzed using the EthoVision XT 10 software package (Noldus Information Technology; Leesburg, VA, USA). Entry and duration in the light was analyzed over a 10-minute period.

Open-field Test

The open-field test was performed in 50 x 50 cm2 white Plexiglas arenas, recorded using an overhead camera, and tracked and analyzed using the EthoVision XT 4 software package (Noldus Information Technology; Leesburg, VA, USA). Prior to testing, the arena was disinfected using Rescue disinfectant (Virox technologies, Oakville, ON, Canada) then allowed to evaporate. Mice were then introduced to the arena and allowed to explore for 10 min while being tracked. The total distance traveled, and the number of entries and time spent in a 17 x 17 cm^2 center square were analyzed. Fecal pellets left during the assay were quantified.

Marble Burying

Marble burying was performed in a normal cage bottom (Lab Products; Seaford, DE) filled with 3-4 cm of fresh, autoclaved wood chip bedding (Aspen chip bedding, Northeastern Products Corp; Warrensburg, NY). Mice were first habituated to the cage for 10 min, and subsequently transferred to a holding cage while the bedding was leveled and 20 glass marbles (4 x 5) were placed on top. Mice were then returned to their own cage and removed after 10 min. The number of buried marbles (50% or more covered) was then recorded and photographed for reference and

scored by an additional blinded researcher. A fresh cage was used for each mouse, and marbles were soaked in Rescue disinfectant (Virox technologies, Oakville, ON, Canada) and dried in bedding in between tests.

Grooming

Mice were placed in autoclaved, empty standard cages (Lab Products; Seaford, DE) and video recorded from the side for 15 minutes. The final 10 minutes were scored manually by two independent blinded, trained researchers for grooming behavior.

Social Interaction

Each mouse was introduced to a fresh, empty, standard, autoclaved cage (Lab Products; Seaford, DE) and allowed to habituate for 10 min before a novel mouse matched in age and sex was introduced to the cage for 5 additional minutes for scoring of social activity. Two blinded, trained researchers scored videos for any social behavior using the ETHOM software[77].

Ultrasonic Vocalization

Mice were single-housed and exposed to a new SPF C57BL/6J female for 10 min every day in the five days prior to the test. On the fourth day, mice were habituated to an empty cage (no bedding) with a filter soaked with 10ul of fresh pooled female urine for 10 min. Subsequently, a novel female was introduced to the cage and ultrasonic vocalizations were recorded using Avisoft UltraSoundGate 116Hme microphone (Avisoft Bioacoustics, Nordbahn, Germany) and the Avisoft Sas-lab Recorder software (Avisoft Bioacoustics, Nordbahn, Germany). Total vocalization and vocalization counts were recorded during 3-minute sessions of male-female interaction.

Novel Object Recognition

Novel object recognition (NOR) was performed as described previously with sand filled flasks and Duplo towers[72]. Mice were habituated to the open field arenas (50 x 50cm^2 white Plexiglass) for 10 minutes on day 1. On day 2, mice were reintroduced to the arena with duplicate copies of one of two objects. On day 3, mice were reintroduced to the arena with one copy of the familiar object and one copy of a novel object. Within each group of mice, mice were split so that both objects were used as the familiar object to control for inherent interest levels in the different objects. Time spent with the nose cone directed toward the objects and within 2cm from the objects was scored the EthoVision XT 10 software package (Noldus Information Technology; Leesburg, VA). NOR index was calculated as time at novel object / total time at objects * 100.

Y-maze

Y-maze alternations test was performed in a white Y-maze (Maze Engineers, Boston, MA) video-taped from above. Entries into each arm were scored manually by a blinded researcher and the number of repetitive, spontaneous alternations were calculated.

Beam Traversal

Beam traversal was performed as previously described[73] on a 1 meter plexiglass beam (Stark's Plastics, Forest Park, OH) constructed of four segments of 0.25m in length, with each segment decreasing in widths from 3.5cm, 2.5cm, 1.5cm, and 0.5cm, with 1cm overhangs placed 1cm below the surface of the beam. The widest segment acted as a loading platform for the animals

and the narrowest end placed into home cage. Animals had two days of training to traverse the length of the beam before testing. On the first day of training, animals received 1 trial with the home cage positioned close to the loading platform and guided the animals forward along the narrowing beam. Animals received two more trials with limited or no assistance to encourage forward movement and stability on the beam. On the second day of training, animals had three trials to traverse the beam and generally did not require assistance in forward movement. On the third day, animals were timed using a stopwatch to traverse from the loading platform and to the home cage. Timing began when the animals placed their forelimbs onto the 2.5cm segment and ended when one forelimb reached the home cage.

Pole Descent

Pole descent was performed as previously described[73] with a 0.5m long pole, 1cm in diameter, wrapped with non-adhesive shelf liner to facilitate the animals grip, which was placed into the home cage. Animals received two days of training to descend from the top of the pole and into the home cage. On day one of training, animals received 3 trials. The first trial, animals were placed head-down 1/3 the distance above the floor, the second trial from 2/3 the distance, and the third trial animals were placed at the top. The second day of training, animals were given 3 trials to descend, head-down, from the top of the pole. On the test day, animals were placed head-down on the top of the pole and timed to descend back into the home cage. Timing began when the experimenter released the animal and ended when one hind-limb reached the home cage base.

Wire Hang

Wire hang was performed as previously described[73]. Animals were placed in the center of a 30 x 30 cm^2 screen with 1cm wide mesh. The screen was inverted head-over-tail and placed on supports ~40cm above an open, clean cage with bedding. Animals were timed until they released their grip or remained for 60s.

Statistical Information

All data are represented as mean ± standard error mean (SEM). Two-tailed unpaired Welch's *t*-tests were used to compare data between two independent groups (ie 4EP- vs 4EP+). Data with more than two independent groups were analyzed by one-way ANOVA with Dunnett's multiple comparison correction or Sidak multiple comparison correction, according to specific experimental design. All data was analyzed using Graphpad Prism, with a *p*-value (or adjusted *p*-value in the case of ANOVA with multiple comparison correction) of less than 0.05 was deemed statistically significant. The number of biological replicates is indicated in all figures and the statistical methods are noted in the figure legends and Methods. The number of asterisks indicates the difference in the figures, with exact *p*-values in the legends. For comprehensive statistical information regarding the autoradiography, fUSi, and QuantSeq experiments, see the corresponding detailed paragraphs above in the Methods section.

Data Availability

All data analyzed for this study is included in this published article with source data for all graphs in the supplementary information files, with additional 2DG data available at https://gin.g-node.org/bneedham/Needham_Nature_2022. The WoL database annotation files are

publicly available at: https://biocore.github.io/wol/download. Greengenes database is publicly available at: https://greengenes.secondgenome.com/.

Code Availability

Custom scripts used in fUSi analysis can be accessed at https://github.com/brittanyneedham/Needham_Nature2022.

Method References:

45. Martens, E. C., Chiang, H. C. & Gordon, J. I. Mucosal Glycan Foraging Enhances Fitness and Transmission of a Saccharolytic Human Gut Bacterial Symbiont. *Cell Host Microbe* **4**, 447–457 (2008).

46. Koropatkin, N. M., Martens, E. C., Gordon, J. I. & Smith, T. J. Starch catabolism by a prominent human gut symbiont is directed by the recognition of amylose helices. *Structure* **16**, 1105–1115 (2008).

47. Bolyen, E. *et al.* Reproducible, interactive, scalable and extensible microbiome data science using QIIME 2. *Nature Biotechnology* **37**, 852–857 (2019).

48. Callahan, B. J. *et al.* DADA2: High-resolution sample inference from Illumina amplicon data. *Nature Methods* **13**, 581–583 (2016).

49. BANOGLU, E. & KING, R. S. Sulfation of indoxyl by human and rat aryl (phenol) sulfotransferases to form indoxyl sulfate. *Eur J Drug Metab Pharmacokinet* **27**, 135–140 (2002).

50. Teubner, W., Meinl, W., Florian, S., Kretzschmar, M. & Glatt, H. Identification and localization of soluble sulfotransferases in the human gastrointestinal tract. *Biochem J* **404**, 207–215 (2007).

51. Sharon, G. *et al.* Human Gut Microbiota from Autism Spectrum Disorder Promote Behavioral Symptoms in Mice. *Cell* **177**, 1600-1618.e17 (2019).

52. Iadecola, C. The Neurovascular Unit Coming of Age: A Journey through Neurovascular Coupling in Health and Disease. *Neuron* **96**, 17–42 (2017).

53. Mace, E. *et al.* Functional ultrasound imaging of the brain: theory and basic principles. *IEEE Transactions on Ultrasonics, Ferroelectrics, and Frequency Control* **60**, 492–506 (2013).

54. Tiran, E. *et al.* Transcranial Functional Ultrasound Imaging in Freely Moving Awake Mice and Anesthetized Young Rats without Contrast Agent. *Ultrasound in Medicine & Biology* **43**, 1679–1689 (2017).

55. github.com/*brittanyneedham/Needham_Nature2022*.

56. Demené, C. *et al.* Spatiotemporal Clutter Filtering of Ultrafast Ultrasound Data Highly Increases Doppler and fUltrasound Sensitivity. *IEEE Transactions on Medical Imaging* **34**, 2271–2285 (2015).

57. Osmanski, B.-F., Pezet, S., Ricobaraza, A., Lenkei, Z. & Tanter, M. Functional ultrasound imaging of intrinsic connectivity in the living rat brain with high spatiotemporal resolution. *Nat Commun* **5**, 1–14 (2014).

58. Armstrong, R. A. When to use the Bonferroni correction. *Ophthalmic Physiol Opt* **34**, 502–508 (2014).

59. Holschneider, D. P., Guo, Y., Wang, Z., Vidal, M. & Scremin, O. U. Positive Allosteric Modulation of Cholinergic Receptors Improves Spatial Learning after Cortical Contusion Injury in Mice. *J. Neurotrauma* **36**, 2233–2245 (2019).

60. Sokoloff, L. Localization of functional activity in the central nervous system by measurement of glucose utilization with radioactive deoxyglucose. *J. Cereb. Blood Flow Metab.* **1**, 7–36 (1981).

61. Wang, Z., Pang, R. D., Hernandez, M., Ocampo, M. A. & Holschneider, D. P. Anxiolytic-like effect of pregabalin on unconditioned fear in the rat: an autoradiographic brain perfusion mapping and functional connectivity study. *Neuroimage* **59**, 4168–4188 (2012).

62. STAR: ultrafast universal RNA-seq aligner | Bioinformatics | Oxford Academic. https://academic.oup.com/bioinformatics/article/29/1/15/272537.

63. Salmon provides fast and bias-aware quantification of transcript expression | Nature Methods. https://www.nature.com/articles/nmeth.4197.

64. Xu, X., Wells, A. B., O'Brien, D. R., Nehorai, A. & Dougherty, J. D. Cell Type-Specific Expression Analysis to Identify Putative Cellular Mechanisms for Neurogenetic Disorders. *J. Neurosci.* **34**, 1420–1431 (2014).

65. Zhang, Y. *et al.* An RNA-sequencing transcriptome and splicing database of glia, neurons, and vascular cells of the cerebral cortex. *J Neurosci* **34**, 11929–11947 (2014).

66. Zambon, A. C. *et al.* GO-Elite: a flexible solution for pathway and ontology over-representation. *Bioinformatics* **28**, 2209–2210 (2012).

67. Tyszka, J. M., Readhead, C., Bearer, E. L., Pautler, R. G. & Jacobs, R. E. Statistical diffusion tensor histology reveals regional dysmyelination effects in the shiverer mouse mutant. *Neuroimage* **29**, 1058–1065 (2006).

68. Mastronarde, D. N. Automated electron microscope tomography using robust prediction of specimen movements. *J. Struct. Biol.* **152**, 36–51 (2005).

69. Kremer, J. R., Mastronarde, D. N. & McIntosh, J. R. Computer visualization of three-dimensional image data using IMOD. *J. Struct. Biol.* **116**, 71–76 (1996).

70. Mastronarde, D. N. Correction for non-perpendicularity of beam and tilt axis in tomographic reconstructions with the IMOD package. *J Microsc* **230**, 212–217 (2008).

71. Carranza-Torres, I. E. *et al.* Organotypic Culture of Breast Tumor Explants as a Multicellular System for the Screening of Natural Compounds with Antineoplastic Potential. *Biomed Res Int* **2015**, (2015).

72. Leger, M. *et al.* Object recognition test in mice. *Nature Protocols* **8**, 2531–2537 (2013).

73. Sampson, T. R. *et al.* Gut Microbiota Regulate Motor Deficits and Neuroinflammation in a Model of Parkinson's Disease. *Cell* **167**, 1469-1480.e12 (2016).

74. Komada, M., Takao, K. & Miyakawa, T. Elevated Plus Maze for Mice. *J Vis Exp* (2008) doi:10.3791/1088.

75. Takao, K. & Miyakawa, T. Light/dark Transition Test for Mice. *J Vis Exp* (2006) doi:10.3791/104.

76. Miedel, C. J., Patton, J. M., Miedel, A. N., Miedel, E. S. & Levenson, J. M. Assessment of Spontaneous Alternation, Novel Object Recognition and Limb Clasping in Transgenic Mouse Models of Amyloid-β and Tau Neuropathology. *J Vis Exp* (2017) doi:10.3791/55523.

77. Shih, H.-T. & Mok, H.-K. ETHOM: Event-Recording Computer Software for the Study of Animal Behavior. in (2000). doi:10.6576/AZT.2000.11.(1).4.

Acknowledgements: We thank members of the Mazmanian laboratory for critical evaluation of the manuscript, Sarah Reisman and Lauren Chapman (Caltech) for synthesizing 4EPS, the Caltech Kavli Nanoscience Institute for aid in maintaining the TF30 electron microscope, and the Gordon and Betty Moore and Beckman Foundations for gifts to Caltech to support electron microscopy. **Funding:** This work was supported by funds from the Center for Environmental Microbial Interactions to B.D.N., National Science Foundation MRI grant 1920364 for Bruker console upgrading, the Human Frontier Science Program (Grant No. LT000217/2020-C) to C.R., the National Institutes of Health (NIH) (2 P50 GM082545-08) to P.J.B., the Ministry of Science and Technology in Taiwan (MOST107- 2320-B-006-072-MY3; MOST108-2321-B-006-025-MY2) to W-L.W, and the Heritage Medical Research Institute, Lynda and Blaine Fetter, and the NIH (MH100556 and AG063744) to S.K.M.

Author contributions: Conceptualization: BDN, SKM. Methodology: BDN, MF, MDA, ZW, W-LW, JH, MSL, JAG, CR, SJH, DPH. Formal Analysis: BDN, MDA, ZW, JH. Investigation: BDN, MF, MDA, ZW, W-LW, JCB, CR, JH, SJH, QZ, MSL, YG. Biochemical pathway investigation and strain engineering: MF, MAF. Gene abundance analysis: QZ, JCB, RK. fUSi imaging: CR, JCB, BDN, MGS. 2DG analysis: ZW, BDN, YG, DPH. QuantSeq analysis: JH, W-LW, BDN, DHG. Oligodendrocyte characterization: BDN, MDA, JCB, MSL, JAG. ET: MSL, BDN, MDA. MRI/DTI: SJH, BDN. Animal behavior: BDN, MDA. Resources: PJB, DG, DPH, MAF, RK, MGS, SKM. Writing original draft: BDN. Writing Review and Editing: BDN, MF, MDA, ZW, W-LW, JH, MSL, JAG, DPH, MAF, SKM. Visualization: BDN, MF, MDA, ZW, W-LW, JH, JCB, CR, SJH, MSL, MAF. Supervision: SKM. Project administration: BDN. Funding acquisition: BDN, WLW, PJB, SKM.

Competing interests: S.K.M. has financial interests in Axial Biotherapeutics. All other authors declare no competing interests related to this work.

Additional Information:

Correspondence and requests for materials should be addressed to Sarkis Mazmanian, sarkis@caltech.edu.

Extended Data Figure Legends:

Extended Data Fig. 1 Strain engineering and 4EPS quantification.
a, Strain legend corresponding to Figure 1b-d, containing further details for strain names and cloning strategy. Additional information can be found in Methods and Supplementary Information Tables 1-3. **b-e,** Maps for integration vectors. **b**, The BO1194 gene was cloned into the pNBU2 vector with an erythromycin resistant marker under the phage promoter. **c**, The PAD gene was cloned into pNBU2 vector with an erythromycin resistant marker under the phage promoter. **d**, The PAD gene was cloned into the pNBU2 vector with a tetracycline resistant marker under the phage promoter. **e**, BO1194 and PAD were tandemly connected, putting the phage promoter in front of both genes, then icloned into the pNBU2 vector with the erythromycin resistant marker. **f**, Creatinine corrected urinary levels of 4EPS from SPF, GF, gnotobiotic mice colonized with strains as labeled, and a mouse model of atypical behavior including anxiety-like phenotypes. This data corresponds to abbreviated data in Fig. 1f. SPF, specific pathogen free mice; GF, germ-free mice; BO, *Bacteroides ovatus* mono-colonized mice; 4EP-, GF mice colonized with non-producing strain pair (*B. ovatus* Δ1194 and WT *L. plantarum* with endogenous VPR) used throughout; WT, GF mice colonized with wild type strain pair (WT *B. ovatus* and WT *L. plantarum* with endogenous VPR) before optimal engineering; 4EP+, colonized with strain pair engineered for higher production of 4EP+ (*B. ovatus*+1194/PAD and WT *L. plantarum* with endogenous VPR), used throughout; CNTNAP2, conventionally colonized mouse model of atypical behavior (left to right columns: n=15, 5, 5, 9, 7, 9, 11). **g**, 4EPS levels (creatinine corrected) in urine of wild type, specific pathogen free (SPF) mice fed one of two isocaloric diets matched for protein, mineral, carbohydrate, and fat levels but differing in either high tyrosine fish meal (fish diet), or a high plant protein (soy diet) (n=8 each group)p=0.002. **h,** 4EPS levels (creatinine corrected) in urine of gnotobiotic mice colonized with isogenic strain pairs of *B. ovatus* and wild type *L. plantarum*, which differ only in the presence or absence of gene 1194, and thus the tyrosine lyase activity requires to convert tyrosine to p-coumaric acid (n=2 each group). **i,** Alignments of genes used to engineer the 4EP synthesis pathway to the reference genomes in the WoL database, showing that these genes are found in ~25 genomes each, most of which are common human gut lineages. **j**, 4EP and 4EPS levels (ug/ml) in serum of colonized mice (n=7 each group). **k**, 4EP+ and 4EP- colonized mice were injected with the organic anion transporter to inhibit potential 4EPS transport out of the brain, then analyzed by LCMS (n=6 each group). Extended data from Figure 1G. **l**, Conventionally colonized (SPF) mice were injected with probenecid and then injected with high dose 4EPS (n=8) or saline vehicle (n=8), and whole brain lysate was analyzed by LCMS compared to 4EPS injection alone (n=4)p<0.0001. **m**, Conventionally colonized (SPF) mice were injected with probenecid and then gavaged with 4EP, then whole brains were harvested at 30-minute intervals and 4EPS levels were quantified by LCMS (n=4; vehicle group n=3)p=0.01. Two independent trials on biological replicates were used for the experiments in the figure. Abbreviations: SPF, specific pathogen-free; GF, germ-free; BO, *Bacteroides ovatus*; WT, wild type; LP, *Lactobacillus* plantarum. Data represent mean ± SEM analyzed by a two-tailed Welch's t-test or one-way ANOVA with Dunnett multiple comparisons test as appropriate. * $p \leq 0.05$; ** $p \leq 0.01$; *** $p \leq 0.001$; **** $p \leq 0.0001$.

Extended Data Fig. 2 4EP sulfation, experimental timeline, normal weight gain, colonization and intestinal barrier of 4EP+ mice.

a, *In vitro* recombinant SULT1A1 sulfotransferase assay with 4EP as potential sulfate acceptor (n=5)$p<0.0001$. **b**, Results of the sulfotransferase assay using various recombinant SULTs (n=3)$p<0.0001$. **c**, 4EP sulfation capacity of cytosolic fractions of brain, colon, liver, and small intestinal tissue, each containing endogenous sulfotransferases (n=2 datapoints of samples pooled from triplicate biological replicates, with only 1 pool for SI). Ion intensity of 4EPS measured by LCMS is plotted along the y-axis. **d**, Confirmation of expression of the *Sult1a1* gene measured by qPCR in tissue from the brain, colon, liver, and small intestine of colonized mice (n=8; brain n=6)$p<0.0001$. **e**, Schematic of mouse experimental timeline, showing ages of mice at colonization of GF mice with 4EP+/- strains, behavior testing and tissue collection. **f,** Weights of mice (grams) after colonization of GF mice with 4EP- or 4EP+ bacteria (n=13). **g**, Ambulatory activity of 4EP- and 4EP+ mice over ten minutes, measured by distance moved when mice were placed in an open arena and allowed to explore (4EP- n=21; 4EP+ n=24). **h**, FITC-dextran levels in serum as a measure of intestinal permeability (4EP- n=5, 4EP+ n=6). **i**, Fecal output of colonized mice over 10 minutes (n=13). **j**, Images of hematoxylin and eosin (H&E) stained small intestine and colon of 4EP+/- mice (representative images of n=4). Scale bar 50μm. **k**, Colonization of ex-GF mice with engineered *Bacteroides ovatus* (BO) and *Lactobacillus plantarum* (LP), plotted as colony forming units (CFU) per gram of intestinal contents (n=4). **l**, Quantification of bacterial distance from the intestinal epithelium imaged by electron tomography, where each data point represents a separate animal comprised of an average of 5-10 bacterial cells per image per mouse (4EP- n=4; 4EP+ n=5). **m,** Example images of bacterial cells near the intestinal epithelial layer of 4EP+/- mice. Two independent trials using multiple randomized litters were used for the experiments in the figure. Abbreviations: SULT, sulfotransferase; SI, small intestine. Data represent mean ± SEM. Panel f was analyzed by a 2-way ANOVA with a Bonferroni multiple comparison correction. Panels g-i and l were analyzed using two-tailed Welch's t-tests and panels a-d, k by a one-way ANOVA with Dunnett multiple comparisons test.

Extended Data Fig. 3 Lack of inflammatory signals in peripheral and brain cytokine and immune profiles of 4EP+/- mice.

a-b, Cytokine and chemokine levels presented in bar graph where grey (-) is 4EP- and green (+) is 4EP+, measured by bioplex in colon (n=9) **a**, and serum (n=9) **b**. No significant differences were observed. **c-d,** Flow cytometry of spleens of 4EP+ and 4EP- mice. For gating strategy see Supplementary Information Figure 2. **c**, Percentages of CD4+ or CD8+ T cells (4EP- n=11, 4EP+ n=10). **d,** Percentage of B cells (4EP- n=11, 4EP+ n=10)$p<0.0001$. **e**, Cytokine and chemokine levels presented in bar graph where grey (-) is 4EP- and green (+) is 4EP+, measured by bioplex (n=9) in brain tissue (Il-3 $p=0.046$; Il-5 $p=0.01$; KC $p=0.02$; TNF-a $p=0.01$). **f,** Flow cytometry percentages of microglia in the brain of 4EP- and 4EP+ mice. For gating strategy see Supplementary Information Figure 2. **g,** Relative expression of microglial genes in microglial-enriched samples (n=8). Multiple randomized litters were used for the experiments in the figure. Each data point represents biologically independent mice from multiple randomized litters examined over one (a-b) or two (c-h) respective experiments. Data represent mean ± SEM. Panels a, b, d, f, and h were analyzed by one-way ANOVA with Dunnett multiple comparisons test comparing each 4EP+/4EP- pair, and panels g and e by a two-tailed Welch's t-test. * $p \leq 0.05$; ** $p \leq 0.01$; *** $p \leq 0.001$.

Extended Data Fig. 4 Extended information on functional connectivity experiments fUSi and autoradiography.

a, Schematic representation of the functional ultrasound (fUSi) set-up. Functional acquisitions are acquired non-invasively through intact skull and scalp in anesthetized mice during 15 minutes per coronal plane. **b,** Maps overlaid with regions of interest colored in a gradient for easier visualization. Significant pairs are indicated, corresponding to the data in main Fig. 2b. Three coronal planes per mouse were studied: Bregma -0.9 mm, Bregma -1.6 mm, Bregma -2mm. 50, 52 and 52 ROIS are respectively delineated for each plane according the Paxinos Atlas. Coronal plane B-0.9mm: ROIs #1 to #8 are located in the left cortex, ROI#9 is the left hippocampus, ROIs#11 to #21 are located in the thalamus, ROI#22 is the right hippocampus, ROIs#23 to #30 are located in the right cortex and finally ROIs#31 to #48 are subthalamic regions. Coronal plane B-1.6mm: ROIs #1 to #20 are located in the cortex, ROIs#21 #22 are the left and right hippocampi, ROIs#23 to #38 are located in the thalamus and ROIs#39 to #42 are subthalamic regions. Coronal plane B-2mm: ROIs #1 to #9 are located in the left cortex, ROI#10 is the left hippocampus, ROIs#11 to #22 are located in the thalamus, ROI#23 is the right hippocampus, ROIs#24 to #32 are located in the right cortex and finally ROIs#33 to #50 are subthalamic regions. **c-d,** Color-coded overlays over representative coronal (c) and sagittal (d) sections of the mouse brain template showing significant differences in regional cerebral glucose uptake following open field exposure in 4EP+ mice compared to 4EP- mice (n=11) (t-test, $p \leq 0.05$, extent threshold > 200 contiguous voxels, with both conditions met to be deemed significant; red/blue: increase/decrease in glucose uptake in 4EP+ compared to 4EP- mice). **e,** Quantitated 2DG-uptake by region of interest, including the amygdala, hypothalamus and PVT, confirming changes in relative 2DG uptake in the open field groups (n=11 each group) From left to right, p=0.01; 0.03; 0.02; 0.009; 0.003). Average optical density of each ROI in each animal was normalized to whole-brain average of that animal. Abbreviations: AM, amygdala; HY, hypothalamus; PVT, paraventricular nucleus of the thalamus; BNST, bed nucleus of the stria terminalis; S1, primary somatosensory cortex; CPu, caudate putamen; Hb, habenular nucleus; RT, reticular nucleus of the thalamus; VPL/VPM, Posterior Lateral/Ventral Posterior Medial Thalamus; R, right; L, left. Two cohorts of mice from multiple litters were used for each experiment in this figure. Panel e was analyzed by one-way ANOVA with multiple comparison correction and two-stage linear step-up procedure of Benjamini, Krieger and Yekutieli. * $p \leq 0.05$.

Extended Data Fig. 5 Extended results of mRNA high throughput sequencing (QuantSeq), and oligodendrocyte analysis by immunofluorescence implicating oligodendrocyte differences in 4EP+ mice.

a, Principal component analysis of all samples analyzed by QuantSeq, with tight clustering by brain region. Each brain region is colored according to the legend. **b**, Differential gene analysis summary showing number of significantly different genes in 6 tested brain regions. Top pie chart refers to total number of differential genes by one-way group ANOVA with all the 4EP- and 4EP+, at baseline and post-EPM. The bottom pie chart was generated according to the specific significant ($p<0.05$) contrasts between 4EP+ and 4EP- conditions of post-EPM conditions as calculated with the post-hoc Tukey HSD test. **c-d**, Gene ontology terms enriched in genes that are upregulated (c) or downregulated (d) in the PVT in 4EP+ relative to 4EP- mice in the baseline, home cage condition. X-axis represents -log10(P) of enrichment analysis. **e**, p-value

histogram of PVT sequencing at baseline, graphed as p-values binned by 0.05 along the x-axis and number of genes along the y-axis. **f**, Adjusted *p*-values for 4EP+/4EP- comparison of expression of oligodendrocyte specific genes in all 6 brain regions analyzed by QuantSeq, corresponding to data presented in Main Figure 3c for the PVT. $p<0.05$ in bold. **g,** PVT seed analysis correlating 2DG uptake in the PVT to the rest of the brain. Images show 3D rendered, average whole brain correlation data (n=11). The center of the PVT is indicated at the cross section of the red lines, and the number of negatively correlated voxels is shown below in each. Significance is illustrated according to the legend. A minimum threshold of 200 contiguous voxels with $p<0.05$ was used. **h,** Schematic of immature OPC and mature, myelinating oligodendrocyte markers used for immunostaining, flow cytometry, or western blots in this study. **i,** Raw counts of mature oligodendrocytes, measured by CC1+ and OLIG2+ staining in 4EP+ and 4EP- mice in the PVT, used to calculate maturity quotient in Figure 3f (n=8). $p=0.04$. **j,** Raw counts of immature oligodendrocytes, measured by NG2+ and OLIG2+ staining in 4EP+ and 4EP- mice in the PVT, used to calculate maturity quotient in Figure 3f (n=8 each group). $p=0.055$. **k,** Representative images (corresponding to main Fig. 3e-f) of the PVT in brain sections from 4EP- and 4EP+ mice, stained for OLIG2, using total cumulative counts from 3-5 images per replicate (n=8). Scale bar 100µm. **l**, Raw counts of OLIG2+ cells in the PVT of 4EP+/- mice. Each data point represents an individual mouse, with total cumulative counts from the PVT (n=8) $p=0.8$. **m**, Raw counts of NeuN+ staining in the PVT (4EP- n=10, 4EP+ n=9), using average counts from 3-5 images per replicate. **n,** Representative images of pan-neuronal NeuN staining in the PVT, with 3-5 images per replicate (4EP- n=10, 4EP+ n=9). Scale bar 100µm. **o,** NG2+ staining in extended regions of the brain (n=3 each group) $p=0.009$. Abbreviations: PVT, the paraventricular nucleus of the thalamus; BNST, bed nucleus of the stria terminalis; BLA, basolateral amygdala; mPFC, medial prefrontal cortex; HY, hypothalamus; vHPC, ventral hippocampus; OLIG2, oligodendrocyte transcription factor 2; NG2, neural/glial antigen 2; CC1, antibody (anti-adenomatous polyposis coli (APC) clone) that binds mature oligodendrocyte marker; MOG, myelin oligodendrocyte glycoprotein; MBP, myelin basic protein; ACA, anterior commissure; CC, corpus callosum; LHB, lateral habenula; LS, lateral septum; MHB, medial habenula; MS, medial septum; ME, median eminence; PFC, prefrontal cortex; PVN, paraventricular nucleus of the hypothalamus; SM, stria medullaris of thalamus. Two cohorts of mice from multiple litters were used for experiments in panels g-o in this figure. Data represent mean ± SEM. Analysis performed using two-tailed Welch's t-tests (i-m) or one-way ANOVA with Dunnett multiple comparison between 4EP+/- pairs (o). * $p \leq 0.05$.

Extended Data Fig. 6 Extended results of oligodendrocyte analysis implicating oligodendrocyte differences in 4EP+ mice *in vivo and in vitro*.
a, Extended quantitation of flow cytometry with MOG+/NG2+ ratio by quadrant in the cerebellum, cortex, and hypothalamus (n=4). **b-c**, Western blot analysis of MOG ($p=0.03$) and MBP ($p=0.002$) markers (respectively) of mature oligodendrocytes from the PVT brain region. PVT punches from two mice were pooled per data point in quantitative data (n=6 pooled samples each group). For gel source data, see Supplementary Information Figure 1. **d-g,** Organotypic brain slices were cultured in the presence of 10uM 4EPS. **d,** Representative images of CC1, NG2 and Olig2 staining. Two cohorts of mice were used, with each data point in Fig 3i representing quantified images from samples from individual mice. Scale bar 20µm. **e,** Example high-magnification image of axon in organotypic brain slices, stained with antibodies specific to NF (red), and PLP (green), with DAPI (blue), taken from image set used for quantification in 3i and

Extended Data Fig 6d. Scale bar 8µm. **f,** qPCR results of oligodendrocyte genes, *Cspg4* (p=0.04)*, Mog* (p=0.03)*, and Mpb* from organotypic brain slices (n=7). **g,** Western blot image of mature oligodendrocyte marker MBP (quantified in main Fig. 3l). For gel source data, see Supplementary Figure 1. Abbreviations: NG2, neural/glial antigen 2; CC1, antibody (anti-adenomatous polyposis coli (APC) clone) that binds mature oligodendrocyte marker; MOG, myelin oligodendrocyte glycoprotein; MBP, myelin basic protein. Two cohorts of mice from multiple litters were used for experiments in this figure. Data represent mean ± SEM. Statistics were performed using two-tailed Welch's t-tests. * $p \leq 0.05$; ** $p \leq 0.01$.

Extended Data Fig. 7 Extended results of myelin analysis by electron microscopy and DTI. **a**, Additional ET of myelinated axons in 4EP- (top) and 4EP+ (bottom) mice visualized longitudinally along an axon (n=3; 4 images each). These longitudinal images were used only for qualitative visual assessment of myelin to accompany the other quantitative measures. **b**, Axon diameters (measured from cell membrane, not including myelin layer) from all axons used to calculate g-ratio (4EP-, 56; 4EP+, 70 axons) (n=4; 4 images each). p=0.1. **c**, g-ratio (r/R), the inner axon diameter/outer diameter of the myelin sheath, of 4EP+ and 4EP- mice. Each data point represents a mouse (n=4), which is an average of the g-ratio of all axons quantified from 4 images per mouse, where a larger g-ratio indicates a thinner layer of myelin. p=0.046. **d**, Plot of g-ratio (r/R) on the y-axis and axon diameter on the x-axis, with linear regression noted by lines (4EP-, 56; 4EP+, 70 axons) (n=4; 4 images each). **e**, Average g-ratio of each animal, binned by axon size, indicating that mid-sized range of axons are driving the change in overall g-ratio phenotype observed in the mice (n=4). **f-g,** Defined regions of interest for the PVT and corpus callosum (CC) overlaid on representative sagittal MRI image. **h-i,** representative tracts observed from a bilateral coronal plane view (left) and fractional anisotropy (FA) analysis (right) for the corpus callosum (CC), and whole brain (p=0.009), respectively (n=4). Two independent trials using multiple litters were used for experiments in this figure. Data represent mean ± SEM. Statistics were performed using two-tailed Welch's t-tests (b,c,h,i), simple linear regression test (d), or one-way ANOVA with Dunnett multiple comparison between 4EP+/- groups at each size group. * $p \leq 0.05$; ** $p \leq 0.01$.

Extended Data Fig. 8 Additional behavior tests in 4EP- and 4EP+ mice. **a**, Distance traveled (p=0.06), time in center (p=0.01), and thigmotaxis time (p=0.007), during open field test over a period of 10 minutes (distance traveled data was also shown in Extended Data Fig. 2g) (4EP- n=21, 4EP+ n=24). **b,** Time spent in the open arms of the elevated plus maze (EPM) (left)(p=0.02) and ratio of time spent in the open/time spent in the closed arms of the EPM (right) (4EP- n=21, 4EP+ n=24). **c**, Light/dark box: time mice spent in the open, lit portion of the arena. Test time, 10 minutes (4EP- n=25, 4EP+ n=23) p=0.02. **d**, Grooming: total time mice spent self-grooming over a period of 10 minutes (4EP- n=27, 4EP+ n=24). **e**, Social interaction: with an unfamiliar, age-matched male intruder. Total time socializing (left) and percent of total socializing that is anogenital sniffing (right) (4EP- n=25, 4EP+ n=22) p=0.0009. **f**, Ultrasonic vocalization: time spent vocalizing to an unfamiliar, age-matched female for 3 minutes (4EP- n=23, 4EP+ n=21) p=0.01. **g**, Novel object recognition (NOR): time spent investigating a novel object when presented with a novel and a familiar object (n=22). **h**, Y-maze alternations: percent of times mice repeated entry into an arm it had just visited rather than alternate to all arms in succession (4EP- n=15, 4EP+ n=16). **i**, Beam traversal: time required for the mouse to cross the narrowing beam (4EP- n=19, 4EP+ n=22). **j**, Pole descent: time required

for the mouse to descend from the pole to the home cage (4EP- n=19, 4EP+ n=22). **k**, Wire hang: time the mouse hung on and explored the underside of the wire grid before releasing into cage below (4EP- n=19, 4EP+ n=22). **l,** Fecal 16s profiles of 4EP+/- mice after behavior tests, where tan is the colonization group and contamination from exposure to behavior tests is colored according to the legend (left panel) and a magnified view of contaminants only (right panel) (4EP- n=8, 4EP+ n=10). Two independent cohorts of mice from multiple litters were used for each experiment in this figure. Data a-k represent mean ± SEM analyzed by two-tailed Welch's t-test. * $p \leq 0.05$; ** $p \leq 0.01$.

Extended Data Fig. 9 Behavior results from 4EP or 4EPS administration by drinking water and anxiety behavior tests of 4EP+/- mice relative to GF and SPF mice.
a-f, Behavior tests of conventionally colonized mice administered 4EP or 4EPS by drinking water. **a**, Left panel: EPM, time spent in open arms over time spent in closed arms (seconds). Right panel: time spent at terminus (outer 1/3 of open arms)(Veh. n=15; 4EPS n=17; 4EP n=16) (Open/closed: Veh. vs 4EPS $p<0.0001$; Veh vs 4EP $p=0.007$; 4EPS vs 4EP $p=0.03$; Terminus: Veh vs 4EPS $p=0.004$). **b**, Open field test, from left to right: time spent in center area over thigmotaxis, time spent in center (seconds), distance moved in open field test, showing an increase in activity in 4EP-treated animals (Veh. n=16; 4EPS n=16; 4EP n=18) p=02. **c**, Grooming test, total percent of time spent grooming, showing an increase in grooming in the 4EPS-treated animals (Veh. n=16; 4EPS n=18; 4EP n=17). **d**, Number of marbles buried (Veh. n=16; 4EPS n=17; 4EP n=18). **e**, Social interaction. Left panel: total socialization time (seconds). Right panel: % of total socialization time spent as anogenital sniffing (Veh. n=8; 4EPS n=7; 4EP n=7). **f**, USV test. Left panel: Vocalization events. Right panel: Total duration spent vocalizing (seconds) (Veh. n=16; 4EPS n=15; 4EP n=18). **g**, 4EPS levels in urine of mice administered 4EP or 4EPS in the drinking water (creatinine corrected)(Veh. n=12; 4EPS n=9; 4EP n=11)(Veh. vs 4EPS p=0.0005; Veh vs 4EP p=0.008; 4EPS vs 4EP p=0.03). **h,** 4EPS levels in serum of mice administered 4EP or 4EPS in the drinking water (Veh. n=4; 4EPS n=4; 4EP n=3). **i,** Quantified flow cytometry data of PVT of mice administered 4EP or 4EPS in the drinking water, with ratio of MOG+ quartile percentages/NG2+ quartile percentages presented (Veh. n=5; 4EPS n=5; 4EP n=4) p=0.03. For gating strategy see Supplementary Information Figure 2 and main Fig. 3h. **j**, Quantified western blot data for MOG and MBP in the PVT of mice administered 4EP or 4EPS in the drinking water, with blots shown below (n=4 each group). (MBP: H2O vs 4EPS p=0.04; vs 4EP p=0.02). For gel source data, see Supplementary Figure 1. **k-m,** Anxiety behavior tests contextualizing 4EP+/- mice to GF and SPF mice. **k,** Open field test, from left to right: time spent in center area over time spent along walls (4EP- vs 4EP+ p=0.04; 4EP+ vs GF p=0.02; 4EP+ vs SPF p=0.04), time spent in center (seconds), distance moved in open field test(4EP+ vs SPF p=0.047; GF vs SPF p-0.01) (4EP- n=8; 4EP+ n=9; GF n=9; SPF n=11). **l,** Elevated plus maze, time spent in the open arms/time spent in the closed arms ration (left)(4EP- vs 4EP+ p=0.03; 4EP+ vs SPF p=0.03) and time spent at the terminus (right) (4EP- n=9; 4EP+ n=9; GF n=11; SPF n=13). **m,** Marble burying (4EP- n=9; 4EP+ n=9; GF n=9; SPF n=112)(4EP- vs 4EP+ p=0.02; 4EP- vs SPF p=0.03; 4EP+ vs GF p=0.02; GF vs SPF p=0.03). Abbreviations: Veh., vehicle control; MOG, myelin oligodendrocyte glycoprotein; MBP, myelin basic protein. Two independent cohorts of mice from multiple litters were used for the experiments in this figure. Data represent mean ± SEM analyzed by one-way ANOVA with Dunnett multiple comparison between all groups. * $p \leq 0.05$; ** $p \leq 0.01$; *** $p \leq 0.001$; **** $p \leq 0.0001$.

Extended Data Fig. 10 Fluorescence imaging and extended behavior test results of clemastine fumarate and miconazole-treated mice, and preliminary behavior tests performed on both sexes, used to determine continued studies on males for the study. **a-i,** 4EP+/- mice were administered vehicle (control), clemastine fumarate (clem.), or miconazole and then behavior tested and imaged.. **a,** Representative images of CC1 (green), NG2 (red), and OLIG2 (blue) staining in 4EP+/- mice with or without treatment. Representative of group of individual mice used for quantification: 4EP- control=7, treated=10; 4EP+ control=6, treated=6, which came from two cohorts (Scale bar 100μm). **b,** Quantification of fluorescent imaging, presented as a ratio of CC1+/NG2+ cells (from left to right n=7, 10, 6, 6, 4, 4). The first four columns are also shown in Main Fig. 4i (Cont 4EP-vs 4EP+ p=0.04; 4EP+Cont vs 4EP+Clem p=0.01). **c-d,** Confirmation that treatment does not reduce 4EPS levels with clemastine (c) (Control. 4EP- n=4; Control. 4EP+ n=6, Clem 4EP- n=3; Clem 4EP+ n=4) or miconazole (d) (Control. 4EP- n=4; Control. 4EP+ n=4, Mic 4EP- n=4; Mic 4EP+ n=5) treatment. **e,** Extended EPM results (Control 4EP- n=13; Control 4EP+ n=13; Clem 4EP- n=12; Clem 4EP+ n=14). **f,** Extended open field results (Control 4EP- n=15; Control 4EP+ n=17; Clem 4EP- n=17; Clem 4EP+ n=17). **g-i,** Behavioral results for mice treated with miconazole, including **g,** Open field (Control 4EP- n=24; Control 4EP+ n=25; Mic. 4EP- n=18; Mic. 4EP+ n=20)(left graph: 4EP-Cont vs 4EP+ Cont p=0.02; 4EP+cont vs 4EP+Mic p=0.008)(middle graph: 4EP-Cont vs 4EP+ Cont p=0.02; 4EP+cont vs 4EP+Mic p=0.005). **h,** EPM (Control 4EP- n=24; Control 4EP+ n=25; Mic. 4EP- n=15; Mic. 4EP+ n=17)(left graph: 4EP-Cont vs 4EP+ Cont p=0.002; 4EP+cont vs 4EP+Mic p=0.03)(right graph: 4EP-Cont vs 4EP+Cont p=0.0009). **i,** Marble Burying (Control 4EP- n=24; Control 4EP+ n=26; Mic. 4EP- n=21; Mic. 4EP+ n=21)(p=0.001) **j**, Left panel: EPM, time spent in open arms over time spent in closed arms. Right panel: time spent at terminus (outer 1/3 of open arms) (Males 4EP- n=17; Males 4EP+ n=17; Females 4EP- n=20; Females 4EP+ n=21)p=0.02. **k,** Open field test, time spent in center area over time spent in thigmotaxis left), time spent in center (right) (Males 4EP- n=16; Males 4EP+ n=14; Females 4EP- n=18; Females 4EP+ n=13)p-values left to right: 0.005, 0.003. **l,** Number of marbles buried in marble burying test (Males 4EP- n=24; Males 4EP+ n=23; Females 4EP- n=17; Females 4EP+ n=26)p=0.03. Abbreviations: NG2, neural/glial antigen 2; CC1, antibody (anti-adenomatous polyposis coli (APC) clone) that binds mature oligodendrocyte marker; OLIG2, oligodendrocyte transcription factor 2; clem, clemastine fumarate; mic, miconazole. Two independent cohorts of mice from multiple litters were used for each experiment in this figure. Data represent mean ± SEM analyzed by two-way ANOVA with Dunnett multiple comparison to 4EP+ group (panels b-i) or Sidak multiple comparison between 4EP+/- groups within each sex (panels j-l). * $p \leq 0.05$, ** $p \leq 0.01$.

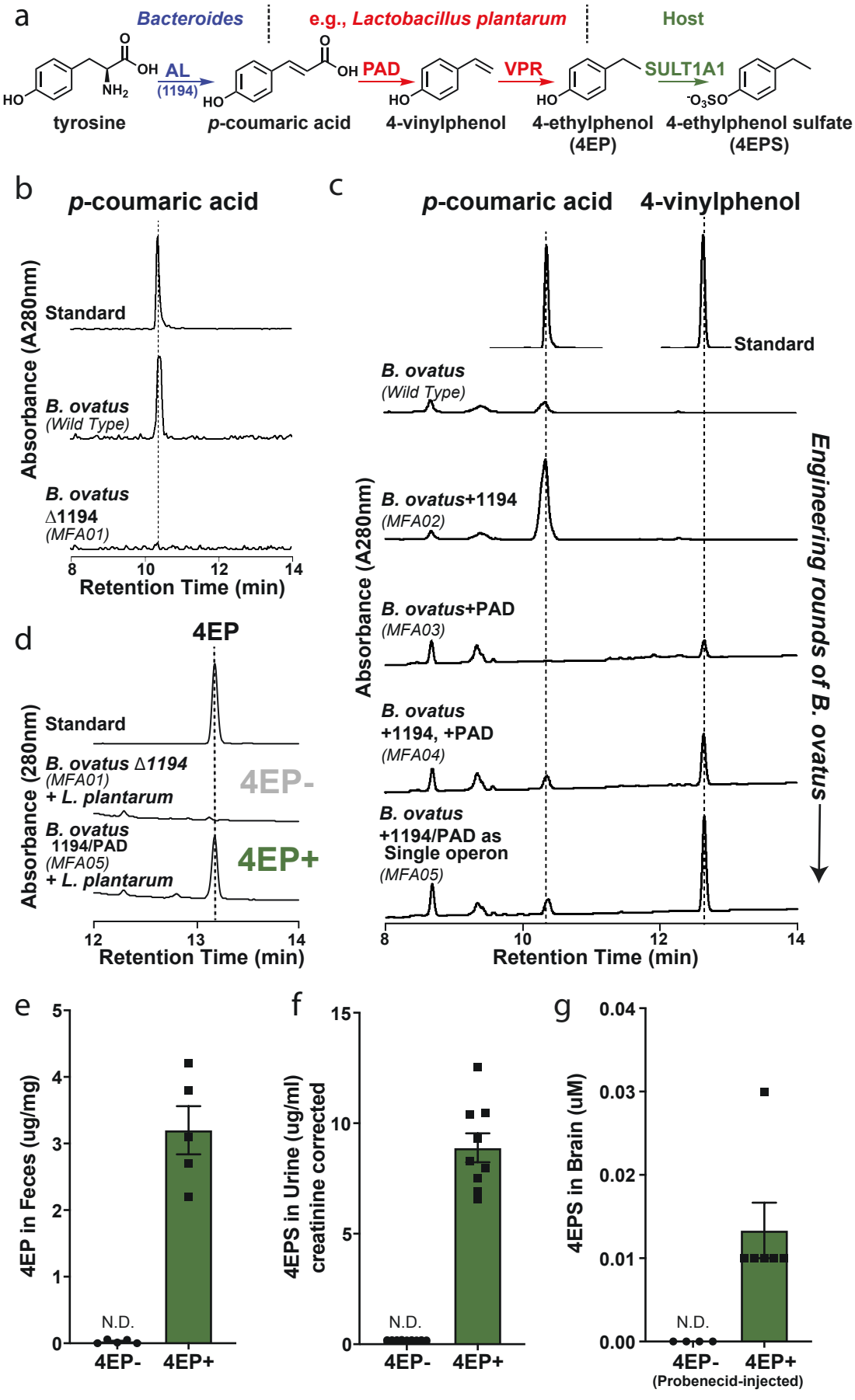
a
Bacteroides
e.g., Lactobacillus plantarum
Host
AL
(1194)
PAD
VPR
SULT1A1
tyrosine
p-coumaric acid
4-vinylphenol
4-ethylphenol
(4EP)
4-ethylphenol sulfate
(4EPS)
b
p-coumaric acid
Absorbance (A280nm)
Standard
B. ovatus
(Wild Type)
B. ovatus
Δ1194
(MFA01)
Retention Time (min)
c
p-coumaric acid
4-vinylphenol
Standard
B. ovatus
(Wild Type)
B. ovatus+1194
(MFA02)
B. ovatus+PAD
(MFA03)
B. ovatus
+1194, +PAD
(MFA04)
B. ovatus
+1194/PAD as
Single operon
(MFA05)
Engineering rounds of B. ovatus
d
4EP
Absorbance (280nm)
Standard
B. ovatus Δ1194
(MFA01)
+ L. plantarum
4EP-
B. ovatus
1194/PAD
(MFA05)
+ L. plantarum
4EP+
e
4EP in Feces (ug/mg)
N.D.
4EP-
4EP+
f
4EPS in Urine (ug/ml)
creatinine corrected
g
4EPS in Brain (uM)
(Probenecid-injected)

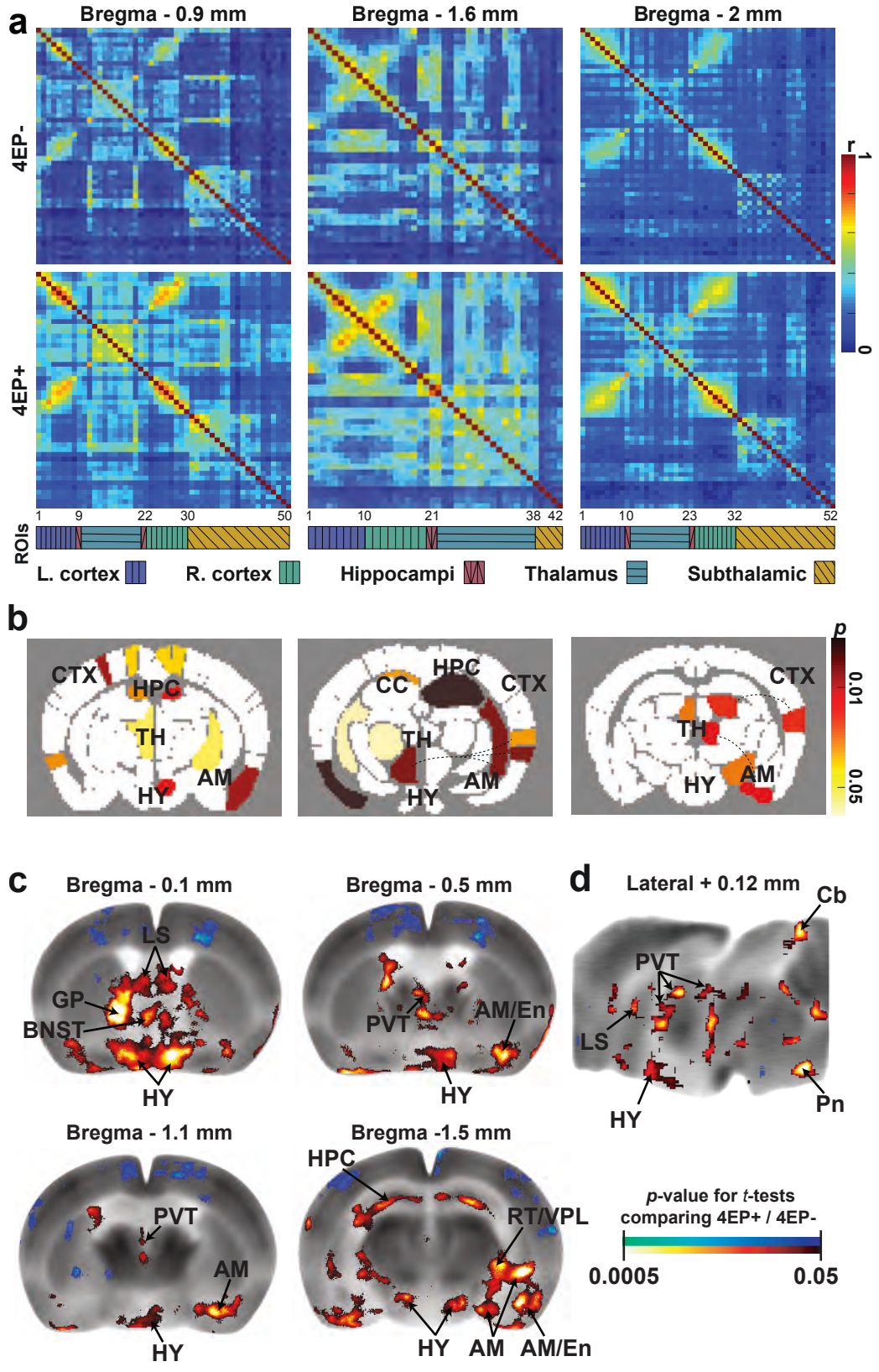
a
Bregma - 0.9 mm
Bregma - 1.6 mm
Bregma - 2 mm
4EP-
4EP+
r
1
0
1 9 22 30 50
1 10 21 38 42
1 10 23 32 52
ROIs
L. cortex
R. cortex
Hippocampi
Thalamus
Subthalamic
b
p
0.01
0.05
CTX
HPC
TH
AM
HY
CC
c
Bregma - 0.1 mm
Bregma - 0.5 mm
Bregma - 1.1 mm
Bregma -1.5 mm
LS
GP
BNST
PVT
AM/En
RT/VPL
d
Lateral + 0.12 mm
Cb
Pn
p-value for t-tests
comparing 4EP+ / 4EP-
0.0005
0.05

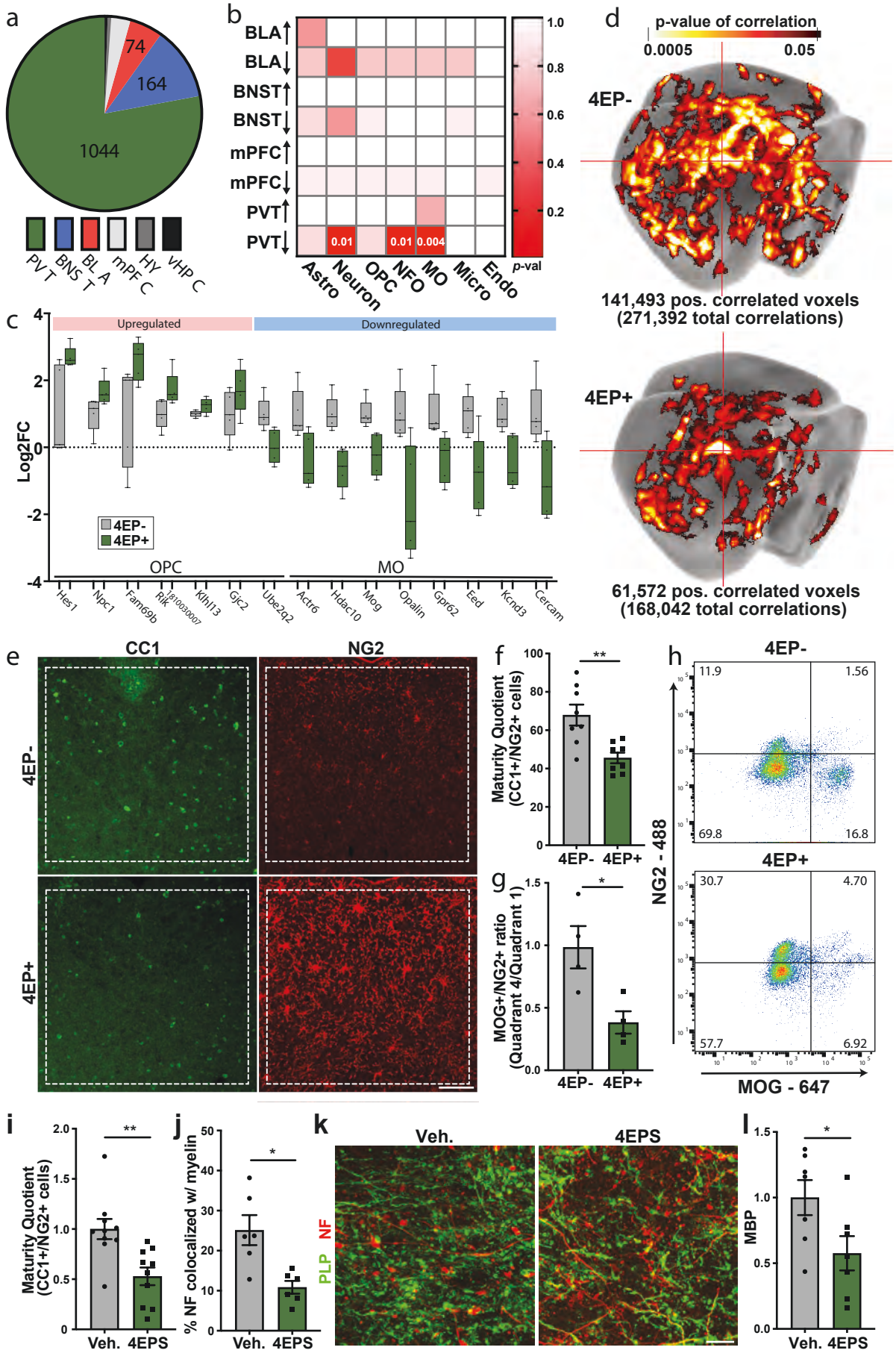
a
74
164
1044
PVT
BNST
BLA
mPFC
HY
vHPC
b
BLA↑
BLA↓
BNST↑
BNST↓
mPFC↑
mPFC↓
PVT↑
PVT↓
0.01
0.01
0.004
Astro
Neuron
OPC
NFO
MO
Micro
Endo
p-val
1.0
0.8
0.6
0.4
0.2
c
Upregulated
Downregulated
Log2FC
4EP-
4EP+
OPC
MO
Hes1
Npc1
Fam69b
Rik
Klhl13
Gjc2
Ube2q2
Actr6
Hdac10
Mog
Opalin
Gpr62
Eed
Kcnd3
Cercam
d
p-value of correlation
0.0005
0.05
4EP-
141,493 pos. correlated voxels
(271,392 total correlations)
4EP+
61,572 pos. correlated voxels
(168,042 total correlations)
e
CC1
NG2
4EP-
4EP+
f
Maturity Quotient
(CC1+/NG2+ cells)
**
4EP-
4EP+
g
MOG+/NG2+ ratio
(Quadrant 4/Quadrant 1)
*
4EP-
4EP+
h
4EP-
11.9
1.56
69.8
16.8
4EP+
30.7
4.70
57.7
6.92
NG2 - 488
MOG - 647
i
Maturity Quotient
(CC1+/NG2+ cells)
**
Veh.
4EPS
j
% NF colocalized w/ myelin
*
Veh.
4EPS
k
Veh.
4EPS
PLP
NF
l
MBP
*
Veh.
4EPS

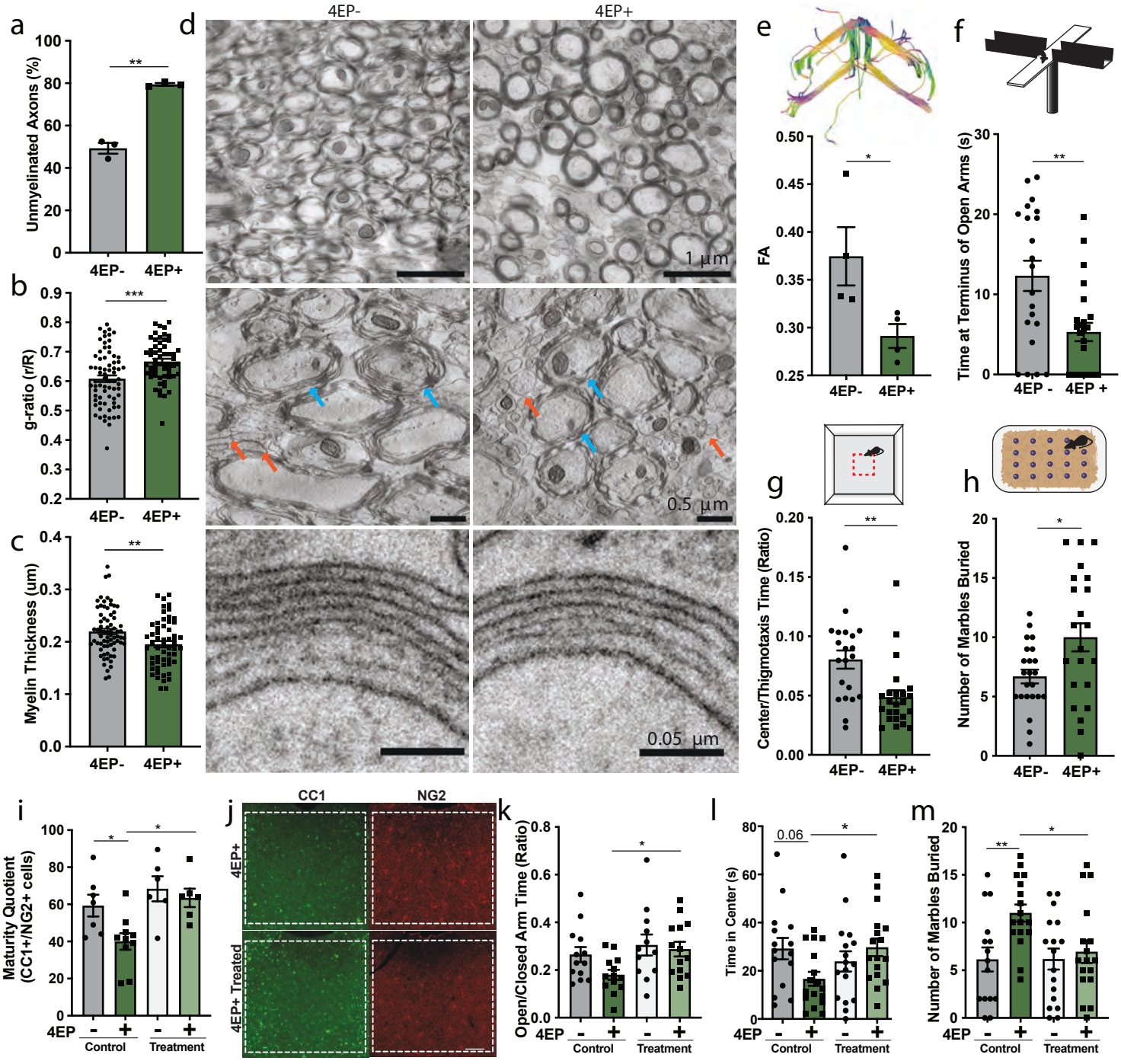
a
Unmyelinated Axons (%)
**
4EP-
4EP+
b
g-ratio (r/R)
***
c
Myelin Thickness (um)
**
d
4EP-
4EP+
1 µm
0.5 µm
0.05 µm
e
FA
*
f
Time at Terminus of Open Arms (s)
**
4EP -
4EP +
g
Center/Thigmotaxis Time (Ratio)
**
h
Number of Marbles Buried
*
i
Maturity Quotient (CC1+/NG2+ cells)
4EP
Control
Treatment
j
CC1
NG2
4EP+
4EP+ Treated
k
Open/Closed Arm Time (Ratio)
l
Time in Center (s)
0.06
m
Number of Marbles Buried

a

Strain	Deleted/ Inserted Genes	Additional Cloning Information
Wild Type	*ATCC 8483Δtdk*	*Used as background for additional strains generated*
MFA01	*ΔBO1194*	*B. ovatus gene 01194 deleted*
MFA02	*BO1194*	*Additional copy of B. ovatus gene under control of phage promoter*
MFA03	*PAD*	*B.subtilis gene under control of phage promoter*
MFA04	*BO1194/PAD*	*Each gene introduced separately under phage promoter*
MFA05	*BO1194_PAD*	*Single operon under control of phage promoter*

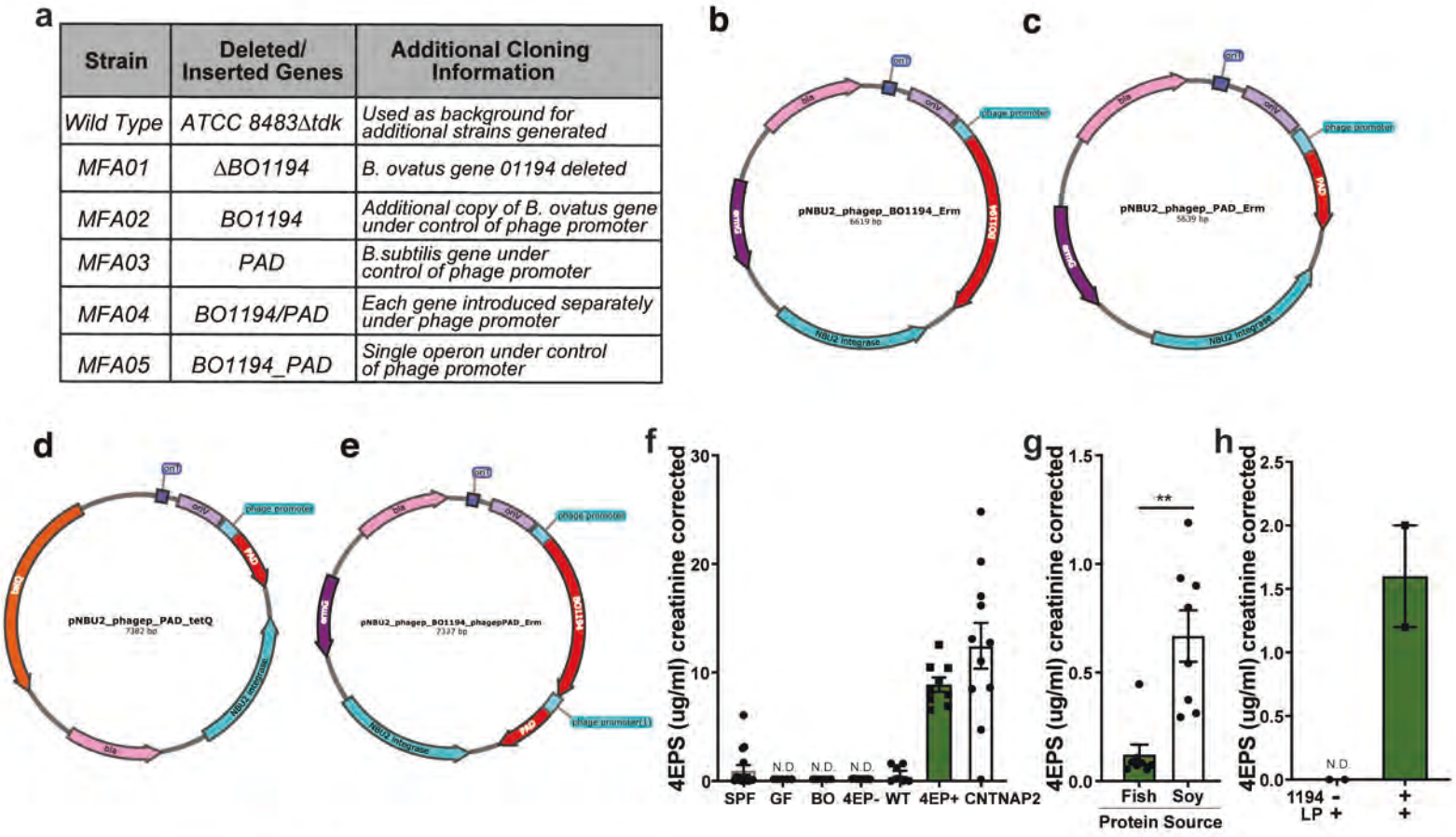

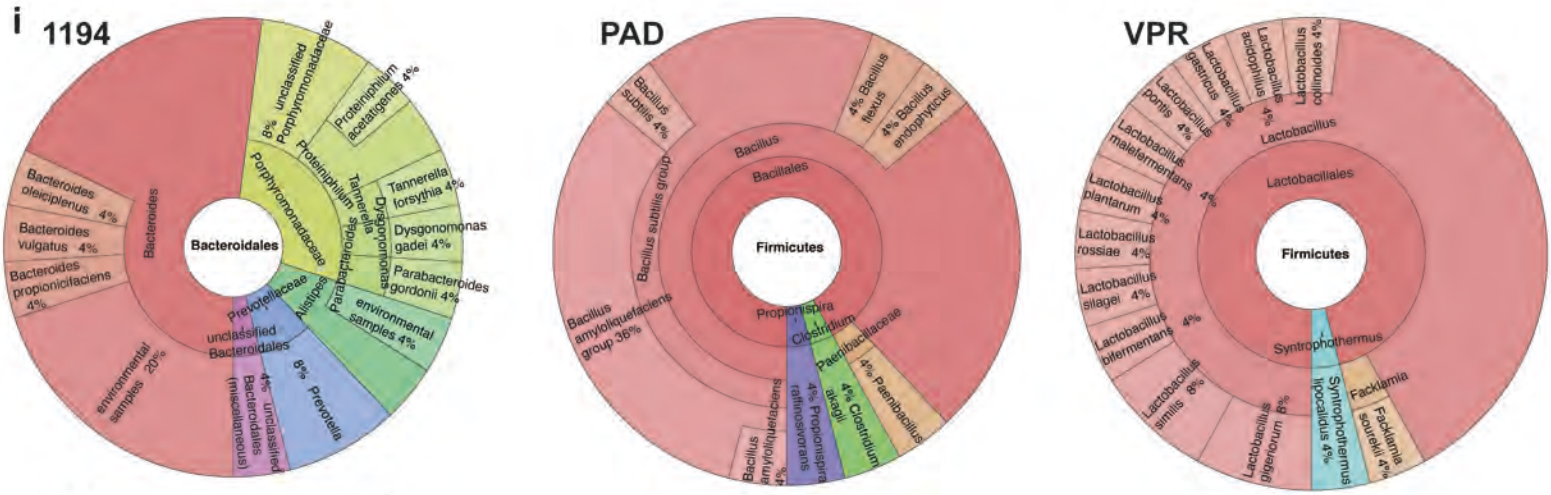

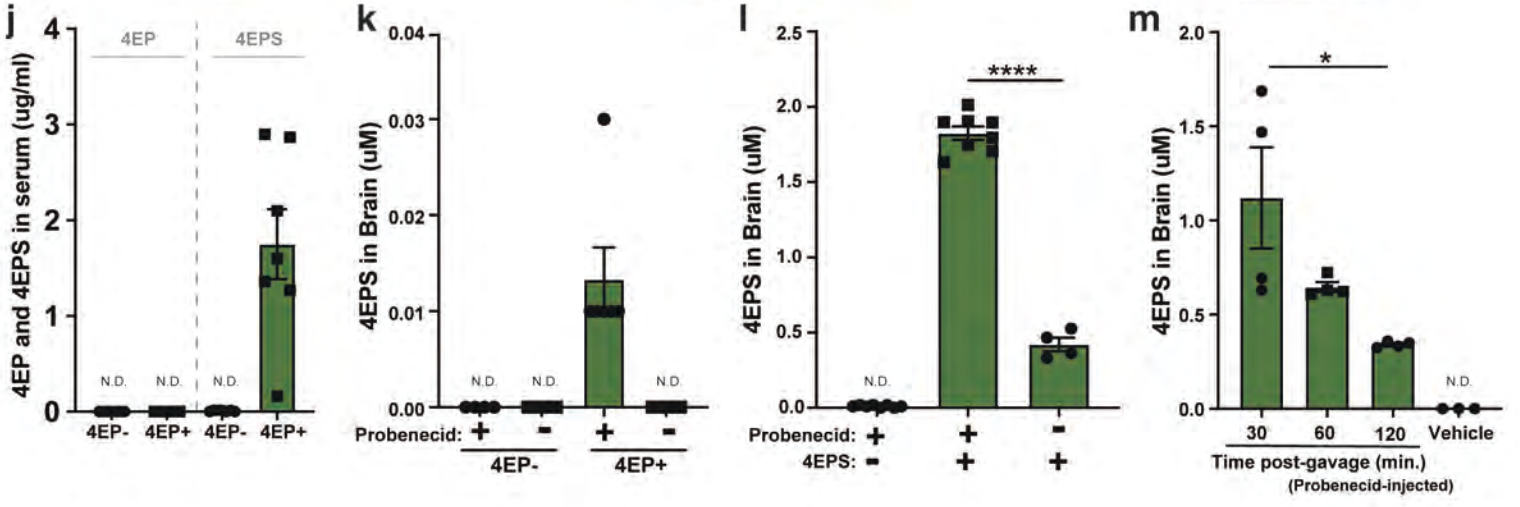

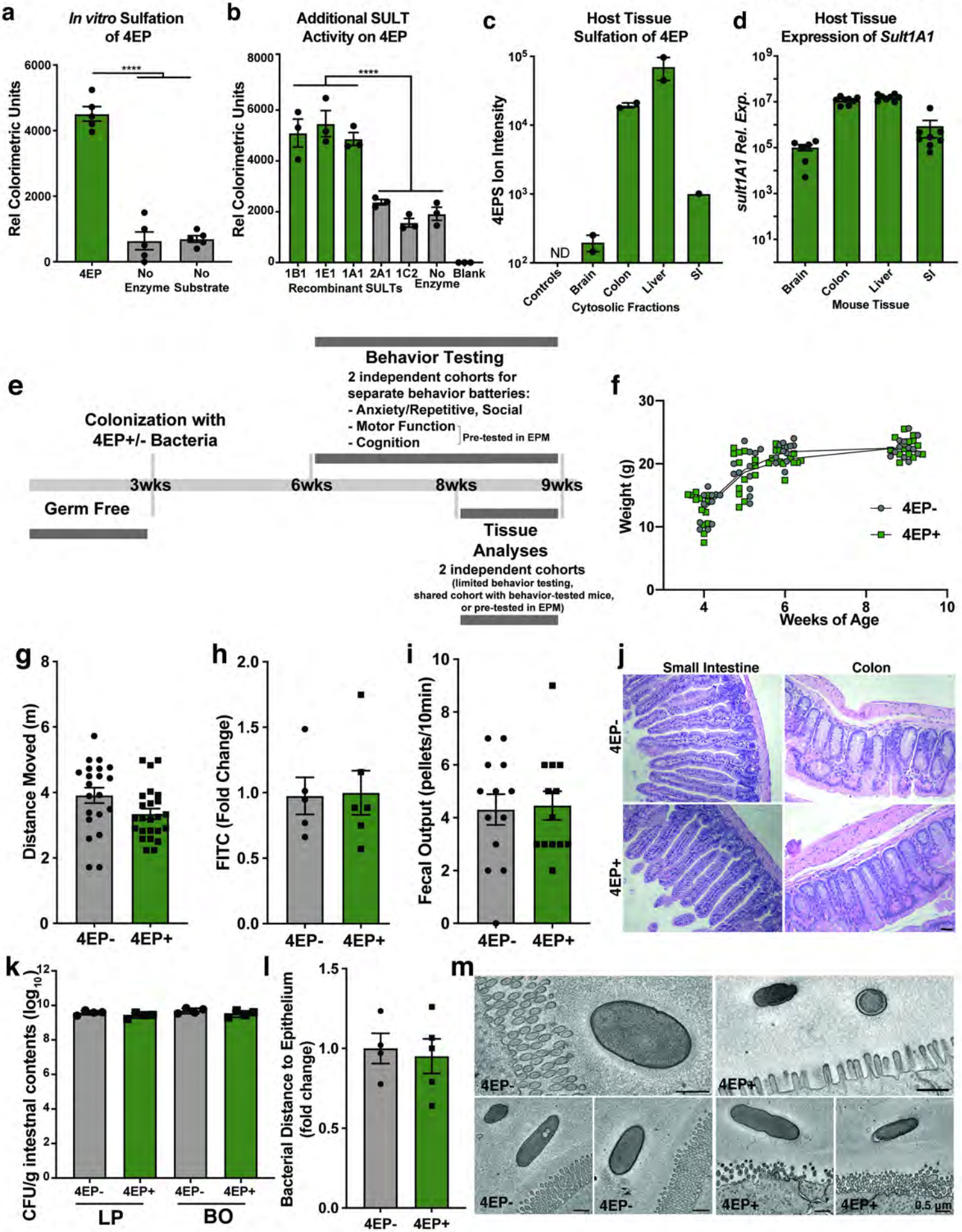
a
In vitro Sulfation of 4EP
Rel Colorimetric Units
6000
4000
2000
0
****
4EP
No Enzyme
No Substrate
b
Additional SULT Activity on 4EP
Rel Colorimetric Units
8000
6000
4000
2000
0
****
1B1 1E1 1A1 2A1 1C2 No Enzyme Blank
Recombinant SULTs
c
Host Tissue Sulfation of 4EP
4EPS Ion Intensity
10^5
10^4
10^3
10^2
ND
Controls
Brain
Colon
Liver
SI
Cytosolic Fractions
d
Host Tissue Expression of Sult1A1
sult1A1 Rel. Exp.
10^9
10^7
10^5
10^3
10^1
Brain
Colon
Liver
SI
Mouse Tissue
e
Behavior Testing
2 independent cohorts for separate behavior batteries:
- Anxiety/Repetitive, Social
- Motor Function
- Cognition
Pre-tested in EPM
Colonization with 4EP+/- Bacteria
3wks
6wks
8wks
9wks
Germ Free
Tissue Analyses
2 independent cohorts
(limited behavior testing, shared cohort with behavior-tested mice, or pre-tested in EPM)
f
Weight (g)
30
20
10
0
4EP-
4EP+
4
6
8
10
Weeks of Age
g
Distance Moved (m)
8
6
4
2
0
4EP-
4EP+
h
FITC (Fold Change)
2.0
1.5
1.0
0.5
0.0
4EP-
4EP+
i
Fecal Output (pellets/10min)
10
8
6
4
2
0
4EP-
4EP+
j
Small Intestine
Colon
4EP-
4EP+
k
CFU/g intestnal contents (log_{10})
12
10
8
6
4
2
0
4EP-
4EP+
4EP-
4EP+
LP
BO
l
Bacterial Distance to Epithelium (fold change)
1.5
1.0
0.5
0.0
4EP-
4EP+
m
4EP-
4EP+
4EP-
4EP-
4EP+
4EP+
0.5 µm

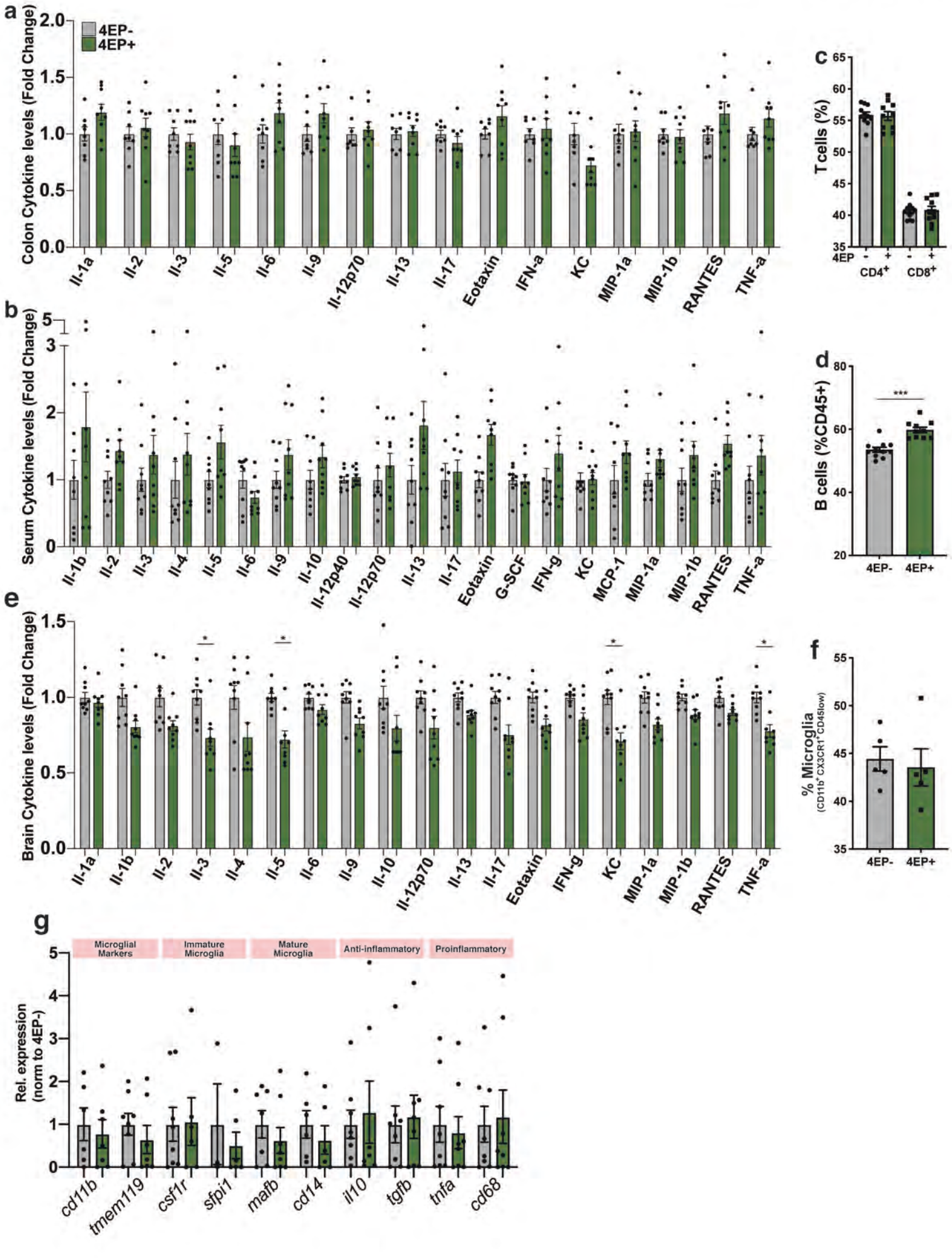
a
4EP-
4EP+
Colon Cytokine levels (Fold Change)
Il-1a
Il-2
Il-3
Il-5
Il-6
Il-9
Il-12p70
Il-13
Il-17
Eotaxin
IFN-a
KC
MIP-1a
MIP-1b
RANTES
TNF-a
b
Serum Cytokine levels (Fold Change)
Il-1b
Il-2
Il-3
Il-4
Il-5
Il-6
Il-9
Il-10
Il-12p40
Il-12p70
Il-13
Il-17
Eotaxin
G-SCF
IFN-g
KC
MCP-1
MIP-1a
MIP-1b
RANTES
TNF-a
c
T cells (%)
4EP
CD4+
CD8+
d
B cells (%CD45+)
***
4EP-
4EP+
e
Brain Cytokine levels (Fold Change)
Il-1a
Il-1b
Il-2
Il-3
Il-4
Il-5
Il-6
Il-9
Il-10
Il-12p70
Il-13
Il-17
Eotaxin
IFN-g
KC
MIP-1a
MIP-1b
RANTES
TNF-a
f
% Microglia
(CD11b+ CX3CR1+CD45low)
4EP-
4EP+
g
Microglial Markers
Immature Microglia
Mature Microglia
Anti-inflammatory
Proinflammatory
Rel. expression (norm to 4EP-)
cd11b
tmem119
csf1r
sfpi1
mafb
cd14
il10
tgfb
tnfa
cd68

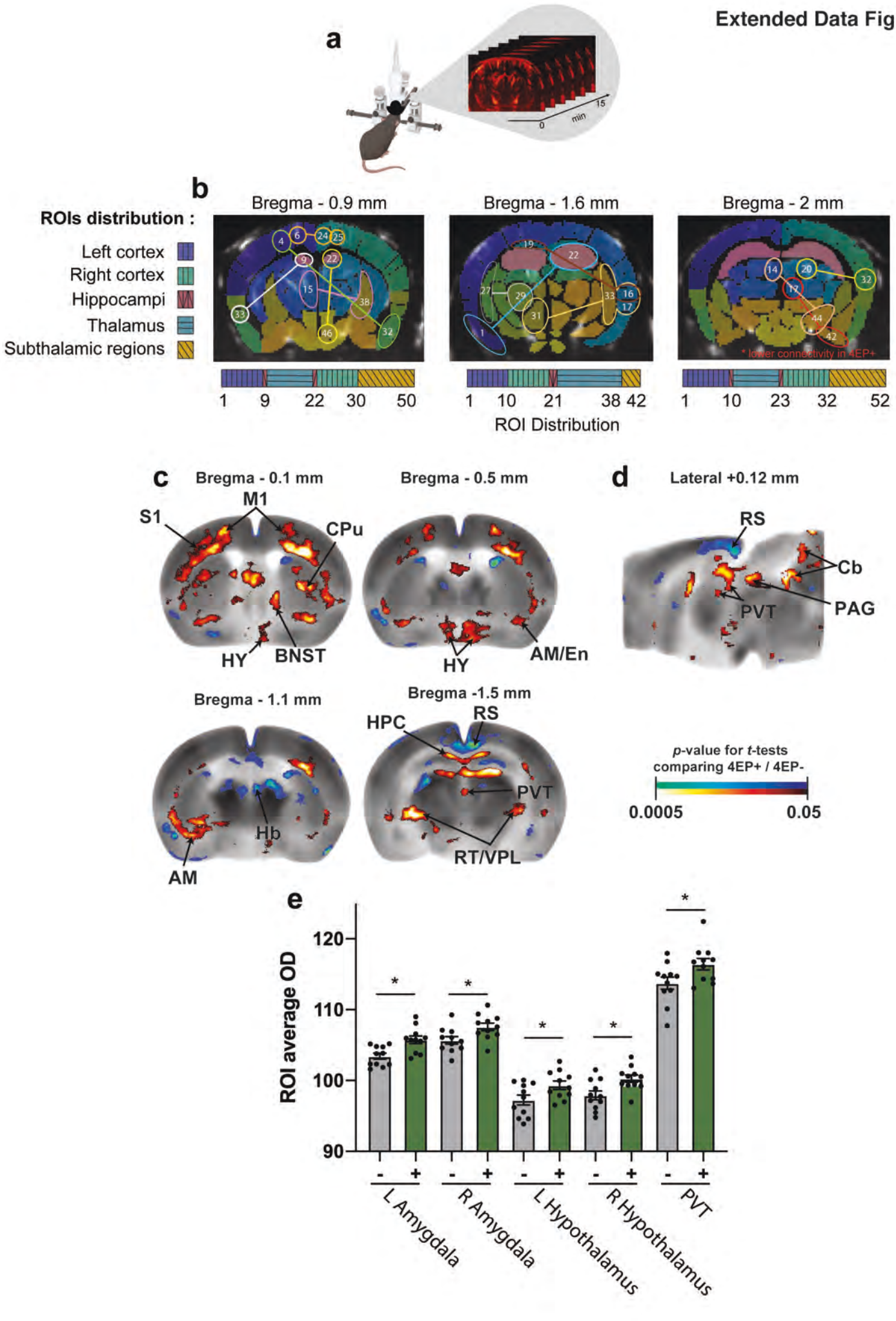
a
0
min
15
b
ROIs distribution :
Left cortex
Right cortex
Hippocampi
Thalamus
Subthalamic regions
Bregma - 0.9 mm
Bregma - 1.6 mm
Bregma - 2 mm
* lower connectivity in 4EP+
1 9 22 30 50
1 10 21 38 42
1 10 23 32 52
ROI Distribution
c
Bregma - 0.1 mm
M1
S1
CPu
HY
BNST
Bregma - 0.5 mm
HY
AM/En
Bregma - 1.1 mm
Hb
AM
Bregma -1.5 mm
HPC
RS
PVT
RT/VPL
d
Lateral +0.12 mm
RS
Cb
PVT
PAG
p-value for t-tests
comparing 4EP+ / 4EP-
0.0005
0.05
e
ROI average OD
120
110
100
90
L Amygdala
R Amygdala
L Hypothalamus
R Hypothalamus
PVT

Extended Data Figure 5

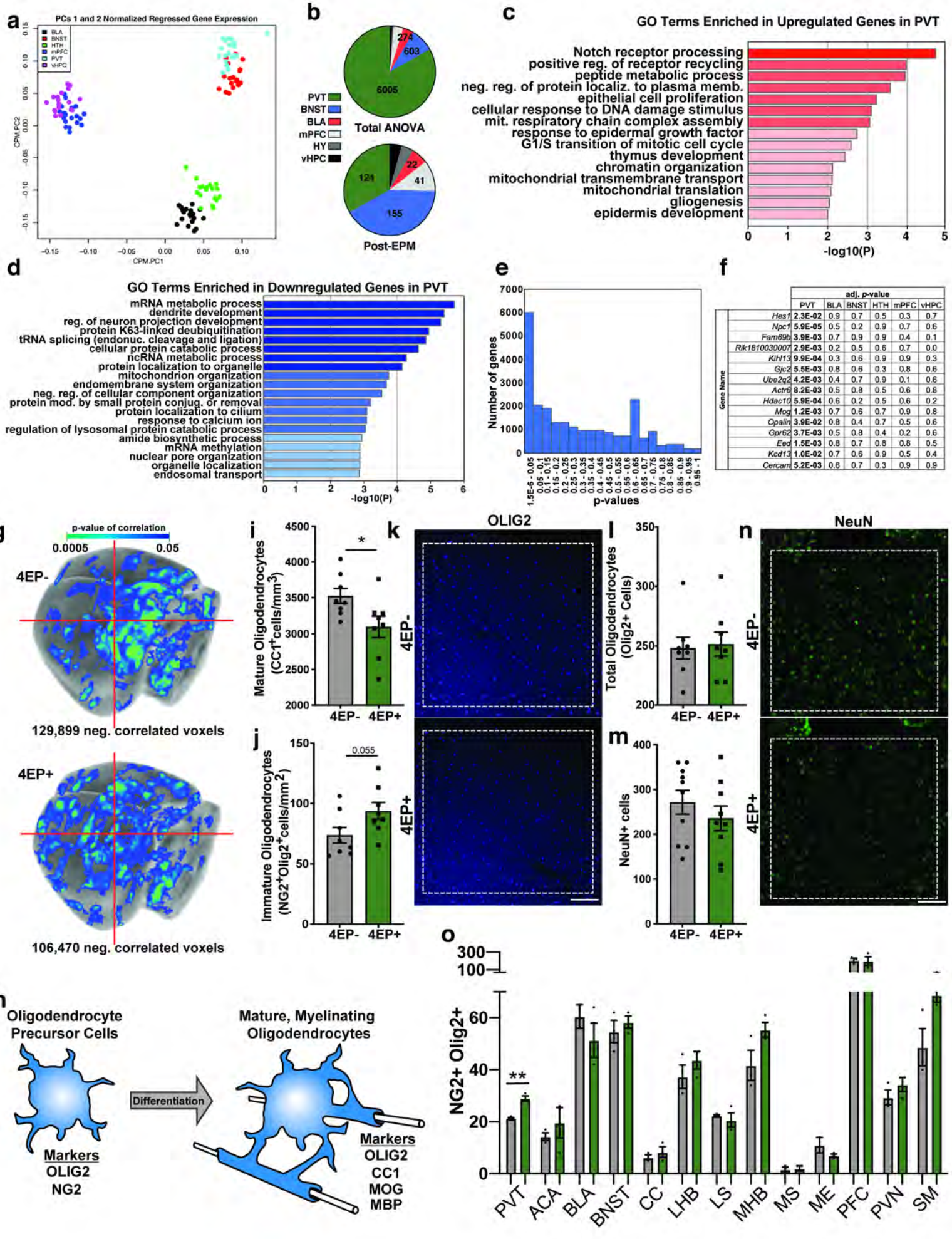

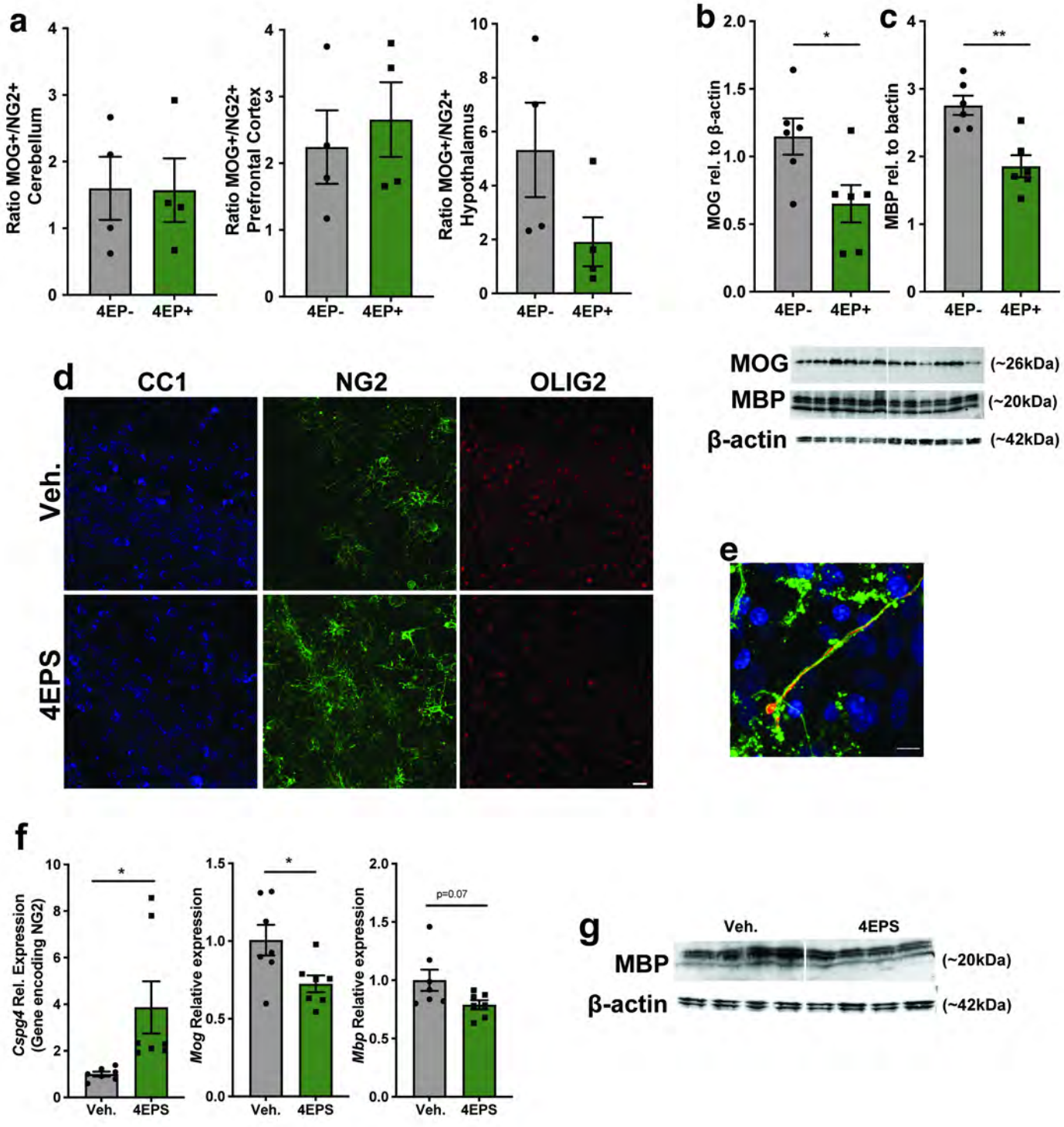
a
Ratio MOG+/NG2+ Cerebellum
Ratio MOG+/NG2+ Prefrontal Cortex
Ratio MOG+/NG2+ Hypothalamus
4EP-
4EP+
b
MOG rel. to β-actin
c
MBP rel. to bactin
MOG
MBP
β-actin
(~26kDa)
(~20kDa)
(~42kDa)
d
CC1
NG2
OLIG2
Veh.
4EPS
e
f
Cspg4 Rel. Expression (Gene encoding NG2)
Mog Relative expression
Mbp Relative expression
p=0.07
Veh.
4EPS
g
Veh.
4EPS
MBP
β-actin
(~20kDa)
(~42kDa)

Extended Data Figure 7

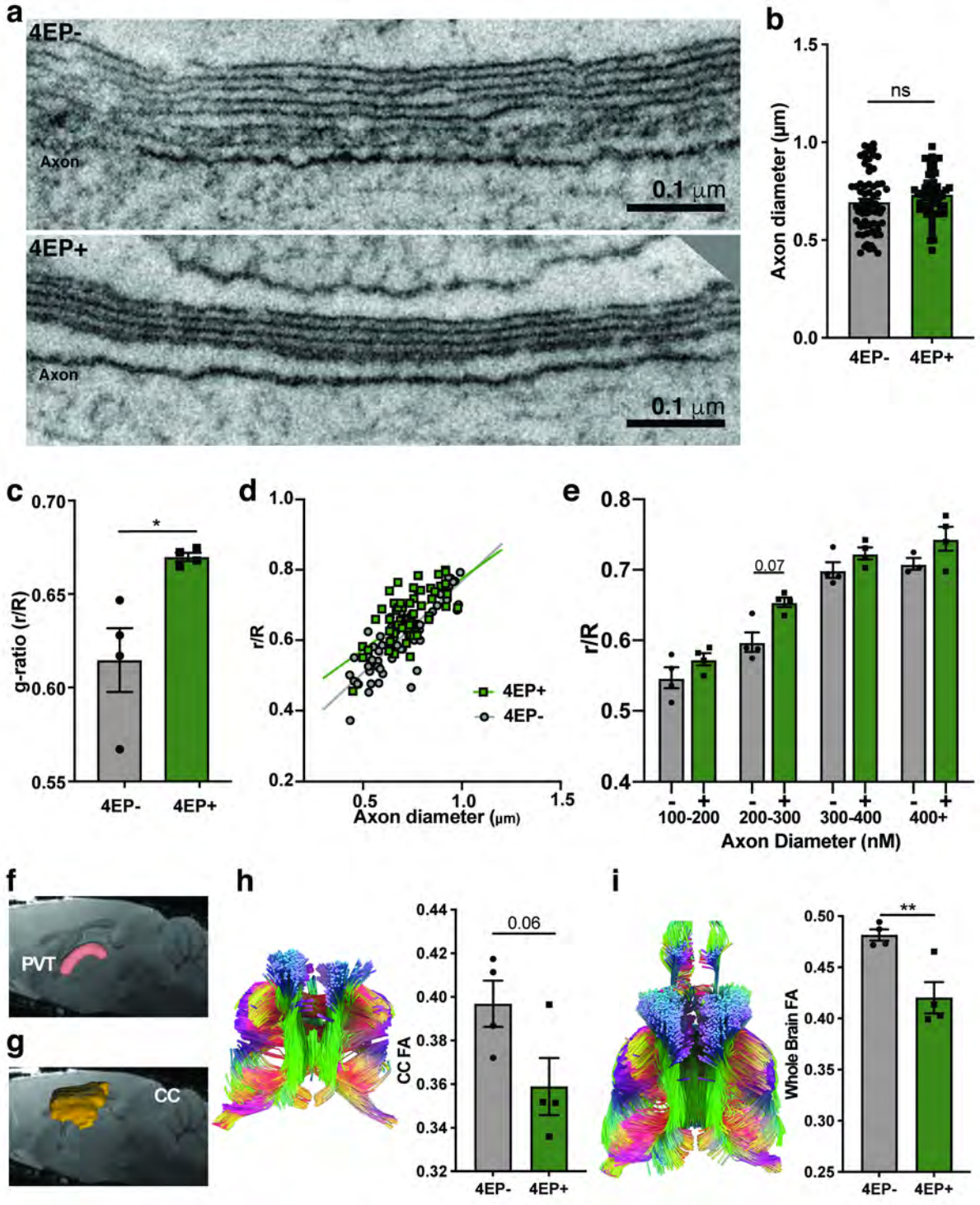

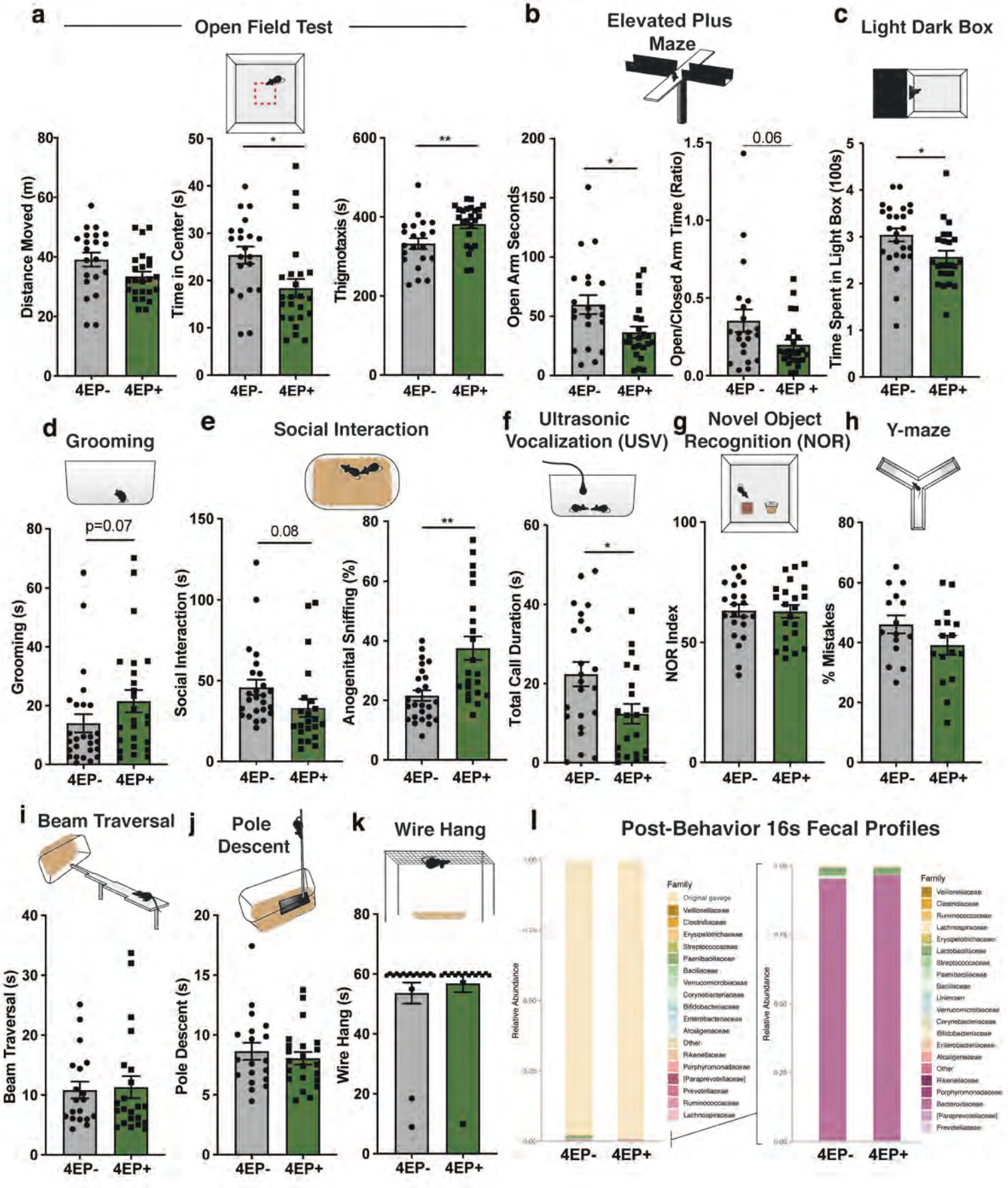
a
Open Field Test
Distance Moved (m)
Time in Center (s)
Thigmotaxis (s)
b
Elevated Plus Maze
Open Arm Seconds
Open/Closed Arm Time (Ratio)
0.06
c
Light Dark Box
Time Spent in Light Box (100s)
d
Grooming
p=0.07
Grooming (s)
e
Social Interaction
0.08
Social Interaction (s)
Anogenital Sniffing (%)
f
Ultrasonic Vocalization (USV)
Total Call Duration (s)
g
Novel Object Recognition (NOR)
NOR Index
h
Y-maze
% Mistakes
i
Beam Traversal
Beam Traversal (s)
j
Pole Descent
Pole Descent (s)
k
Wire Hang
Wire Hang (s)
l
Post-Behavior 16s Fecal Profiles
Relative Abundance
Family
Original gavage
Veillonellaceae
Clostridiaceae
Erysipelotrichaceae
Streptococcaceae
Paenibacillaceae
Bacillaceae
Verrucomicrobiaceae
Corynebacteriaceae
Bifidobacteriaceae
Enterobacteriaceae
Alcaligenaceae
Other
Rikenellaceae
Porphyromonadaceae
[Paraprevotellaceae]
Prevotellaceae
Ruminococcaceae
Lachnospiraceae
Unknown
Lactobacillaceae
Bacteroidaceae
4EP-
4EP+

Extended Data Figure 9

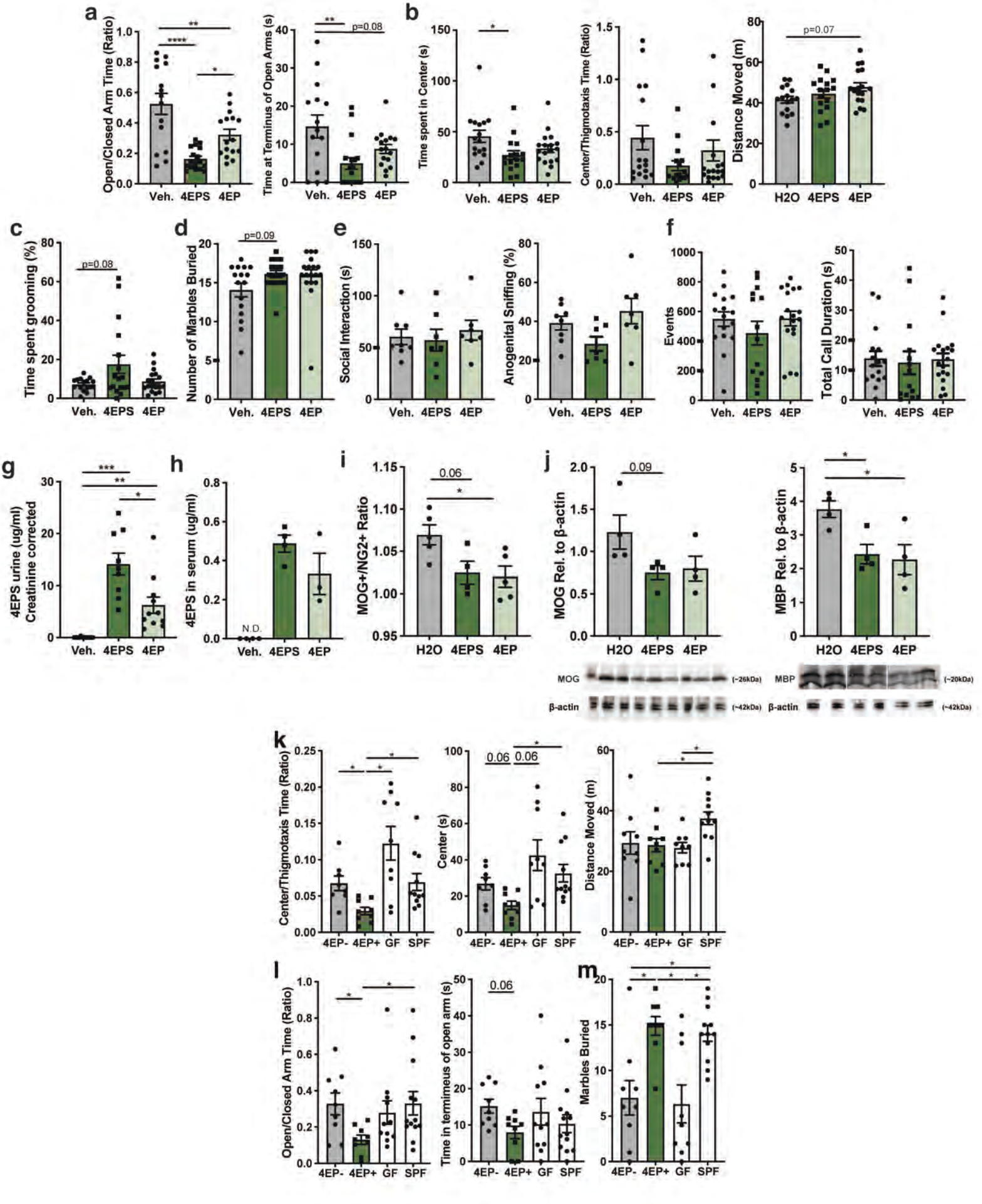

Extended Data Figure 10

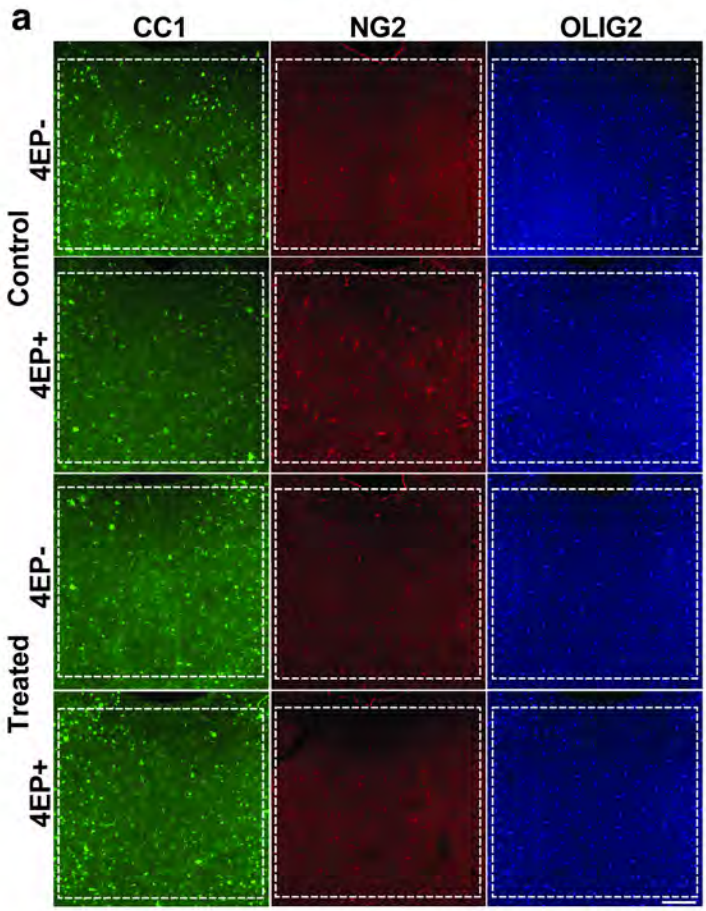

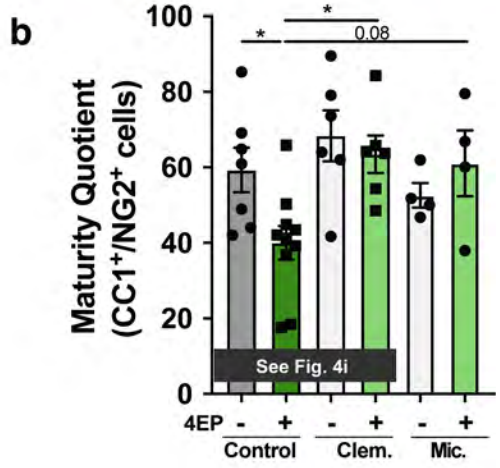

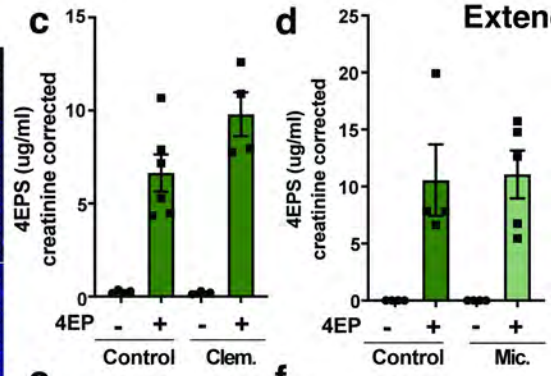

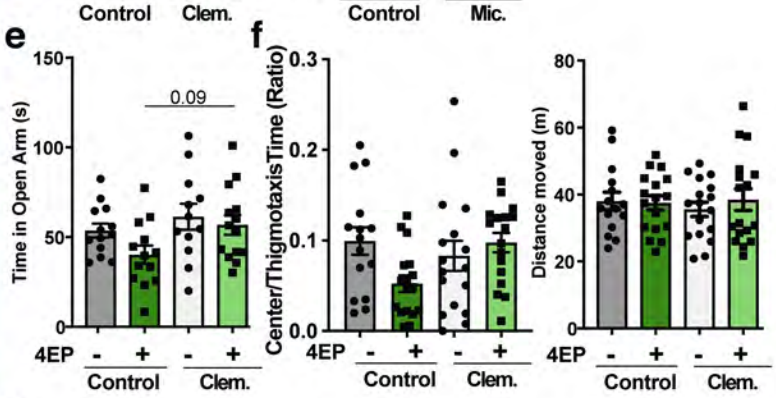

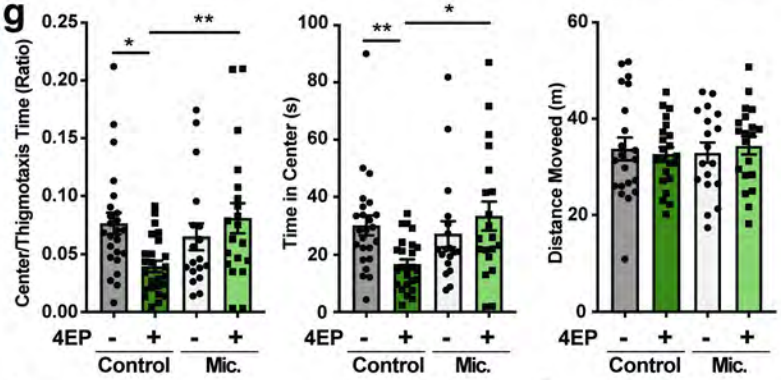

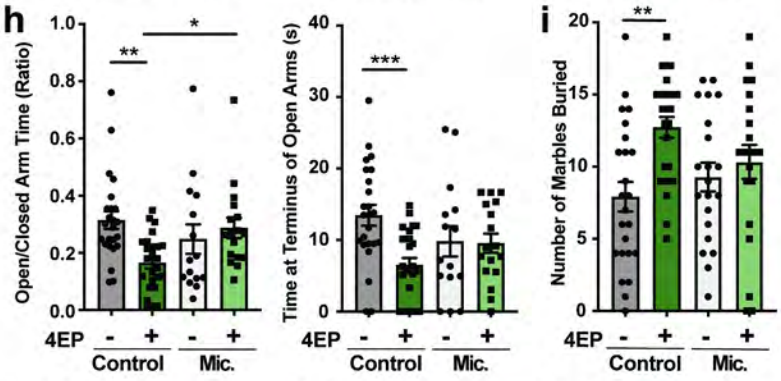

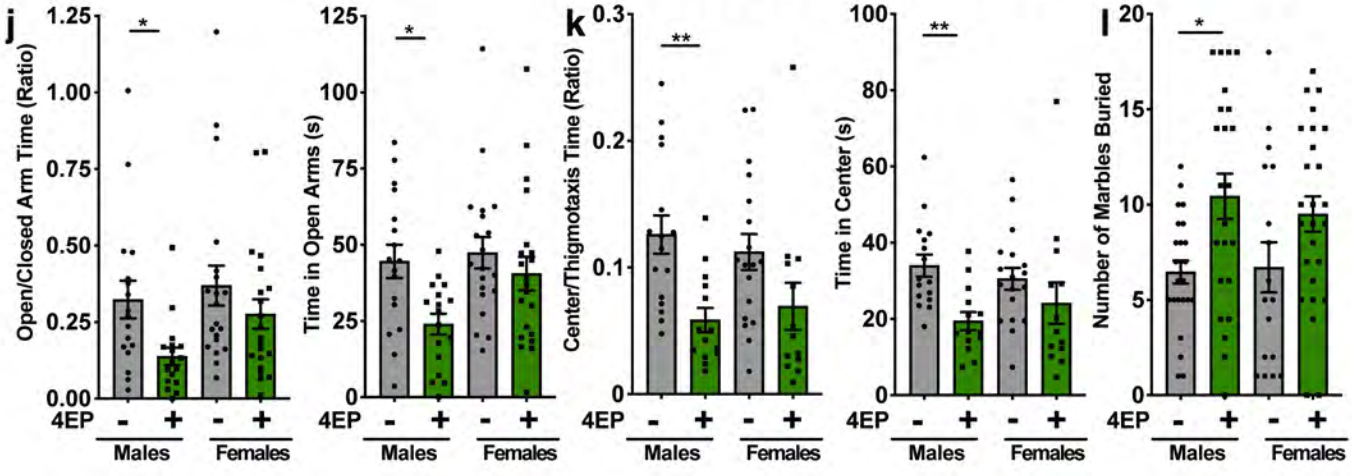

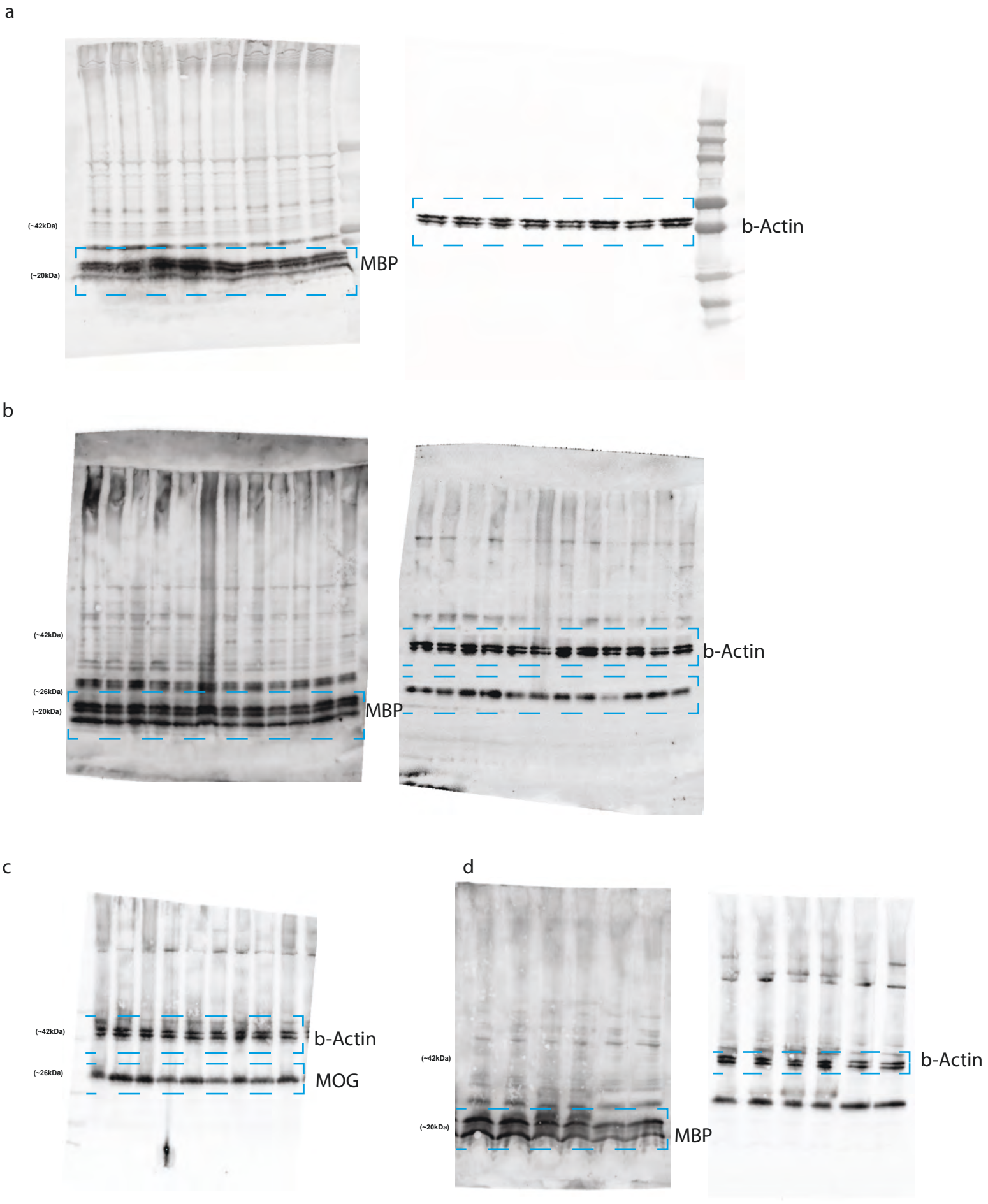

Supplementary Data Figure 1. Raw scans of western blots in the paper.
a, Blot scans corresponding to Extended Data Figure 6h. b, Blot scans corresponding to Extended Data Figure 6 b,c. c, Blot scans corresponding to Extended Data Figure 6j (left). d, Blot scans corresponding to Extended Data Figure 6j (right).

a

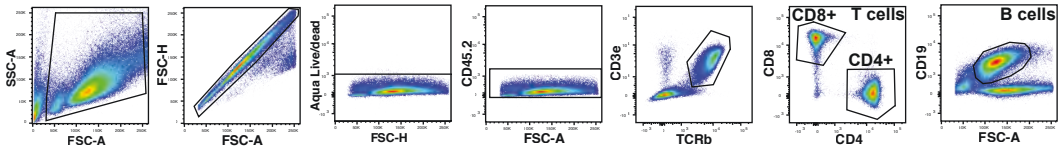

b

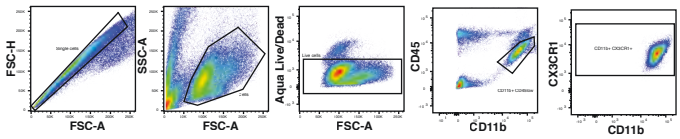

c

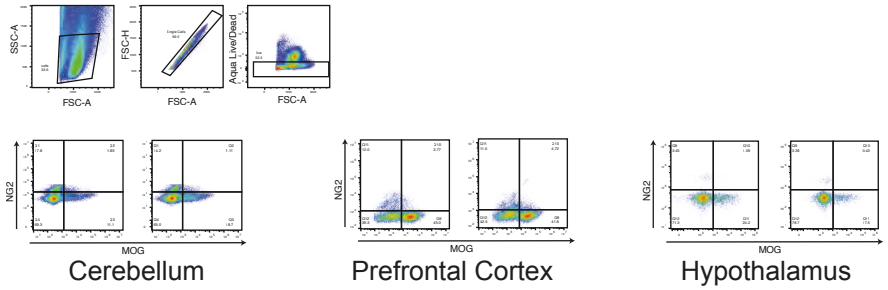

Supplementary Data Figure 2. Glow cytometry gating strategies used in the paper. a, Gating for Figure 3g,h and Extended Data Figure 3c,d. b, Gating strategy for Extended Data Figure 3f. c, Gating strategy for Extended Data Figure 6a.

Supplementary Data Table1. Strains used in this study

Name	Strain	Specific Genotype	plasmid	source
	B. ovatus ATCC 8483 Δ*tdk*			lab stock
	Lactobacillus plantarum BAA-793			ATCC
	E. coli S17-1 λ pir			lab stock
MFA01	*B. ovatus* ATCC 8483 Δ*tdk*	ΔBO_01194		this study
MFA02	*B. ovatus* ATCC 8483 Δ*tdk*		pMFA01	this study
MFA03	*B. ovatus* ATCC 8483 Δ*tdk*		pMFA02	this study
MFA04	*B. ovatus* ATCC 8483 Δ*tdk*		pMFA01 and pMF03	this study
MFA05	*B. ovatus* ATCC 8483 Δ*tdk*		pMFA04	this study

Supplementary Data Table 2. Plasmids used in this study

plasmids	back bone	promoter	introduced gene	source
pExchange_tdk_ΔBO_01194	pEchange_tdk		up and down stream of BACOVA_01194	this study
pMFA01	pNBU2_bla_ermGb	phage promoter	BACOVA_01194	this study
pMFA02	pNBU2_bla_ermGb	phage promoter	bsPAD	this study
pMFA03	pNBU2_bla_tetQb	phage promoter	bsPAD	this study
pMFA04	pNBU2_bla_tetQb	phage promoter	BACOVA_01194. bsPAD	this study

Supplementary Data Table 3. primers used in this study for generation of engineered bacterial strains

primer #	primer name	sequence (5'-3')	
Upstream of BACOVA_01194			
1	BO_01194_US_F	GCG*GGATCC* AAAGATGTTATTCACCTTACC	*Bam* HI
2	BO_01194_US_R	GCG*GTCGAC* TTTCTGTACTAGATATTTTATG	*Sal* I
Downstream of BACOVA_01194			
3	BO_01194_DS_F	GCG*GTCGAC* AATGAAATATGCATTAGTAACC	*Sal* I
4	BO_01194_DS_R	GCG*CTGCAG* ACTGCGTTAATAACAGGAGC	*Pst* I
pNBU2 vector for gibson assembly			
5	pNBU2_F	TCTAGAACTAGTGGATCCCC	
6	pNBU2_R	GCGGCCGCCACCGCGG	
phage promoter_BO_01194			
7	3'pNBU2_phageP_F	CCTCCACCGCGGTGGCGGCCGCGATAAAACGAAAGGCTCAG	
8	phageP_5'BO_01194_R	GTCAGCTATCATCTACTTTGTTTCTTTCGACAC	
9	3'phageP_BO_01194_F	GAAAGAAACAAAGTAGATGATAGCTGACAAAAGTATAA	
10	5'pNBU2_BO_01194_R	CGGGGGATCCACTAGTTCTAGATTATTTATCTTCTTTTTTGAG	
phage promoter_bsPAD			
7	3'pNBU2_phageP_F	CCT CCA CCG CGG TGG CGG CCG CGA TAA AAC GAA AGG CTC AG	
11	phageP_5'bsPAD_R	ACTGTACTTCATCTACTTTGTTTCTTTCGACAC	
12	3'phageP_bsPAD_F	GAAACAAAGTAGATGAAGTACAGTAAAAGACTAAG	
13	5'pNBU2_bsPAD_R	CGGGGGATCCACTAGTTCTAGATTATAATCTTCCCGCGCG	
phage promoter_BO_01194_phage promoter_bsPAD			
7	3'pNBU2_phageP_F	CCTCCACCGCGGTGGCGGCCGCGATAAAACGAAAGGCTCAG	
14	5'phageP_BO_01194_R	TCTCAAAAAAGAAGATAAATAAGATAAAACGAAAGGCTCAG	
12	3'phageP_bsPAD_F	GAAACAAAGTAGATGAAGTACAGTAAAAGACTAAG	
13	5'pNBU2_bsPAD_R	CGGGGGATCCACTAGTTCTAGATTATAATCTTCCCGCGCG	

Supplementary Data Table 4. Region of Interest (ROI) Definitions corresponding to Fig. 2a-b, ED Fig. 4a-b

Bregma - 0.9 mm			Bregma - 1.6 mm			Bregma - 2 mm		
ROIs number	ROIs label	ROIs full name	ROIs number	ROIs label	ROIs full name	ROIs number	ROIs label	ROIs full name
1	L - S2	Left secondary somatosensory cortex	1	L - Pir	Left piriform cortex	1	L - AuV	Left secondary auditory cortex, ventral area
2	L - S1ULp	Left primary somatosensory cortex, upper lip region	2	L - PRh	Left perirhinal cortex	2	L - AuD	Left secondary auditory cortex, dorsal area
3	L - S1BF	Left primary somatosensory cortex, barrel field	3	L - Ect	Left ectorhinal cortex	3	L - S1	Left primary somatosensory cortex
4	L - S1Sh	Left primary somatosensory cortex, shoulder region	4	L - S2	Left secondary somatosensory cortex	4	L - S1BF	Left primary somatosensory cortex, barrel field
5	L - S1HL	Left primary somatosensory cortex, hindlimb region	5	L - S1ULp	Left primary somatosensory cortex, upper lip region	5	L - Pt	Left parietal cortex, posterior area
6	L - M1-M2	Left primary and secondary motor cortex	6	L - S1BF	Left primary somatosensory cortex, barrel field	6	L - LPtA	Left lateral parietal association cortex
7	L - RSD	Left retrosplenial dysgranular cortex	7	L - S1Tr	Left primary somatosensory cortex, trunk region	7	L - MPtA	Left medial parietal association cortex
8	L - RSG	Left retrosplenial granular cortex	8	L - PtA	Left parietal association cortex	8	L - RSD	Left retrosplenial dysgranular cortex
9	L - CA	Left hippocampus	9	L - RS	Left retrosplenial cortex	9	L - RSG	Left retrosplenial granular cortex
10	L - LV	Left lateral ventricle	10	R - RS	Right retrosplenial cortex	10	L - CA	Left hippocampus
11	L - Cpu	Left caudate putamen (striatum)	11	R - PtA	Right parietal association cortex	11	L - fi - ic	Left fimbria of the hippocampus and internal capsule
12	L - Rt	Left reticular nucleus	12	R - S1Tr	Right primary somatosensory cortex, trunk region	12	L - DLG	Left dorsal lateral geniculate nucleus
13	L - LD	Left laterodorsal and anteroventral thalamic nucleus	13	R - S1BF	Right primary somatosensory cortex, barrel field	13	L - LP	Left lateral posterior thalamic nucleus
14	L - VL	Left ventrolateral thalamic nucleus	14	R - S1ULp	Right primary somatosensory cortex, upper lip region	14	L - Hb	Left habenular nucleus
15	L - AM	Left anteromedial thalamic nucleus	15	R - S2	Right secondary somatosensory cortex	15	L - VP	Left ventral thalamic nucleus
16	R - AM	Right anteromedial thalamic nucleus	16	R - Ect	Right ectorhinal cortex	16	L -MDD	Left mediodorsal thalamic nucleus
17	R - VL	Right ventrolateral thalamic nucleus	17	R - PRh	Right perirhinal cortex	17	R -MDD	Right mediodorsal thalamic nucleus
18	R - LD	Right laterodorsal and anteroventral thalamic nucleus	18	R - Pir	Right piriform cortex	18	R - VP	Right ventral thalamic nucleus
19	R - Rt	Right reticular nucleus	19	L - cc	Left corpus callosum	19	R - Hb	Right habenular nucleus
20	R - Cpu	Right caudate putamen (striatum)	20	R - cc	Right corpus callosum	20	R - LP	Right lateral posterior thalamic nucleus
21	R - LV	Right lateral ventricle	21	L - CA	Left hippocampus	21	R - DLG	Right dorsal lateral geniculate nucleus
22	R - CA	Right hippocampus	22	R - CA	Right hippocampus	22	R - fi - ic	Right fimbria of the hippocampus and internal capsule
23	R - RSG	Right retrosplenial granular cortex	23	L - Hb	Left habenular nucleus	23	R - CA	Right hippocampus
24	R - RSD	Right retrosplenial dysgranular cortex	24	R - Hb	Left habenular nucleus	24	R - RSG	Right retrosplenial granular cortex
25	R - M1-M2	Right primary and secondary motor cortex	25	L - LD	Left laterodorsal thalamic nucleus	25	R - RSD	Right retrosplenial dysgranular cortex
26	R - S1HL	Right primary somatosensory cortex, hindlimb region	26	R - LD	Right laterodorsal thalamic nucleus	26	R - MPtA	Right medial parietal association cortex
27	R - S1Sh	Right primary somatosensory cortex, shoulder region	27	L - Cpu	Left caudate putamen (striatum)	27	R - LPtA	Right lateral parietal association cortex
28	R - S1BF	Right primary somatosensory cortex, barrel field	28	L -ic	Left internal capsule	28	R - Pt	Right parietal cortex, posterior area
29	R - S1ULp	Right primary somatosensory cortex, upper lip region	29	L -VL	Left ventral thalamic nucleus	29	R - S1BF	Right primary somatosensory cortex, barrel field
30	R - S2	Right secondary somatosensory cortex	30	L - Me	Left medial amygdaloid nucleus	30	R - S1	Right primary somatosensory cortex
31	L- Pir	Left piriform cortex	31	L - VM	Left ventromedial thalamic nucleus	31	R - AuD	Right secondary auditory cortex, dorsal area
32	R- Pir	Right piriform cortex	32	L - MD	Left mediodorsal thalamic nucleus	32	R - AuV	Right secondary auditory cortex, ventral area
33	L - AIP	Left agranular insular cortex, posterior part	33	R - Cpu	Right caudate putamen (striatum)	33	L - Pir	Left piriform cortex
34	R - AIP	Right agranular insular cortex, posterior part	34	R -ic	Right internal capsule	34	R - Pir	Right piriform cortex
35	L - GI	Left gigantocellular reticular nucleus	35	R - VL	Right ventral thalamic nucleus	35	L - Ent	Left entorhinal cortex
36	R- GI	Right gigantocellular reticular nucleus	36	R - Me	Right medial amygdaloid nucleus	36	R - Ent	Right entorhinal cortex
37	L -ic-GP	Left internal capsule and globus pallidus	37	R - VM	Right ventromedial thalamic nucleus	37	L - CPu	Left caudate putamen (striatum)
38	R -ic-GP	Right internal capsule and globus pallidus	38	R - MD	Right mediodorsal thalamic nucleus	38	R - CPu	Right caudate putamen (striatum)
39	L - Ce	Left central amygdaloid nucleus	39	L - DM	Left dorsomedial hypothalamic nucleus	39	L - BL	Left basolateral amygdaloid nucleus
40	R - Ce	Right central amygdaloid nucleus	40	L -VMHC	Left ventromedial hypothalamic nucleus	40	R - BL	Right basolateral amygdaloid nucleus
41	L - AA	Left anterior amygdaloid area	41	R - DM	Right dorsomedial hypothalamic nucleus	41	L - Co	Left cortical amygdaloid area
42	R - AA	Right anterior amygdaloid area	42	R -VMH	Right ventromedial hypothalamic nucleus	42	R - Co	Right cortical amygdaloid area
43	L - PLH	Left peduncular part of lateral hypothalamus				43	L - STh	Left subthalamic nucleus
44	R - PLH	Right peduncular part of lateral hypothalamus				44	R - STh	Right subthalamic nucleus
45	L - AH	Left anterior hypothalamic area,				45	L - VM	Left ventromedial thalamic nucleus
46	R - AH	Right anterior hypothalamic area,				46	R - VM	Right ventromedial thalamic nucleus
47	L - RCh	Left - retrochiasmatic area				47	L - PH	Left posterior hypothalamic nucleus
48	R - RCh	Right - retrochiasmatic area				48	R - PH	Right posterior hypothalamic nucleus
49	L - Pa	Left - hypothalamic nucleus				49	L -VMH	Left ventromedial hypothalamic nucleus
50	R - Pa	Right - hypothalamic nucleus				50	R -VMH	Right ventromedial hypothalamic nucleus
						51	L - PLH	Left - lateral hypothalamus
						52	R - PLH	Right - lateral hypothalamus

Supplementary Data Table 5. Primers used in this study for qPCR

	primer name	sequence (5'-3')
Sult1A1		
	sult1a1for	CCCGGATACCCTTCCTTGAG
	sult1a1rev	CCATAGGACACTTTCCCATCCA
B-actin		
	bactinfor	AGAGGGAAATCGTGCGTGAC
	bactinrev	CAATAGTGATGACCTGGCCGT
Mog		
	mogfor	CGGACAGAGCTGCTGAAAGA
	mogrev	TGCTCGAAGTTTTCCTCTCAGT
Mbp		
	mbpfor	CGGACAGAGCTGCTGAAAGA
	mbprev	TGCTCGAAGTTTTCCTCTCAGT
Cspg4		
	cspg4for	CCTTCACTGTCACTGTCCTGC
	cspg4rev	CAGGGTTCCTCTGTGTGAGAACA
Cd11b		
	cd11bfor	AAGCTCTTCTGGTCACAGCC
	cd11brev	GCAACAACCACACTGGTTCC
Tmem119		
	tmem119for	TCACCCAGAGCTGGTTCCAT
	tmem119rev	GTGACACAGAGTAGGCCACC
Csfl1r		
	tmem119for	GGTTGTAGAGCCGGGTGAAA
	tmem119rev	AAGAGTGGGCCGGATCTTTG
Sfpi1		
	sfpi1for	CCCAAGGGGACTATCTCCCA
	sfpi1rev	TGTCGAGCCTGAGAGGGG
Mafb		
	mafbfor	TTGGCTAAGAAGAGGGCAGC
	mafbrev	TTCCTTAGCTCAGCCTTGCC
Cd14		
	cd14for	ACTGAAGCCTTTCTCGGAGC
	cd14rev	AAGCACACGCTCCATGGTC
Il10		
	il10for	CAGAGAAGCATGGCCCAGAA
	il10rev	GACACCTTGGTCTTGGAGCTTA
Tgfb		
	tgfbfor	GCTGAACCAAGGAGACGGAA
	tgfbrev	ATGTCATGGATGGTGCCCAG
Tnfa		
	tnfafor	CCCTCACACTCAGATCATCTTCT
	tnfarev	GCTACGACGTGGGCTACAG
Cd68		
	cd68for	TTACCTTTGGATTCAAACAGGACC
	cd68rev	GAGGCAGCAAGAGGGACTG

Supplementary QuantSeq Data of the PVT. Corresponding to Fig. 3c.

Ensembl ID	diff	lwr	upr	p.adj	external_ger
ENSMUSG00000062393.13	-9.1902232	-10.969512	-7.410934	4.12E-08	Dgkk
ENSMUSG00000075590.2	1.63400261	0.93075942	2.3372458	0.00011493	Nrbp2
ENSMUSG00000021258.9	1.3799642	0.69122751	2.0687009	0.0004224	Ccnk
ENSMUSG00000102990.1	-7.14378	-9.12013	-5.1674301	1.63E-06	Gm37764
ENSMUSG00000034839.5	0.98142587	0.05294042	1.90991132	0.03755739	Larp6
ENSMUSG00000098905.1	-9.1702681	-11.220953	-7.119583	1.82E-07	Zfp953
ENSMUSG00000010538.14	-7.3013634	-9.2859287	-5.3167981	1.36E-06	Tsacc
ENSMUSG00000028082.13	-1.9440313	-2.8989155	-0.9891471	0.00036849	Sh3d19
ENSMUSG00000038121.6	-0.863599	-1.605057	-0.1221409	0.02182864	Fam210a
ENSMUSG00000037376.14	-1.5261407	-2.2828448	-0.7694366	0.00039938	Trmt6
ENSMUSG00000021520.4	2.6000043	1.49194416	3.70806443	0.00010515	Uqcrb
ENSMUSG00000024413.13	2.06122033	1.18228419	2.94015648	0.00010569	Npc1
ENSMUSG00000031701.6	-1.1808137	-1.7091713	-0.6524561	0.00016297	Dnaja2
ENSMUSG00000106691.1	-6.1956007	-8.5643589	-3.8268426	3.86E-05	2700029L08F
ENSMUSG00000108194.1	-8.0423081	-10.346274	-5.738342	2.32E-06	1700097M23
ENSMUSG00000035011.15	-0.3037901	-0.5751115	-0.0324687	0.02739306	Zbtb7a
ENSMUSG00000056708.5	1.40608956	0.56247357	2.24970555	0.00188881	Ier5
ENSMUSG00000105270.1	-6.907755	-9.3523359	-4.463174	1.85E-05	Gm42863
ENSMUSG00000025959.13	1.08621855	0.24506883	1.92736827	0.01156818	Klf7
ENSMUSG00000019689.4	2.43579701	1.2954561	3.57613791	0.00024304	Fmc1
ENSMUSG00000097479.1	-0.904214	-1.4501729	-0.3582552	0.00198365	Gm26582
ENSMUSG00000019777.16	-0.9701305	-1.6953137	-0.2449474	0.00918467	Hdac2
ENSMUSG00000024735.13	-0.51007	-0.7849737	-0.2351664	0.00080311	Prpf19
ENSMUSG00000026109.14	-2.3771148	-3.3916768	-1.3625528	0.00010657	Tmeff2
ENSMUSG00000064247.14	-1.6550233	-2.6500542	-0.6599924	0.00191932	Plcxd1
ENSMUSG00000074909.4	-0.8997635	-1.7578112	-0.0417158	0.03917823	Ranbp6
ENSMUSG00000021065.15	-7.0165049	-9.5137284	-4.5192813	1.95E-05	Fut8
ENSMUSG00000078591.1	-2.0040411	-3.0832651	-0.9248171	0.00079788	Hs3st4
ENSMUSG00000106702.1	2.43002927	1.22086407	3.63919447	0.00041167	Gm42846
ENSMUSG00000032251.12	-1.5842992	-2.5476405	-0.620958	0.00209383	Irak1bp1
ENSMUSG00000038740.9	2.05266381	0.88453883	3.22078879	0.00124703	Mvb12b
ENSMUSG00000031703.8	-1.1726677	-2.1194498	-0.2258857	0.01506018	Itfg1
ENSMUSG00000021087.17	-0.2898531	-0.5629019	-0.0168042	0.03671203	Rtn1
ENSMUSG00000082127.2	0.87639733	0.08573507	1.66705959	0.02898888	Gm13577
ENSMUSG00000109362.1	-6.8194269	-9.3129317	-4.3259221	2.53E-05	Gm44562
ENSMUSG00000038000.10	1.63245385	0.59421235	2.67069535	0.00294131	Acd
ENSMUSG00000027133.3	1.18736361	0.29544802	2.0792792	0.00948643	Nop10
ENSMUSG00000069495.12	-1.6866894	-2.7384864	-0.6348925	0.00253692	Epc2
ENSMUSG00000018770.9	1.5545885	0.47381237	2.63536463	0.00560088	Atp5g3
ENSMUSG00000073684.13	1.27406792	0.26526882	2.28286702	0.01333017	Faap20
ENSMUSG00000047843.16	0.76378327	0.16498747	1.36257908	0.01251814	Bri3
ENSMUSG00000020664.9	-1.2781038	-2.2816511	-0.2745565	0.01264041	Dld
ENSMUSG00000058318.15	0.62109581	0.10055817	1.14163346	0.01891645	Phf21a
ENSMUSG00000021413.8	-0.4770054	-0.8081903	-0.1458205	0.00554929	Prpf4b
ENSMUSG00000043284.12	1.22733013	0.19272356	2.26193671	0.01958496	Tmem11
ENSMUSG00000024603.7	-0.7234576	-1.2321612	-0.214754	0.00606288	Dctn4
ENSMUSG00000101671.1	1.32054426	0.38873335	2.25235517	0.00621228	Gm28221
ENSMUSG00000056050.12	-1.1198894	-2.0896536	-0.1501252	0.02294762	Mia3
ENSMUSG00000105361.1	0.20033087	0.05117675	0.34948499	0.00894494	AY036118
ENSMUSG00000024780.6	2.22488998	0.90934307	3.54043689	0.00168654	Cdc37l1
ENSMUSG00000029088.16	-1.5232445	-2.4054615	-0.6410274	0.00143363	Kcnip4
ENSMUSG00000030967.14	-1.3976763	-2.5082354	-0.2871173	0.01362822	Zranb1
ENSMUSG00000070498.3	-2.7311564	-4.9843828	-0.4779299	0.01719976	Tmem132b
ENSMUSG00000079614.3	-3.0097908	-5.0245886	-0.994993	0.00428091	Seh1l
ENSMUSG00000022000.10	-1.116854	-2.1956185	-0.0380896	0.04188803	Zc3h13
ENSMUSG00000057315.14	-2.3222423	-4.5886033	-0.0558812	0.04418888	Arhgap24
ENSMUSG00000027677.17	-1.2646546	-2.3737337	-0.1555756	0.02469087	Ttc14
ENSMUSG00000047921.15	-1.4458658	-2.5321797	-0.359552	0.00949903	Trappc9
ENSMUSG00000078440.9	0.47371824	0.06727746	0.88015902	0.02174114	Dohh
ENSMUSG00000033938.5	-0.5515067	-1.0076518	-0.0953615	0.0174653	Ndufb7
ENSMUSG00000022437.6	-0.7641956	-1.1270779	-0.4013133	0.00027512	Samm50
ENSMUSG00000022808.4	-1.6361222	-2.8998004	-0.3724441	0.01137493	Snx4
ENSMUSG00000026782.15	-0.8832514	-1.3201427	-0.4463601	0.00039127	Abi2
ENSMUSG00000097224.1	1.24201419	0.12466279	2.35936558	0.02853438	Gm26716
ENSMUSG00000029674.13	-1.1670034	-2.103195	-0.2308118	0.01447128	Limk1
ENSMUSG00000072692.7	0.65889452	0.11915684	1.19863219	0.01646793	Rpl37rt
ENSMUSG00000062203.14	-1.5759524	-2.7055333	-0.4463715	0.00692007	Gspt1
ENSMUSG00000027080.6	-1.884819	-3.1141276	-0.6555105	0.00354312	Med19
ENSMUSG00000039917.10	-0.5151421	-0.9157019	-0.1145823	0.01187764	Rhbdd2
ENSMUSG00000058558.12	1.27059155	0.03619038	2.50499272	0.04316712	Rpl5
ENSMUSG00000019659.8	1.59066768	0.45833873	2.72299662	0.00660137	Ccdc12
ENSMUSG00000008301.11	1.15231423	0.64810716	1.65652131	0.00013342	Phax
ENSMUSG00000013089.15	-1.1715616	-2.1990353	-0.1440878	0.02469579	Etv5
ENSMUSG00000054568.7	-1.7139258	-3.123607	-0.3042445	0.01688174	Usp17la
ENSMUSG00000103849.1	-5.8115998	-8.6608619	-2.9623376	0.00036263	Gm37806
ENSMUSG00000079557.10	-2.2386144	-3.3716934	-1.1055354	0.00047585	2-Mar
ENSMUSG00000034327.17	-2.1362343	-3.4020107	-0.8704579	0.00171432	Kctd9
ENSMUSG00000013367.5	-1.977456	-3.2728858	-0.6820262	0.00365942	Iglon5
ENSMUSG00000000346.8	3.20176679	1.68277835	4.72075523	0.00027294	Dazap2
ENSMUSG00000001472.17	-0.4994186	-0.8104459	-0.1883912	0.00251221	Tcf25
ENSMUSG00000028648.13	1.21774181	0.14891384	2.28656979	0.02480938	Ndufs5
ENSMUSG00000069020.9	-1.7420376	-3.1241127	-0.3599625	0.01349817	Urm1
ENSMUSG00000020476.14	-0.9930912	-1.5177857	-0.4683967	0.00068166	Dbnl
ENSMUSG00000023236.7	-0.6151814	-1.2135927	-0.0167701	0.04344836	Scg5
ENSMUSG00000019863.6	-2.7508179	-5.1761499	-0.3254858	0.02545812	Qrsl1
ENSMUSG00000059923.13	-0.3965078	-0.7086544	-0.0843613	0.01285208	Grb2
ENSMUSG00000041777.11	-1.3921366	-2.4841401	-0.3001332	0.01256108	Cir1
ENSMUSG00000062328.7	-0.6116795	-0.85603	-0.367329	5.81E-05	Rpl17
ENSMUSG00000010609.15	2.34604343	1.14832695	3.54375991	0.00051171	Psen2
ENSMUSG00000020738.16	2.30960092	1.02199664	3.5972052	0.00105758	Sumo2
ENSMUSG00000024824.6	-1.8863771	-3.1821697	-0.5905846	0.00514699	Rad9a
ENSMUSG00000027710.14	-2.3399038	-3.6235413	-1.0562664	0.00092817	Acad9
ENSMUSG00000034361.10	-2.168863	-3.4206428	-0.9170833	0.00139478	Cpne2
ENSMUSG00000018042.17	-0.689631	-1.313388	-0.0658741	0.02940471	Cyb5r3
ENSMUSG00000030652.11	-0.4608889	-0.7391717	-0.1826061	0.0019837	Coq7
ENSMUSG00000025428.15	-1.2300108	-2.0056478	-0.4543737	0.00275943	Atp5a1
ENSMUSG00000035601.9	-6.9890958	-10.360111	-3.6180805	0.00031501	Trmt10b
ENSMUSG00000015971.4	1.57621945	0.33984787	2.81259104	0.01255928	Actr8
ENSMUSG00000031157.10	-1.3436948	-2.3265316	-0.360858	0.00794274	Pqbp1
ENSMUSG00000029438.9	-1.6228044	-2.9818071	-0.2638017	0.01882791	Bcl7a
ENSMUSG00000045348.16	-2.8035975	-4.3013168	-1.3058782	0.00074683	Nyap1
ENSMUSG00000020964.14	-0.6057546	-1.0806675	-0.1308418	0.01251972	Sel1l
ENSMUSG00000031109.16	-2.178576	-3.4532272	-0.9039247	0.001553	Enox2
ENSMUSG00000029823.16	-1.3942009	-2.6410069	-0.1473949	0.02759408	Luc7l2

ENSMUSG00000052539.15	-1.2798442	-2.4848314	-0.074857	0.03660506	Magi3
ENSMUSG00000059479.7	-1.9459905	-3.1970828	-0.6948983	0.00318707	B3gnt8
ENSMUSG00000047067.7	-1.0653596	-2.1224002	-0.008319	0.04806846	Dusp28
ENSMUSG00000020238.14	-1.7995438	-3.0849001	-0.5141874	0.00675664	Ncln
ENSMUSG00000041986.15	1.68178222	0.58794555	2.77561889	0.00347149	Elmod1
ENSMUSG00000078681.10	0.50522016	0.08025928	0.93018103	0.01933185	Tm2d3
ENSMUSG00000009575.14	0.32536274	0.0424842	0.60824128	0.02348809	Cbx5
ENSMUSG00000027522.15	-2.0818749	-3.6547149	-0.509035	0.00985149	Stx16
ENSMUSG00000102474.1	-4.6490735	-7.5146642	-1.7834828	0.00232297	2610012C04I
ENSMUSG00000067148.15	-1.4988503	-2.7895224	-0.2081782	0.02220972	Polr1c
ENSMUSG00000039148.4	-1.6635861	-2.7612427	-0.5659294	0.00385587	Sart1
ENSMUSG00000032329.3	1.5779619	0.33296841	2.8229554	0.01303422	Hmg20a
ENSMUSG00000061313.8	-0.7167888	-1.4116589	-0.0219186	0.04268754	Ddhd2
ENSMUSG00000021221.15	-2.3315031	-4.6189367	-0.0440695	0.04540011	Dpf3
ENSMUSG00000004562.16	0.63203255	0.36688525	0.89717985	9.11E-05	Arhgef40
ENSMUSG00000059187.12	-3.0999484	-5.5936755	-0.6062213	0.01472318	Fam19a1
ENSMUSG00000040563.13	-1.6725569	-3.0543273	-0.2907866	0.01734415	Plppr2
ENSMUSG00000037940.16	1.76109072	0.62875099	2.89343044	0.0031896	Inpp4b
ENSMUSG00000031781.14	-1.4599127	-2.7829379	-0.1368875	0.02972402	Ciapin1
ENSMUSG00000007670.9	-1.8429265	-3.157717	-0.5281359	0.00670206	Khsrp
ENSMUSG00000035776.14	-0.9674451	-1.5661578	-0.3687325	0.00239494	Cd99l2
ENSMUSG00000026749.11	-1.8834227	-3.2498353	-0.5170101	0.00751581	Nek6
ENSMUSG00000003402.13	-1.8537808	-3.1955319	-0.5120297	0.0073968	Prkcsh
ENSMUSG00000047417.17	-1.2217847	-2.4222152	-0.0213543	0.04573761	Rexo1
ENSMUSG00000042303.16	-1.9706296	-3.4191416	-0.5221177	0.00821011	Sgsm3
ENSMUSG00000068856.3	-1.3715861	-2.2784415	-0.4647308	0.00391398	Sf3b4
ENSMUSG00000049881.13	-1.5317517	-2.4042095	-0.659294	0.00125586	2810025M15
ENSMUSG00000041341.9	-2.2035283	-3.5387248	-0.8683318	0.00203844	Atg2b
ENSMUSG00000071454.13	-1.7257965	-3.1918281	-0.2597649	0.02050146	Dtnb
ENSMUSG00000014551.8	0.73841782	0.30865276	1.16818288	0.00148996	Mrps25
ENSMUSG00000015942.9	-1.7567548	-3.0193261	-0.4941834	0.00704889	Gtf2ird2
ENSMUSG00000041096.13	-2.5581099	-4.0028387	-1.113381	0.00117348	Tspyl2
ENSMUSG00000062012.13	-1.5211639	-2.7807606	-0.2615671	0.01758859	Zfp13
ENSMUSG00000009647.13	2.61818686	0.98149032	4.2548834	0.00258455	Mcu
ENSMUSG00000024548.11	-1.7276527	-3.3062869	-0.1490184	0.03111388	Setbp1
ENSMUSG00000097910.2	-3.5324814	-6.2143899	-0.850573	0.01017412	5033428I22R
ENSMUSG00000019923.13	-1.1609674	-1.8350914	-0.4868434	0.00146293	Zwint
ENSMUSG00000085586.1	-3.0822559	-5.8190959	-0.3454159	0.02650465	Gm11613
ENSMUSG00000029815.12	-4.6335839	-7.4978192	-1.7693486	0.00237409	Malsu1
ENSMUSG00000021486.6	-1.7633968	-3.3280534	-0.1987402	0.02639683	Prelid1
ENSMUSG00000003444.8	-2.0561449	-3.3222193	-0.7900704	0.00230504	Med29
ENSMUSG00000031988.9	-1.7949522	-3.1153165	-0.4745879	0.00825133	Vps26b
ENSMUSG00000108956.1	-6.2207261	-9.5706727	-2.8707794	0.00079776	Gm45179
ENSMUSG00000027809.14	-2.8949636	-5.5462052	-0.243722	0.03150345	Etfdh
ENSMUSG00000009292.17	-1.51967	-2.9761525	-0.0631875	0.0402226	Trpm2
ENSMUSG00000000399.10	-1.7773061	-3.3138938	-0.2407184	0.02273454	Ndufa9
ENSMUSG00000021192.15	-7.0639365	-10.152894	-3.9749792	0.00013267	Golga5
ENSMUSG00000109506.1	-5.673983	-8.9736453	-2.3743207	0.0014806	Gm44724
ENSMUSG00000028207.18	-1.594806	-2.910647	-0.278965	0.01720875	Asph
ENSMUSG00000005575.16	-1.675046	-3.1046816	-0.2454105	0.02108019	Ube2m
ENSMUSG00000019189.13	1.89039344	0.17018394	3.61060294	0.03041092	Rnf145
ENSMUSG00000057554.13	-1.6846847	-2.97148	-0.3978894	0.01058386	Lgals8
ENSMUSG00000029993.16	-2.4567598	-4.0823595	-0.8311602	0.00393603	Nfu1
ENSMUSG00000027562.12	-1.5316364	-2.6292314	-0.4340413	0.00691049	Car2
ENSMUSG00000026944.18	-1.1682487	-2.1074998	-0.2289977	0.01467087	Abca2
ENSMUSG00000046020.13	-1.6571998	-2.9425291	-0.3718704	0.01168589	Pofut1
ENSMUSG00000063065.13	1.80083169	0.07295061	3.52871277	0.04045857	Mapk3
ENSMUSG00000056367.14	1.0897358	0.6059413	1.57353031	0.00015195	Actr3b
ENSMUSG00000016477.17	-1.7270208	-3.0492522	-0.4047895	0.01074665	E2f3
ENSMUSG00000052031.7	-1.6155337	-3.0538517	-0.1772157	0.02690838	Tagap1
ENSMUSG00000024472.9	-1.8531682	-3.4111134	-0.295223	0.01927045	Dcp2
ENSMUSG00000015829.13	-1.4133995	-2.8131031	-0.0136959	0.04760965	Tnr
ENSMUSG00000105083.1	-6.662964	-10.161084	-3.1648442	0.00064675	Gm42699
ENSMUSG00000067722.3	-1.5941967	-2.8061582	-0.3822352	0.01026382	BC003965
ENSMUSG00000004798.14	1.52995619	0.2388849	2.82102747	0.01970839	Ulk2
ENSMUSG00000085127.1	-4.4636928	-7.8014846	-1.125901	0.00920535	4930444E06I
ENSMUSG00000066643.12	-1.7298573	-2.8093428	-0.6503718	0.00255062	Wdr35
ENSMUSG00000062906.12	-7.3238637	-10.910486	-3.7372411	0.00035913	Hdac10
ENSMUSG00000001774.7	-1.759578	-3.4102073	-0.1089487	0.0358969	Chordc1
ENSMUSG00000087352.1	-1.2212836	-2.3898599	-0.0527073	0.03987633	Gm12999
ENSMUSG00000068205.14	-1.3429054	-2.4796384	-0.2061725	0.02007429	Macrod2
ENSMUSG00000023456.14	-1.0589852	-1.7416983	-0.3762722	0.00325286	Tpi1
ENSMUSG00000009739.16	-1.6539799	-3.0541588	-0.2538009	0.02008537	Pou6f1
ENSMUSG00000025551.13	-4.9946737	-8.237933	-1.7514144	0.00343013	Fgf14
ENSMUSG00000037234.17	-0.595835	-0.9928047	-0.1988653	0.00413663	Hook3
ENSMUSG00000041921.16	-2.0081892	-3.6330112	-0.3833672	0.01526069	Metap1d
ENSMUSG00000063511.11	-1.1225286	-1.9655544	-0.2795029	0.00947251	Snrnp70
ENSMUSG00000028876.7	-1.423883	-2.6829486	-0.1648175	0.02588482	Epha10
ENSMUSG00000028788.14	0.35894445	0.12289018	0.59499872	0.00376408	Ptp4a2
ENSMUSG00000033569.17	-1.6714648	-3.0063087	-0.3366208	0.01406855	Adgrb3
ENSMUSG00000024019.17	-0.4430392	-0.817247	-0.0688314	0.01981673	Cmtr1
ENSMUSG00000023030.16	-1.7388135	-3.271815	-0.205812	0.02545149	Slc11a2
ENSMUSG00000020124.9	-1.4506069	-2.6602594	-0.2409544	0.01835318	Usp15
ENSMUSG00000055240.16	-2.1176685	-3.5085975	-0.7267396	0.00373025	Zfp101
ENSMUSG00000034973.16	-1.6034281	-3.1656918	-0.0411644	0.04381519	Dopey1
ENSMUSG00000025521.15	-3.1118075	-4.9087195	-1.3148954	0.00140034	Tmem192
ENSMUSG00000023143.10	-1.9340851	-3.396411	-0.4717591	0.00990209	Nagpa
ENSMUSG00000023990.18	-1.3619006	-2.1472571	-0.5765441	0.0013853	Tfeb
ENSMUSG00000027692.16	-1.6298336	-2.9909173	-0.26875	0.01851445	Tnik
ENSMUSG00000026568.6	-1.2057147	-2.3186121	-0.0928173	0.0328861	Mpc2
ENSMUSG00000037890.13	-3.0904263	-5.9272963	-0.2535562	0.03191059	Wdr19
ENSMUSG00000021578.16	-1.3426648	-2.5884176	-0.096912	0.03382814	Ccdc127
ENSMUSG00000022884.14	1.25023105	0.00887143	2.49159067	0.04824296	Eif4a2
ENSMUSG00000033943.15	-1.4761889	-2.8496761	-0.1027017	0.03434645	Mga
ENSMUSG00000037826.5	-1.181642	-2.3596843	-0.0035996	0.04924124	Ppm1k
ENSMUSG00000091542.1	-7.8855312	-11.95569	-3.8153725	0.00056112	Gm17167
ENSMUSG00000020312.11	-4.106307	-7.0871718	-1.1254422	0.00754603	Shc2
ENSMUSG00000008140.17	-0.5234224	-0.9562118	-0.090633	0.01743406	Emc10
ENSMUSG00000024392.17	-1.9843111	-3.3398692	-0.628753	0.00494947	Bag6
ENSMUSG00000039860.19	-0.4346919	-0.8566582	-0.0127255	0.04298557	Srrm3
ENSMUSG00000046058.7	1.43788368	0.00707826	2.8686891	0.04877721	Eid2
ENSMUSG00000021113.4	-2.747043	-4.4926637	-1.0014224	0.00292252	Snapc1
ENSMUSG00000022339.8	-1.3389218	-2.5838885	-0.0939552	0.03422669	Ebag9
ENSMUSG00000040028.10	-3.1805271	-5.1121386	-1.2489157	0.0020746	Elavl1
ENSMUSG00000026860.16	-1.6664459	-3.2382621	-0.0946296	0.03696018	Sh3glb2

ENSMUSG00000064302.13	-2.255917	-3.748502	-0.763332	0.00393373	Clasp1
ENSMUSG00000002524.15	-0.9576352	-1.6106042	-0.3046661	0.00488385	Puf60
ENSMUSG00000028890.13	-1.6671846	-3.0469354	-0.2874338	0.01753004	Mtf1
ENSMUSG00000019876.15	-4.677482	-8.0388751	-1.316089	0.00704472	Pkib
ENSMUSG00000029670.12	-1.5741212	-3.1459882	-0.0022542	0.04964248	Ing3
ENSMUSG00000063801.7	-1.2161666	-2.2912516	-0.1410816	0.02584263	Ap3s2
ENSMUSG00000021468.7	-1.5144073	-2.8873555	-0.1414591	0.02978886	Sptlc1
ENSMUSG00000009927.8	0.85668175	0.13681638	1.57654713	0.01921594	Rps25
ENSMUSG00000047592.17	-5.1742663	-8.2611696	-2.0873631	0.00180781	Nxpe5
ENSMUSG00000006519.11	-5.9548186	-9.4666155	-2.4430217	0.00165243	Cyba
ENSMUSG00000021647.6	-5.7614446	-9.0385179	-2.4843712	0.00124207	Cartpt
ENSMUSG00000031168.14	-1.4084718	-2.7706427	-0.0463008	0.04216625	Ebp
ENSMUSG00000005410.6	-4.1805343	-7.3399708	-1.0210978	0.00987356	Mcm5
ENSMUSG00000043542.12	-1.5007202	-2.8752639	-0.1261766	0.03152445	Zc2hc1a
ENSMUSG00000042203.7	-1.772648	-3.0366019	-0.5086942	0.00667665	Tbc1d22b
ENSMUSG00000029434.12	-1.6836893	-3.0789742	-0.2884044	0.01767365	Vps33a
ENSMUSG00000057716.6	-1.3650604	-2.5843286	-0.1457921	0.0274062	Tmem178b
ENSMUSG00000089824.10	1.80867494	0.52996257	3.0873873	0.00629583	Rbm12
ENSMUSG00000041229.15	-3.8828248	-6.8172601	-0.9483894	0.0098734	Phf8
ENSMUSG00000028618.11	1.78341888	0.139858	3.42697976	0.03260683	Tmem59
ENSMUSG00000009995.17	-2.1724677	-3.8643941	-0.4805413	0.01199885	Taz
ENSMUSG00000060038.14	-2.4723895	-4.2350544	-0.7097245	0.00667075	Dhps
ENSMUSG00000028849.17	-1.5719811	-2.9232443	-0.2207179	0.02198185	Map7d1
ENSMUSG00000062591.5	-0.7238759	-1.2241613	-0.2235905	0.00537313	Tubb4a
ENSMUSG00000039849.5	-1.6025861	-3.1335671	-0.0716052	0.03954357	Pcif1
ENSMUSG00000050538.8	-1.9682181	-3.3532356	-0.5832005	0.006095	B230217C12
ENSMUSG00000015291.10	-1.88653	-3.232175	-0.540885	0.00669339	Gdi1
ENSMUSG00000023032.12	-1.7879039	-3.2962477	-0.2795602	0.01967728	Slc4a8
ENSMUSG00000020235.16	-1.6267879	-3.0528837	-0.2006921	0.02463448	Fzr1
ENSMUSG00000075376.10	-1.7310133	-3.1317823	-0.3302443	0.01527484	Rc3h2
ENSMUSG00000026307.12	-5.4110897	-8.8908657	-1.9313138	0.00319349	Scly
ENSMUSG00000096257.2	-6.4415177	-9.9368893	-2.9461461	0.00084914	Ccer2
ENSMUSG00000057858.7	-2.3835227	-4.1556875	-0.611358	0.00886276	Fam204a
ENSMUSG00000098183.1	1.00194263	0.00530555	1.9985797	0.04868537	Gm27010
ENSMUSG00000034109.15	-2.1644258	-3.7173523	-0.6114992	0.00696758	Golim4
ENSMUSG00000027895.9	-2.0579452	-3.5589175	-0.5569729	0.00779087	Kcnc4
ENSMUSG00000036769.14	-7.0203656	-10.841208	-3.199523	0.00087007	Wdr44
ENSMUSG00000030330.15	-1.7128637	-3.0988688	-0.3268585	0.0152696	Ing4
ENSMUSG00000033335.17	-2.3027727	-4.1052829	-0.5002624	0.01239348	Dnm2
ENSMUSG00000053600.7	-6.1756031	-9.8641869	-2.4870194	0.00182422	Zfp472
ENSMUSG00000041141.7	-1.8346174	-3.4089216	-0.2603131	0.02176054	Pnmal1
ENSMUSG00000074093.4	-1.5384197	-2.9362015	-0.1406379	0.03015409	Svip
ENSMUSG00000015937.14	-1.588526	-2.9509573	-0.2260947	0.02169508	H2afy
ENSMUSG00000027566.14	0.38433079	0.0495216	0.71913998	0.02375892	Psma7
ENSMUSG00000028873.16	-6.1328017	-9.9393919	-2.3262115	0.00244926	Cdca8
ENSMUSG00000036893.17	-2.2800491	-3.9661623	-0.5939358	0.00854956	Ehmt1
ENSMUSG00000039994.15	-3.2743314	-4.9351048	-1.613558	0.00048433	Timeless
ENSMUSG00000010277.7	-1.5812333	-3.0403542	-0.1221124	0.0328385	2610507B11
ENSMUSG00000030987.5	-0.6673747	-1.2346377	-0.1001118	0.02057455	Stim1
ENSMUSG00000049047.11	-2.2272419	-3.8539174	-0.6005665	0.00786327	Armcx3
ENSMUSG00000003500.13	-1.8502141	-3.2994364	-0.4009917	0.01244569	Impdh1
ENSMUSG00000043346.8	-3.1327234	-4.8799061	-1.3855408	0.00106094	Gm6741
ENSMUSG00000021027.15	-1.4281467	-2.778507	-0.0777864	0.0374468	Ralgapa1
ENSMUSG00000047264.8	-1.6114369	-3.0329145	-0.1899593	0.02553104	Zfp358
ENSMUSG00000074884.12	-2.5848248	-4.4641306	-0.7055191	0.00762602	Serf2
ENSMUSG00000054387.13	-1.7182205	-3.2696789	-0.166762	0.02912761	Mdm4
ENSMUSG00000025016.10	-0.8580702	-1.4409756	-0.2751647	0.0047561	Tm9sf3
ENSMUSG00000060216.15	-1.5978028	-3.0507401	-0.1448655	0.03029266	Arrb2
ENSMUSG00000031708.16	-0.4298013	-0.8036732	-0.0559293	0.02355806	Tecr
ENSMUSG00000049760.5	-0.8785534	-1.6127556	-0.1443512	0.01859312	2410015M2
ENSMUSG00000007850.16	-2.2869927	-4.097417	-0.4765684	0.01331147	Hnrnph1
ENSMUSG00000073664.11	-0.9908812	-1.9438919	-0.0378704	0.04096633	Nbeal1
ENSMUSG00000020794.13	-5.5494186	-9.8054652	-1.2933719	0.01086769	Ube2g1
ENSMUSG00000032497.15	-2.3632302	-4.0980856	-0.6283749	0.00813929	Lrrfip2
ENSMUSG00000049957.14	-2.3580292	-4.2339247	-0.4821336	0.01373218	Ccdc137
ENSMUSG00000022210.6	1.34641444	0.03794643	2.65488246	0.04323597	Dhrs4
ENSMUSG00000038806.7	-1.7305223	-3.0335619	-0.4274828	0.0096375	Sde2
ENSMUSG00000027363.15	-1.6011218	-3.005833	-0.1964106	0.02474715	Usp8
ENSMUSG00000032870.8	-1.8822882	-3.2396635	-0.5249129	0.00721358	Smap2
ENSMUSG00000021650.6	-1.6271989	-2.9843931	-0.2700048	0.01837623	Ptcd2
ENSMUSG00000060098.11	-2.5012141	-4.2526506	-0.7497776	0.00588967	Prmt7
ENSMUSG00000022295.7	-1.8586386	-3.4496184	-0.2676588	0.02144679	Atp6v1c1
ENSMUSG00000038668.14	-0.7162402	-1.427642	-0.0048385	0.04832644	Lpar1
ENSMUSG00000011751.16	-2.0577809	-3.6252992	-0.4902626	0.01039846	Sptbn4
ENSMUSG00000105753.1	-1.6776056	-3.3178312	-0.03738	0.04460478	Gm43847
ENSMUSG00000032537.14	-1.9190167	-3.6708977	-0.1671358	0.03095647	Ephb1
ENSMUSG00000053293.9	-7.5096316	-11.6129	-3.4063629	0.0008985	Pom121
ENSMUSG00000052676.16	-2.1006826	-3.5672569	-0.6341083	0.0057679	Zmat1
ENSMUSG00000025439.5	-1.4309814	-2.7073792	-0.1545836	0.02719486	Clns1a
ENSMUSG00000038451.13	-2.2418433	-3.9387981	-0.5448884	0.00997666	Spsb2
ENSMUSG00000067870.5	-4.7136065	-8.3405568	-1.0866561	0.01110199	Rpl31-ps8
ENSMUSG00000037710.8	-1.7182502	-3.3344526	-0.1020478	0.03641805	Cisd1
ENSMUSG00000054237.5	-2.2631886	-4.230084	-0.2962933	0.02343433	Fra10ac1
ENSMUSG00000086841.1	1.85496689	0.1005465	3.60938728	0.03750219	2410006H16
ENSMUSG00000037032.16	-0.6097075	-1.1875832	-0.0318318	0.03792452	Apbb1
ENSMUSG00000097312.1	-3.5383994	-7.0164763	-0.0603225	0.04583983	Gm26870
ENSMUSG00000026617.16	-1.6733332	-3.3403835	-0.0062828	0.04906577	Bpnt1
ENSMUSG00000030647.8	1.47238074	0.02156493	2.92319656	0.04641321	Ndufc2
ENSMUSG00000038365.8	-2.7585244	-4.5867035	-0.9303452	0.00398174	Fbxo25
ENSMUSG00000047989.11	0.63610971	0.18793767	1.08428174	0.00614694	Ino80c
ENSMUSG00000026238.14	-0.5595081	-1.113461	-0.0055551	0.04755165	Ptma
ENSMUSG00000036782.13	0.90267798	0.30356004	1.50179592	0.00402434	Klhl13
ENSMUSG00000024962.13	-1.5822375	-2.8949336	-0.2695413	0.01779531	Vegfb
ENSMUSG00000006024.13	-1.4959827	-2.8990401	-0.0929254	0.03585603	Napa
ENSMUSG00000041645.13	-0.3683744	-0.6811209	-0.0556279	0.02043143	Ddx24
ENSMUSG00000032393.14	-2.1720261	-3.7207035	-0.6233487	0.0066753	Dpp8
ENSMUSG00000068747.14	-1.8142767	-3.3705844	-0.2579689	0.02171611	Sort1
ENSMUSG00000034958.11	-0.9427228	-1.6615199	-0.2239257	0.01046251	Atcay
ENSMUSG00000049252.17	-2.1138315	-3.9173672	-0.3102958	0.02103893	Lrp1b
ENSMUSG00000030811.14	-0.9463577	-1.8205129	-0.0722024	0.03301967	Fbxl19
ENSMUSG00000082519.1	-7.3613892	-11.21432	-3.5084584	0.00063041	Vamp7-ps
ENSMUSG00000097730.3	-4.1302483	-7.6207484	-0.6397483	0.01988228	Gm26588
ENSMUSG00000027835.11	-1.5415382	-2.9572622	-0.1258142	0.03199265	Pdcd10
ENSMUSG00000051166.9	-1.7541433	-3.3001573	-0.2081293	0.02540422	Eml5
ENSMUSG00000031667.16	-2.0003095	-3.5735607	-0.4270583	0.01277604	Aktip

ENSMUSG00000069892.9	-5.8768039	-9.2576192	-2.4959885	0.00135925	9930111J21R
ENSMUSG00000062098.11	-0.4228672	-0.8336113	-0.0121231	0.04312452	Btbd3
ENSMUSG00000024942.16	-1.8210011	-3.1822633	-0.4597389	0.00918664	Capn1
ENSMUSG00000032101.6	-2.0967153	-3.8253879	-0.3680426	0.01713117	Ddx25
ENSMUSG00000038909.16	-1.603991	-3.1611058	-0.0468762	0.04299705	Kat7
ENSMUSG00000037916.13	-1.6521767	-3.2557053	-0.0486482	0.04294664	Ndufv1
ENSMUSG00000020098.6	-7.5177276	-11.258975	-3.7764804	0.00041212	Pcbd1
ENSMUSG00000024431.14	-1.6746299	-3.0129451	-0.3363147	0.01413086	Nr3c1
ENSMUSG00000028741.13	-1.8258448	-3.4628431	-0.1888466	0.02799425	Mrto4
ENSMUSG00000027665.13	-1.1708274	-1.9850777	-0.3565771	0.00561398	Pik3ca
ENSMUSG00000040479.11	0.64485344	0.05021009	1.23949678	0.03271495	Dgkz
ENSMUSG00000020721.16	-1.6448186	-3.2572808	-0.0323565	0.04521821	Helz
ENSMUSG00000093445.7	-6.7188738	-10.575473	-2.8622749	0.00133534	Lrch4
ENSMUSG00000034488.14	-0.879959	-1.5758146	-0.1841034	0.01322287	Edil3
ENSMUSG00000029557.7	-1.6886199	-3.3565306	-0.0207093	0.04698607	Mrm2
ENSMUSG00000038527.9	-6.9409126	-10.820182	-3.061643	0.00107914	C1rl
ENSMUSG00000029344.14	-6.1649492	-10.266493	-2.0634056	0.0040946	Tpst2
ENSMUSG00000025545.9	-2.1563952	-4.1402519	-0.1725386	0.0323	Clybl
ENSMUSG00000027957.13	-7.5949395	-11.445405	-3.7444735	0.00048246	Slc35a3
ENSMUSG00000032297.11	-1.8093874	-3.4282478	-0.190527	0.02766733	Celf6
ENSMUSG00000039419.17	-1.7811527	-3.2721802	-0.2901252	0.0187838	Cntnap2
ENSMUSG00000024474.5	-1.7515275	-3.3156867	-0.1873683	0.02737651	Ik
ENSMUSG00000032609.12	-2.5304299	-4.4168264	-0.6440333	0.00902073	Klhdc8b
ENSMUSG00000105679.1	-5.7047639	-9.6045486	-1.8049792	0.00497335	Gm43338
ENSMUSG00000027782.10	-2.3365159	-4.1601665	-0.5128654	0.01216707	Kpna4
ENSMUSG00000057176.4	-1.6290466	-3.2277511	-0.030342	0.04546546	Ccdc189
ENSMUSG00000021103.12	-1.4515934	-2.8335557	-0.069631	0.03883138	Mnat1
ENSMUSG00000024516.12	-0.7962352	-1.3817084	-0.210762	0.008229	Sec11c
ENSMUSG00000102935.1	4.1819784	0.28219498	8.08176181	0.03476625	Gm38355
ENSMUSG00000040249.15	-1.9744225	-3.6543664	-0.2944787	0.02069831	Lrp1
ENSMUSG00000039740.6	-2.5387284	-4.3457896	-0.7316672	0.00659755	Alg2
ENSMUSG00000052296.7	-1.6443228	-3.1667964	-0.1218493	0.03344869	Ppp6r1
ENSMUSG00000034175.13	-2.2580421	-4.0229238	-0.4931603	0.0122769	Rhbdd3
ENSMUSG00000021248.8	-1.7233918	-3.4133279	-0.0334557	0.04527935	Tmed10
ENSMUSG00000031683.16	0.58060595	0.1859705	0.9752414	0.00477481	Lsm6
ENSMUSG00000030255.13	-1.7018539	-3.2109963	-0.1927115	0.02630683	Sspn
ENSMUSG00000039041.15	-1.6559177	-3.1547806	-0.1570548	0.02952737	Adrm1
ENSMUSG00000021460.16	-2.7706823	-4.7469728	-0.7943919	0.0066931	Auh
ENSMUSG00000106411.1	-2.6427961	-4.7052745	-0.5803176	0.01215863	Gm42445
ENSMUSG00000031753.16	-1.113016	-2.0237114	-0.2023206	0.01635322	Cog4
ENSMUSG00000076439.12	-5.1035328	-8.6771447	-1.529921	0.005889	Mog
ENSMUSG00000041354.15	-4.5687234	-8.14481	-0.9926369	0.01239101	Rgl2
ENSMUSG00000063687.3	-6.2920662	-10.351585	-2.2325469	0.00327134	Pcdhb5
ENSMUSG00000024067.13	-7.9336369	-12.137191	-3.7300825	0.0006978	Dpy30
ENSMUSG00000001020.8	-5.0815115	-9.5486028	-0.6144203	0.02503303	S100a4
ENSMUSG00000035198.9	-1.6270958	-3.058273	-0.1959186	0.02511522	Tubg1
ENSMUSG00000021938.11	-2.7679252	-4.4896743	-1.0461762	0.00248964	Pspc1
ENSMUSG00000034390.16	-1.5599854	-3.0950192	-0.0249516	0.04609077	Cmip
ENSMUSG00000042671.12	-1.9514432	-3.7982531	-0.1046333	0.0376258	Rgs8
ENSMUSG00000026463.17	-2.2985002	-4.0739127	-0.5230876	0.01138068	Atp2b4
ENSMUSG00000079442.12	-1.8928099	-3.492575	-0.2930447	0.01989257	St6galnac4
ENSMUSG00000053550.13	-2.1248636	-4.0156587	-0.2340684	0.02682939	Shisa7
ENSMUSG00000046056.15	-1.7250094	-3.2924649	-0.1575539	0.03016919	Sbsn
ENSMUSG00000048070.4	-5.9968577	-10.052636	-1.9410796	0.00460796	Pirt
ENSMUSG00000026977.17	-1.769219	-3.3337266	-0.2047113	0.02589233	7-Mar
ENSMUSG00000033439.12	-5.3845148	-10.176354	-0.5926755	0.02684417	Trmt13
ENSMUSG00000038608.15	-1.6528601	-3.1944904	-0.1112298	0.03480319	Dock10
ENSMUSG00000034401.16	-4.9946265	-9.5817634	-0.4074896	0.03199845	Spata6
ENSMUSG00000057841.5	-1.8493052	-3.4283473	-0.270263	0.02113366	Rpl32
ENSMUSG00000041629.7	-1.6835541	-3.1842901	-0.182818	0.02709776	Fam104a
ENSMUSG00000003452.15	-2.0953259	-3.9650241	-0.2256277	0.02725432	Bicd1
ENSMUSG00000051616.14	-7.6209853	-11.682269	-3.5597015	0.00073191	C230029F24I
ENSMUSG00000022756.15	-2.2302732	-4.216171	-0.2443754	0.02692941	Slc7a4
ENSMUSG00000021242.8	-0.5401222	-1.0755795	-0.004665	0.04786615	Npc2
ENSMUSG00000108189.1	-5.5699009	-10.445107	-0.694695	0.02441607	Gm43887
ENSMUSG00000039671.18	-0.8699603	-1.7240048	-0.0159157	0.04554382	Zmynd8
ENSMUSG00000003929.10	-1.9149584	-3.29094	-0.5389768	0.00703875	Zfp81
ENSMUSG00000012126.16	-2.1370109	-3.4824132	-0.7916087	0.00272607	Ubxn11
ENSMUSG00000075316.11	-1.802836	-3.3644609	-0.2412111	0.02298746	Scn9a
ENSMUSG00000002983.17	-4.8652215	-9.6071558	-0.1232871	0.04389219	Relb
ENSMUSG00000066697.3	-4.7743226	-8.6355851	-0.9130602	0.01522076	Gm10172
ENSMUSG00000025393.12	-0.5451124	-1.0355854	-0.0546394	0.02855861	Atp5b
ENSMUSG00000005362.14	-1.7017925	-3.2953137	-0.1082712	0.03554801	Crbn
ENSMUSG00000002496.9	-1.8583119	-3.4936935	-0.2229303	0.02518827	Tsc2
ENSMUSG00000028165.9	-2.8737696	-4.9970053	-0.7505339	0.00849755	Cisd2
ENSMUSG00000027285.13	-1.8388657	-3.4785472	-0.1991842	0.02714445	Haus2
ENSMUSG00000004360.8	-1.985609	-3.6402001	-0.331018	0.01827334	9330159F19I
ENSMUSG00000024208.15	-1.5103796	-2.795513	-0.2252461	0.02070042	Uqcc2
ENSMUSG00000057963.9	-1.8042998	-3.4049016	-0.203698	0.02636426	Itpk1
ENSMUSG00000048218.5	-1.7238389	-3.4371169	-0.010561	0.04848085	Amigo2
ENSMUSG00000092416.2	-6.3586943	-11.539033	-1.1783559	0.01592351	Zfp141
ENSMUSG00000024713.15	-2.1649101	-3.8780277	-0.4517924	0.01327893	Pcsk5
ENSMUSG00000034681.16	-1.7499985	-3.2741698	-0.2258273	0.02372853	Rnps1
ENSMUSG00000068290.11	-1.8585729	-3.6348836	-0.0822623	0.03963513	Ddrgk1
ENSMUSG00000002320.15	-4.8420106	-8.3756858	-1.3083355	0.0078227	Tm9sf1
ENSMUSG00000023723.17	-1.604115	-3.18058	-0.0276499	0.04579491	Mrps23
ENSMUSG00000048807.2	-1.6289026	-3.0341452	-0.22366	0.02244965	Slc35e4
ENSMUSG00000003809.14	-5.4681587	-9.7411111	-1.1952063	0.01225946	Gcdh
ENSMUSG00000002015.5	-1.9485655	-3.4768367	-0.4202943	0.01255064	Bcap31
ENSMUSG00000034755.18	-4.4962477	-7.7477802	-1.2447152	0.0073534	Pcdh11x
ENSMUSG00000022108.7	-0.8853059	-1.429838	-0.3407739	0.00228591	Itm2b
ENSMUSG00000086604.2	-5.5373909	-9.7798216	-1.2949601	0.01079494	Gm15510
ENSMUSG00000054942.13	-1.5750041	-3.1087916	-0.0412166	0.04370029	Miga1
ENSMUSG00000067194.6	-1.9313731	-3.537483	-0.3252633	0.01804913	Eif1ax
ENSMUSG00000020300.14	-2.4413132	-4.1246605	-0.7579659	0.00528636	Cpeb4
ENSMUSG00000038486.9	-0.3496421	-0.6781839	-0.0211002	0.03622005	Sv2a
ENSMUSG00000035596.14	-0.7800558	-1.3344089	-0.2257027	0.0065251	Mboat7
ENSMUSG00000038390.11	-0.9648736	-1.6532439	-0.2765034	0.00670239	Gpr162
ENSMUSG00000043866.11	0.60430696	0.06972855	1.13888537	0.02594596	Taf10
ENSMUSG00000026841.7	-2.2205759	-3.9425881	-0.4985637	0.01167397	Fibcd1
ENSMUSG00000055026.13	-2.4705795	-4.3139166	-0.6272425	0.00907152	Gabrg3
ENSMUSG00000106948.1	-6.1164593	-10.481236	-1.751682	0.0067141	Gm42785
ENSMUSG00000007944.8	-2.0140191	-3.618937	-0.4091011	0.01387797	Ttc9b
ENSMUSG00000022962.14	-5.6889202	-9.5907383	-1.7871021	0.00509113	Gart
ENSMUSG00000028329.13	-1.5267622	-2.9445451	-0.1089793	0.03398659	Xpa

ENSMUSG00000038122.8	-4.2499685	-7.559198	-0.9407389	0.01198347	Tbc1d32
ENSMUSG00000031201.17	-1.8152876	-3.3832648	-0.2473104	0.02261255	Brcc3
ENSMUSG00000085830.1	-1.7478938	-3.24285	-0.2529375	0.0213435	Grin1os
ENSMUSG00000030701.17	-1.9392236	-3.3996111	-0.4788361	0.00964625	Plekhb1
ENSMUSG00000028937.14	-0.5494176	-1.066783	-0.0320522	0.03663636	Acot7
ENSMUSG00000030619.9	-4.2067998	-7.5450695	-0.86853	0.01351689	Eed
ENSMUSG00000020496.8	-0.3623812	-0.7215863	-0.003176	0.04783511	Rnf187
ENSMUSG00000072572.8	-3.9019523	-6.2874075	-1.5164972	0.00218227	Slc39a2
ENSMUSG00000000131.15	-1.5784237	-3.0240602	-0.1327872	0.03151516	Xpo6
ENSMUSG00000041592.16	-3.8251912	-7.3967923	-0.2535901	0.0350051	Sdk2
ENSMUSG00000019809.16	-6.2538444	-10.640332	-1.8673569	0.0059587	Pex3
ENSMUSG00000001228.14	-4.8332986	-9.2390649	-0.4275323	0.03070237	Uhrf1
ENSMUSG00000019978.15	-2.6998521	-4.7984133	-0.6012908	0.01184984	Epb41l2
ENSMUSG00000033799.9	-6.1591037	-10.929485	-1.3887221	0.01158183	Fam208b
ENSMUSG00000037351.9	-1.9396695	-3.5087629	-0.370576	0.01524326	Actr1b
ENSMUSG00000038884.14	-1.1615136	-2.1173388	-0.2056884	0.01693528	A230050P20I
ENSMUSG00000032997.16	-2.0177768	-3.8920746	-0.1434789	0.03404059	Chpf
ENSMUSG00000033781.6	-4.3786807	-7.4359801	-1.3213813	0.00577264	Asb13
ENSMUSG00000046093.9	-1.7319351	-3.335294	-0.1285762	0.03342208	Hpcal4
ENSMUSG00000037503.12	1.56804396	0.11784014	3.01824778	0.03324314	Fam168b
ENSMUSG00000051111.15	-2.3313617	-4.4346513	-0.2280721	0.02898868	Sv2c
ENSMUSG00000020038.9	-2.2128807	-3.6035452	-0.8222163	0.0026895	Cry1
ENSMUSG00000110542.1	8.12907977	3.51580899	12.7423505	0.00121975	Gm39139
ENSMUSG00000031837.14	-1.7851924	-3.372592	-0.1977927	0.02672033	Necab2
ENSMUSG00000045777.14	-3.2794315	-4.8243528	-1.7345102	0.00025669	Ifitm10
ENSMUSG00000062995.12	-1.6946899	-3.302531	-0.0868488	0.03812888	Ica1
ENSMUSG00000025272.16	-2.0782903	-3.7867702	-0.3698103	0.01682836	Tro
ENSMUSG00000060904.14	-1.7892044	-3.3897069	-0.1887019	0.02763811	Arl1
ENSMUSG00000020706.13	-2.2027985	-4.0770866	-0.3285103	0.02070026	Ftsj3
ENSMUSG00000031885.14	-6.3980441	-9.8012593	-2.9948289	0.00072073	Cbfb
ENSMUSG00000098950.7	-1.4392592	-2.7030697	-0.1754487	0.02487189	Gm28036
ENSMUSG00000031832.15	-1.4204411	-2.5097523	-0.3311299	0.0108628	Taf1c
ENSMUSG00000021822.2	-1.7291399	-2.7033687	-0.754911	0.00115127	Plau
ENSMUSG00000075555.11	-1.2356342	-2.2001659	-0.2711025	0.0121767	Gm10863
ENSMUSG00000110540.1	-1.6160375	-2.8355128	-0.3965622	0.00977598	Gm45743
ENSMUSG00000105294.1	-1.1584919	-2.0286942	-0.2882895	0.0094846	Gm43304
ENSMUSG00000003348.9	-1.3154377	-2.18564	-0.4452353	0.0039294	Mob3a
ENSMUSG00000082088.1	-0.9964913	-1.8666937	-0.1262889	0.02409456	Gm15753
ENSMUSG00000108718.1	-1.403257	-2.2734594	-0.5330547	0.00243248	Gm44749
ENSMUSG00000030670.16	-2.5047906	-3.374993	-1.6345883	1.55E-05	Cyp2r1
ENSMUSG00000098014.1	-1.3226804	-2.1928828	-0.452478	0.00377552	Gm26967
ENSMUSG00000021490.10	-1.1337057	-2.1534455	-0.113966	0.02850707	Slc34a1
ENSMUSG00000109492.1	-0.3278947	-0.4774055	-0.178384	0.00019269	Gm33882
ENSMUSG00000034566.10	-0.6215879	-1.2096237	-0.0335522	0.03754981	Atp5h
ENSMUSG00000025169.6	-4.5449724	-7.9926937	-1.0972511	0.01011857	Ogfod3
ENSMUSG00000046364.14	0.31825097	0.02852866	0.60797329	0.03048197	Rpl27a
ENSMUSG00000029478.16	-1.8297074	-3.4323858	-0.227029	0.02451958	Ncor2
ENSMUSG00000087479.1	-4.1116528	-7.6208586	-0.6024471	0.02107841	Gm16835
ENSMUSG00000031654.16	-1.8397384	-3.5037147	-0.1757622	0.02940186	Cbln1
ENSMUSG00000034379.8	-4.7892992	-8.5940417	-0.9845567	0.01361208	Wdr5b
ENSMUSG00000025485.13	-1.7414697	-3.4070004	-0.075939	0.0397781	Ric8a
ENSMUSG00000027109.16	-2.0002986	-3.8000093	-0.2005879	0.02855081	Sp3
ENSMUSG00000022257.3	-1.6816448	-3.2505789	-0.1127106	0.03485787	Laptm4b
ENSMUSG00000030965.19	-2.3142559	-4.1632127	-0.465299	0.01410557	Abraxas2
ENSMUSG00000035754.7	-2.3698047	-4.4200905	-0.319519	0.02282825	Wdr18
ENSMUSG00000040640.10	-1.595433	-3.1309465	-0.0599195	0.0411138	Erc2
ENSMUSG00000022023.5	-0.9867472	-1.8094187	-0.1640757	0.01833018	Wbp4
ENSMUSG00000063063.12	-0.9091614	-1.7677032	-0.0506197	0.03719223	Ctnna2
ENSMUSG00000086944.1	-4.8863432	-9.3316062	-0.4410802	0.0303661	Gm15859
ENSMUSG00000029821.15	-2.133688	-3.7987229	-0.4686532	0.01215266	Gsdme
ENSMUSG00000044982.6	-2.2811964	-4.1630122	-0.3993805	0.0171892	Sft2d3
ENSMUSG00000056043.5	-5.5854678	-9.5190505	-1.6518851	0.00612888	Rgs9bp
ENSMUSG00000033769.16	-2.0278651	-3.968606	-0.0871242	0.03991876	Exoc6b
ENSMUSG00000034108.5	-4.9109842	-8.8738265	-0.9481419	0.01500928	Ccs
ENSMUSG00000031841.19	-2.7387482	-5.258417	-0.2190794	0.03230384	Cdh13
ENSMUSG00000078619.10	1.17466671	0.16363861	2.18569481	0.02214724	Smarcd2
ENSMUSG00000027263.12	-0.5320565	-1.0387589	-0.0253542	0.03889938	Tubgcp4
ENSMUSG00000033981.14	-0.5105374	-1.0207455	-0.0003293	0.0498388	Gria2
ENSMUSG00000032096.15	-1.7794747	-3.2352965	-0.3236529	0.01634045	Arcn1
ENSMUSG00000034210.13	-0.9388761	-1.6538455	-0.2239067	0.01037749	Efcab14
ENSMUSG00000028218.19	-1.8617158	-3.6315674	-0.0918642	0.03853581	Fam92a
ENSMUSG00000027593.15	-1.6638073	-3.2153383	-0.1122762	0.03476571	Raly
ENSMUSG00000068263.11	-5.7213417	-9.8337143	-1.6089692	0.00705442	Efcc1
ENSMUSG00000023328.14	-2.3462572	-4.110927	-0.5815875	0.00956572	Ache
ENSMUSG00000033773.14	-4.5651619	-8.0044202	-1.1259036	0.00967092	Rpap2
ENSMUSG00000027770.5	-1.8724971	-3.5511674	-0.1938268	0.02797972	Dhx36
ENSMUSG00000099893.1	-8.610855	-13.622411	-3.5992989	0.00148989	Gm29245
ENSMUSG00000063260.2	-7.4743256	-12.063454	-2.8851972	0.00225516	Syt10
ENSMUSG00000029462.18	-1.0621256	-1.8572413	-0.2670099	0.00927432	Vps29
ENSMUSG00000025026.14	-1.5063411	-2.8449975	-0.1676847	0.02663137	Add3
ENSMUSG00000105974.1	-5.8491531	-10.926932	-0.7713741	0.02328467	Gm43318
ENSMUSG00000022503.10	-3.9840872	-7.7014607	-0.2667137	0.03487386	Nubp1
ENSMUSG00000022442.15	-2.0602042	-3.9193378	-0.2010706	0.02903006	Ttll1
ENSMUSG00000027489.15	-2.5346008	-4.6333758	-0.4358257	0.01758879	Necab3
ENSMUSG00000091811.2	-2.0845762	-3.7979431	-0.3712093	0.01681154	Inafm1
ENSMUSG00000056214.8	-5.9998514	-10.270388	-1.7293146	0.00659602	Pard6g
ENSMUSG00000022552.15	-1.8072911	-3.5490508	-0.0655314	0.04140374	Sharpin
ENSMUSG00000004561.14	-5.6874089	-10.582207	-0.792611	0.02213881	Mettl17
ENSMUSG00000053877.12	-2.8174321	-4.7684755	-0.8663887	0.00544848	Srcap
ENSMUSG00000031482.9	-6.4606604	-10.887038	-2.0342824	0.00505262	Slc25a15
ENSMUSG00000000731.15	-5.3269803	-10.195448	-0.4585124	0.03114792	Aire
ENSMUSG00000028863.13	-1.6935603	-3.0199613	-0.3671593	0.0124386	Meaf6
ENSMUSG00000028518.8	-5.5950007	-9.9636391	-1.2263623	0.01219811	Prkaa2
ENSMUSG00000023017.9	-1.9060024	-3.7545451	-0.0574598	0.04278618	Asic1
ENSMUSG00000057497.8	-5.1817473	-9.2121494	-1.1513452	0.01190079	Fam136a
ENSMUSG00000025173.13	-1.0805479	-2.1085112	-0.0525845	0.03868162	Wdr45b
ENSMUSG00000029171.12	-7.1723762	-12.417692	-1.9270603	0.00793385	Pgm1
ENSMUSG00000027939.11	-5.4484443	-9.4666738	-1.4302148	0.00839546	Nup210l
ENSMUSG00000026019.15	-0.7081785	-1.3856827	-0.0306744	0.03984193	Wdr12
ENSMUSG00000022951.15	-1.5507022	-2.982948	-0.1184564	0.03300137	Rcan1
ENSMUSG00000004961.7	-1.8580415	-3.517536	-0.198547	0.02739659	Syt5
ENSMUSG00000038347.14	-7.3702092	-12.796129	-1.9442892	0.00829642	Tcte2
ENSMUSG00000029922.15	2.43287448	0.4892281	4.37652086	0.01410194	Mkrn1
ENSMUSG00000033460.14	-6.0052301	-10.143115	-1.8673448	0.00526054	Armcx1
ENSMUSG00000039307.16	-7.0858491	-11.495351	-2.6763476	0.00249754	Hexdc

ENSMUSG00000092286.1	-2.5447071	-4.3164513	-0.772963	0.00565927	Dtnbos
ENSMUSG00000084416.3	2.1494798	0.2276281	4.07133151	0.02756293	Rpl10a-ps1
ENSMUSG00000036537.6	-6.1420804	-10.513692	-1.770469	0.00659435	Rnf113a1
ENSMUSG00000049470.13	-1.8410372	-3.5918528	-0.0902216	0.03860832	Aff4
ENSMUSG00000063888.6	-1.4480448	-2.8772878	-0.0188018	0.04681244	Rpl7l1
ENSMUSG00000099960.1	-9.6468032	-14.612967	-4.6806395	0.00054887	Gm28590
ENSMUSG00000042401.6	-1.8191631	-3.6158653	-0.022461	0.04696608	Crtac1
ENSMUSG00000052544.9	-6.0683037	-11.007688	-1.1289196	0.01583685	St6galnac3
ENSMUSG00000038205.12	-1.9347807	-3.594249	-0.2753124	0.02170005	Prkab2
ENSMUSG00000078899.9	-1.9288286	-3.6867696	-0.1708876	0.03067614	Gm4631
ENSMUSG00000031808.7	-2.2647448	-4.443011	-0.0864786	0.04097395	Slc27a1
ENSMUSG00000021798.13	-7.2861879	-11.571898	-3.0004778	0.00161891	Ldb3
ENSMUSG00000031388.14	-4.9263668	-8.8816885	-0.9710452	0.01454685	Naa10
ENSMUSG00000039159.16	-1.1090383	-1.9546803	-0.2633962	0.0104653	Ube2h
ENSMUSG00000021905.13	-4.9093296	-8.7689774	-1.0496819	0.01274329	Dph3
ENSMUSG00000019338.13	-1.8223144	-3.5320194	-0.1126094	0.03592212	Zfp687
ENSMUSG00000039515.11	-2.1987687	-4.3716761	-0.0258613	0.04710738	Ptpa
ENSMUSG00000060181.5	0.75256867	0.14640862	1.35872871	0.01483901	Slc35e3
ENSMUSG00000026820.5	-1.9746304	-3.6306214	-0.3186394	0.01898939	Ptges2
ENSMUSG00000052512.17	-2.0182374	-3.9501857	-0.0862891	0.03996452	Nav2
ENSMUSG00000047945.6	-2.5169977	-4.4764512	-0.5575442	0.01196773	Marcksl1
ENSMUSG00000078653.4	0.80911384	0.00307301	1.61515467	0.04905505	Cntd1
ENSMUSG00000024457.16	-2.6275982	-4.9866127	-0.2685838	0.02820773	Trim26
ENSMUSG00000058070.14	-2.370285	-4.4096931	-0.3308769	0.02210401	Eml1
ENSMUSG00000022247.12	-2.2317052	-4.2021478	-0.2612626	0.02566577	Brix1
ENSMUSG00000040356.16	-5.2889024	-9.9376513	-0.6401535	0.02501276	Skiv2l
ENSMUSG00000020153.14	-0.7872466	-1.5523601	-0.0221331	0.04325178	Ndufs7
ENSMUSG00000032399.7	-0.5560698	-1.0618868	-0.0502528	0.03034699	Rpl4
ENSMUSG00000017764.2	-5.2012861	-9.095585	-1.3069873	0.00928339	Zswim1
ENSMUSG00000097290.8	4.87997462	0.61040437	9.14954488	0.02435822	1300002E11I
ENSMUSG00000032403.8	-2.4566636	-4.3179498	-0.5953773	0.01003747	2300009A05I
ENSMUSG00000049295.16	-4.9039788	-8.8685538	-0.9394037	0.01518398	Zfp219
ENSMUSG00000006906.10	-1.6308237	-3.2280275	-0.0336199	0.04499588	Stambp
ENSMUSG00000026571.12	-1.9259956	-3.695709	-0.1562821	0.03208301	Dcaf6
ENSMUSG00000031820.9	-1.6845374	-2.8609461	-0.5081288	0.00578034	Babam1
ENSMUSG00000094936.7	-6.5630523	-11.282182	-1.8439223	0.00707237	Rbm4
ENSMUSG00000053091.16	-6.2769395	-10.586594	-1.9672846	0.00512921	Lins1
ENSMUSG00000022858.15	-2.0643441	-3.9799191	-0.148769	0.03385049	Tra2b
ENSMUSG00000033128.8	-0.9653291	-1.7173342	-0.213324	0.01201961	Gga1
ENSMUSG00000083929.3	-4.810291	-8.8817332	-0.7388488	0.02006437	Gm10600
ENSMUSG00000043541.16	-7.5910645	-12.301698	-2.8804311	0.00244497	Casc1
ENSMUSG00000039509.8	-7.2989199	-12.066689	-2.5311508	0.00358312	Nup133
ENSMUSG00000026275.13	-0.739422	-1.4139628	-0.0648811	0.03083472	Ppp1r7
ENSMUSG00000039231.18	-6.1558236	-10.083186	-2.2284616	0.00301057	Suv39h1
ENSMUSG00000037270.18	-0.986761	-1.8439185	-0.1296036	0.02336813	4932438A13I
ENSMUSG00000027339.15	-1.3455825	-2.4669776	-0.2241873	0.01828639	Rassf2
ENSMUSG00000096188.1	-2.2650993	-3.9788708	-0.5513278	0.00994665	Cmtm4
ENSMUSG00000018451.6	-1.7491141	-3.3214963	-0.1767319	0.02841559	6330403K07I
ENSMUSG00000048108.13	-7.0079071	-12.206392	-1.809422	0.00872832	Tmem72
ENSMUSG00000031441.15	-2.5798965	-4.4288499	-0.730943	0.00691455	Atp11a
ENSMUSG00000003166.19	-2.3857809	-4.4491965	-0.3223653	0.0227837	Dgcr2
ENSMUSG00000034413.14	2.14008984	0.0616689	4.21851078	0.04309072	Neurl1b
ENSMUSG00000092641.2	-5.9349165	-10.61802	-1.2518128	0.01304346	Gm23563
ENSMUSG00000110711.1	2.65085367	0.55883733	4.74287001	0.01305491	Gm45760
ENSMUSG00000026491.13	-4.8464166	-8.7442201	-0.948613	0.01470308	Ahctf1
ENSMUSG00000032372.14	-5.3808877	-10.716857	-0.0449187	0.04793671	Plscr2
ENSMUSG00000040907.15	-0.5384264	-1.0147421	-0.0621107	0.02595098	Atp1a3
ENSMUSG00000047369.15	-2.2312211	-4.3938218	-0.0686203	0.04264749	Dnah14
ENSMUSG00000017868.16	-6.6664597	-11.422084	-1.9108356	0.00669821	Sgk2
ENSMUSG00000025656.17	-1.9208894	-3.7572067	-0.0845721	0.03968607	Arhgef9
ENSMUSG00000050627.13	-1.807162	-3.570032	-0.0442919	0.04408521	Gpd1l
ENSMUSG00000053693.16	-6.1926792	-11.999275	-0.3860829	0.03580918	Mast1
ENSMUSG00000056917.12	-5.5851638	-10.810287	-0.3600401	0.03537647	Sipa1
ENSMUSG00000009535.13	-1.8649436	-3.6738165	-0.0560706	0.04280471	Rnmt
ENSMUSG00000028469.15	-2.1772135	-3.995885	-0.3585419	0.01854315	Npr2
ENSMUSG00000032540.15	-7.0953744	-11.723226	-2.4675225	0.00354389	Abhd5
ENSMUSG00000057738.13	-0.8233038	-1.5800842	-0.0665233	0.03214873	Sptan1
ENSMUSG00000107306.1	-0.811277	-1.6200993	-0.0024547	0.04924634	Gm42577
ENSMUSG00000036062.13	-1.6975496	-3.3945645	-0.0005346	0.04992125	Phf24
ENSMUSG00000068267.5	-1.7633005	-3.469419	-0.057182	0.04226686	Cenpb
ENSMUSG00000026229.17	-1.2289355	-2.2144892	-0.2433818	0.01444189	Psmd1
ENSMUSG00000041907.9	-5.7030203	-9.3100371	-2.0960035	0.00282168	Gpr45
ENSMUSG00000097022.2	-6.9859323	-11.582735	-2.3891292	0.00377972	BC001981
ENSMUSG00000044148.6	2.20033702	0.00395358	4.39672046	0.04955166	1810030O07
ENSMUSG00000024270.11	-1.9653748	-3.6901675	-0.240582	0.02478937	Slc39a6
ENSMUSG00000037419.8	-2.1679878	-4.0592157	-0.2767599	0.02394777	Endod1
ENSMUSG00000040044.11	-1.580241	-3.1052793	-0.0552028	0.04170139	Orc3
ENSMUSG00000031812.16	-0.5890724	-1.1159383	-0.0622065	0.02761483	Map1lc3b
ENSMUSG00000100813.1	-6.5554333	-10.828066	-2.2828003	0.00352539	Gm28874
ENSMUSG00000021549.13	-1.3046011	-2.3387075	-0.2704947	0.01342259	Rasa1
ENSMUSG00000040339.10	2.13348806	0.1893691	4.07760701	0.03064567	Fam102b
ENSMUSG00000040721.9	-1.1967456	-2.1424456	-0.2510457	0.01316424	Zfhx2
ENSMUSG00000029576.17	-9.0333029	-14.237511	-3.829095	0.00137491	Radil
ENSMUSG00000056851.13	-2.3094032	-4.4636343	-0.1551722	0.03482412	Pcbp2
ENSMUSG00000021772.14	0.97050486	0.08369605	1.85731366	0.03111672	Nkiras1
ENSMUSG00000040329.14	-6.4825149	-11.827499	-1.1375307	0.01713828	Il7
ENSMUSG00000073591.4	-5.9844731	-10.20444	-1.7645058	0.00618342	Pcdhb22
ENSMUSG00000021983.15	-7.6971527	-13.198175	-2.1961308	0.00678363	Atp8a2
ENSMUSG00000075702.9	-0.5269612	-1.0445972	-0.0093253	0.04568574	Selenom
ENSMUSG00000030270.11	-2.1072454	-4.1948892	-0.0196016	0.04770406	Cpne9
ENSMUSG00000020925.16	-4.6308306	-8.74248	-0.5191811	0.02649649	Ccdc43
ENSMUSG00000091318.2	-5.9562525	-9.4627769	-2.4497281	0.00163007	Gm5415
ENSMUSG00000048920.8	-1.5459697	-3.0659676	-0.0259718	0.04589892	Fkrp
ENSMUSG00000097527.2	-7.3755303	-12.282849	-2.4682119	0.00409686	1700112J16R
ENSMUSG00000015755.16	-2.0283755	-3.8436065	-0.2131444	0.02770529	Tab2
ENSMUSG00000048040.8	-2.0848581	-3.8941847	-0.2755315	0.02324103	Arxes2
ENSMUSG00000027395.15	-2.1740178	-4.0330098	-0.3150258	0.02131487	Polr1b
ENSMUSG00000100826.6	-0.6720794	-1.1901613	-0.1539974	0.01123329	Snhg14
ENSMUSG00000079492.2	-5.5273516	-9.7997502	-1.254953	0.01143148	Gm11127
ENSMUSG00000000568.15	-1.2781801	-2.2033433	-0.3530169	0.00739827	Hnrnpd
ENSMUSG00000095280.1	-5.0385533	-10.012446	-0.0646602	0.04684886	Gm21738
ENSMUSG00000037149.9	-1.976645	-3.9114079	-0.0418821	0.04486114	Ddx1
ENSMUSG00000103825.1	-5.6812976	-10.983009	-0.3795857	0.03490039	Gm38178
ENSMUSG00000017943.15	-1.1762423	-2.1495882	-0.2028964	0.01751864	Gdap1l1
ENSMUSG00000026150.14	-2.1577162	-4.1573699	-0.1580625	0.03361569	Mff

ENSMUSG00000041594.17	-4.6562468	-8.9730121	-0.3394814	0.03368388	Tmtc4
ENSMUSG00000106671.1	-5.0514913	-9.3404315	-0.7625511	0.02043906	Gm42900
ENSMUSG00000029700.11	-5.8294356	-11.411328	-0.2475432	0.04002821	Slc13a1
ENSMUSG00000039844.19	-1.9756541	-3.9102996	-0.0410086	0.04496256	Rapgef1
ENSMUSG00000025234.11	-3.0301213	-5.4989503	-0.5612924	0.01593272	Arih1
ENSMUSG00000047789.4	-2.4363342	-4.5596621	-0.3130062	0.02381848	Slc38a9
ENSMUSG00000033760.16	-2.0873555	-3.7732897	-0.4014214	0.01509663	Rbm4b
ENSMUSG00000052613.16	-1.8370724	-3.4420446	-0.2321002	0.0241569	Pcdh15
ENSMUSG00000021589.12	-6.402968	-10.24708	-2.5588556	0.00189835	Rhobtb3
ENSMUSG00000017715.11	-7.3633221	-12.488475	-2.2381696	0.0056474	Pgs1
ENSMUSG00000078572.3	0.92932516	0.19673757	1.66191274	0.01296239	Ndufaf8
ENSMUSG00000024487.4	-2.2398116	-4.3626841	-0.1169391	0.03792432	Yipf5
ENSMUSG00000026840.14	-6.6421754	-11.447651	-1.8366995	0.00737511	Lamc3
ENSMUSG00000025742.5	-6.0974575	-11.116164	-1.0787511	0.01695643	Prps2
ENSMUSG00000029036.18	-1.7819267	-3.5600022	-0.0038511	0.04946102	Atad3a
ENSMUSG00000065097.1	1.8912883	0.36989092	3.41268568	0.01472117	Snora16a
ENSMUSG00000032551.6	-5.8831857	-10.679235	-1.0871359	0.01598705	1110059G10
ENSMUSG00000070867.4	-1.504734	-2.8229802	-0.1864878	0.024543	Trabd2b
ENSMUSG00000029712.14	-4.5032784	-8.8581592	-0.1483976	0.0421481	Actl6b
ENSMUSG00000092558.3	-2.0230162	-3.502816	-0.5432165	0.00794556	Med20
ENSMUSG00000013419.6	-1.2706588	-2.3396241	-0.2016936	0.01934952	Zfp651
ENSMUSG00000022472.16	-0.7611704	-1.3115693	-0.2107714	0.00734855	Desi1
ENSMUSG00000090353.2	-5.0008397	-9.4567894	-0.54489	0.02703436	Gm17555
ENSMUSG00000062044.15	-1.9201596	-3.673851	-0.1664682	0.0310313	Lmtk3
ENSMUSG00000029405.16	-2.095123	-4.0304106	-0.1598353	0.0330208	G3bp2
ENSMUSG00000031904.5	-5.1479084	-9.9873537	-0.3084632	0.03630845	Slc7a6
ENSMUSG00000071073.4	0.52442683	0.02238703	1.02646663	0.03997902	Lrrc73
ENSMUSG00000091735.2	-4.3868014	-8.4270797	-0.3465231	0.03249653	Gpr62
ENSMUSG00000038976.12	-0.7359025	-1.3116366	-0.1601684	0.01235258	Ppp1r9b
ENSMUSG00000109865.1	-5.8252198	-10.497967	-1.152473	0.01446448	Hspa14
ENSMUSG00000036402.13	2.27410329	0.58716901	3.96103758	0.00872825	Gng12
ENSMUSG00000034105.9	-5.885778	-10.40812	-1.3634365	0.01099838	Tldc1
ENSMUSG00000003421.13	-1.7712484	-3.276309	-0.2661877	0.02053528	Nosip
ENSMUSG00000017716.15	-6.0711092	-10.262895	-1.8793236	0.00533643	Birc5
ENSMUSG00000032410.13	-0.4706425	-0.9154509	-0.0258341	0.03735742	Xrn1
ENSMUSG00000028960.18	-1.0108764	-1.7457606	-0.2759922	0.00762061	Ube4b
ENSMUSG00000053166.14	-2.2941608	-4.4247201	-0.1636016	0.03399993	Cdh22
ENSMUSG00000063884.6	2.76119607	0.51704842	5.00534372	0.01569104	Ptcd3
ENSMUSG00000020780.15	-2.4432872	-4.5638496	-0.3227247	0.02325225	Srp68
ENSMUSG00000029376.8	5.64579638	1.3887145	9.90287826	0.00972652	Mthfd2l
ENSMUSG00000021701.7	-8.7755597	-14.455179	-3.0959402	0.00334798	Plk2
ENSMUSG00000085748.1	-6.0276909	-9.9396978	-2.1156839	0.00341704	Gm12280
ENSMUSG00000021567.14	-5.1760944	-9.3336689	-1.0185199	0.0145851	Nkd2
ENSMUSG00000052026.7	-2.0282226	-3.8544581	-0.2019871	0.02867378	Slc6a7
ENSMUSG00000032869.15	-2.2725415	-4.4311455	-0.1139376	0.03836603	Psmf1
ENSMUSG00000008999.7	-5.004848	-8.726812	-1.282884	0.00887587	Bmp7
ENSMUSG00000036452.17	-0.7673838	-1.5299001	-0.0048675	0.04842765	Arhgap26
ENSMUSG00000034154.15	-5.2561518	-9.9631205	-0.5491832	0.02780959	Ino80
ENSMUSG00000036186.5	2.77239303	0.56660858	4.97817747	0.01374188	Fam69b
ENSMUSG00000028637.15	-3.3545843	-6.686739	-0.0224296	0.04834339	Ccdc30
ENSMUSG00000019951.9	-2.0872951	-3.9894543	-0.1851358	0.03065754	Uhrf1bp1l
ENSMUSG00000034171.13	-4.368602	-8.5518201	-0.1853839	0.04003453	Faah
ENSMUSG00000019428.16	-1.8285779	-3.4783179	-0.1788379	0.02899339	Fkbp8
ENSMUSG00000027168.21	-2.7640639	-5.1380673	-0.3900605	0.0218755	Pax6
ENSMUSG00000037791.15	-5.0245879	-9.2399446	-0.8092312	0.01903184	Phf12
ENSMUSG00000089833.1	-4.5506999	-8.7066537	-0.3947461	0.03102211	Fhitos
ENSMUSG00000064061.13	-0.9701529	-1.6781712	-0.2621346	0.00782312	Dzip3
ENSMUSG00000034610.14	-1.7732074	-3.5225025	-0.0239122	0.04669188	Zcchc11
ENSMUSG00000039452.5	-2.5858214	-4.6081215	-0.5635213	0.01232455	Snx22
ENSMUSG00000050708.16	-0.6825538	-1.3097149	-0.0553928	0.03208078	Ftl1
ENSMUSG00000033697.15	-0.8286947	-1.6080778	-0.0493116	0.03639431	Arhgap39
ENSMUSG00000021265.3	-1.8488454	-3.3869824	-0.3107085	0.01809574	Slc25a29
ENSMUSG00000030685.5	-6.5711502	-10.84509	-2.2972107	0.00347174	Kctd13
ENSMUSG00000022438.6	-2.7583271	-4.6795332	-0.8371211	0.00567434	Parvb
ENSMUSG00000022781.8	-2.2048536	-4.2317285	-0.1779786	0.03216391	Pak2
ENSMUSG00000001151.9	-1.1983207	-2.3414542	-0.0551872	0.03924524	Pcnt
ENSMUSG00000057667.7	-7.9691531	-13.238114	-2.7001921	0.00391384	Bloc1s3
ENSMUSG00000106446.1	-3.8905798	-7.5203413	-0.2608184	0.03485497	Gm42970
ENSMUSG00000073728.10	-4.2673998	-8.138059	-0.3967406	0.02986908	Tmem51os1
ENSMUSG00000032307.16	-5.6538698	-10.099384	-1.2083552	0.01275276	Ube2q2
ENSMUSG00000097164.1	-2.2872769	-3.9430475	-0.6315062	0.00740466	Cep83os
ENSMUSG00000025795.7	-5.0198263	-9.5299288	-0.5097237	0.02832684	Rassf3
ENSMUSG00000108867.1	-4.5040089	-8.426931	-0.5810867	0.02373307	Gm44643
ENSMUSG00000024772.9	-2.4121698	-4.5931315	-0.2312081	0.02934499	Ehd1
ENSMUSG00000042208.15	-0.8926107	-1.6839154	-0.101306	0.02626338	0610010F05l
ENSMUSG00000062373.7	-2.2030809	-4.2606496	-0.1455122	0.03505472	Tmem65
ENSMUSG00000110529.1	-4.904333	-9.4069513	-0.4017146	0.03193646	Gm45694
ENSMUSG00000038671.15	-2.2030772	-4.3213735	-0.084781	0.0409076	Arfrp1
ENSMUSG00000068663.13	-0.8254067	-1.5374359	-0.1133774	0.0224417	Clec16a
ENSMUSG00000042275.8	-2.267335	-4.449128	-0.085542	0.04107567	Pelo
ENSMUSG00000100143.1	1.10468786	0.08347116	2.12590455	0.03316298	NA
ENSMUSG00000026914.15	-3.5827548	-6.1958425	-0.9696671	0.00779063	Psmd14
ENSMUSG00000061751.15	-2.3464343	-4.6517423	-0.0411262	0.04572594	Kalrn
ENSMUSG00000051786.14	-2.018782	-3.995304	-0.04226	0.04492106	Tubgcp6
ENSMUSG00000001120.15	-2.5574979	-4.7036243	-0.4113716	0.01905974	Pcbp3
ENSMUSG00000027778.15	-2.3701979	-4.5993515	-0.1410443	0.03639384	Ift80
ENSMUSG00000107059.1	-1.8358668	-3.4081799	-0.2635538	0.02151315	Gm43629
ENSMUSG00000021807.5	-1.706069	-3.4105788	-0.0015593	0.04977165	Rtraf
ENSMUSG00000029501.14	-5.0028875	-9.2617219	-0.7440532	0.02075911	Ankle2
ENSMUSG00000021669.14	-2.2792786	-4.2019687	-0.3565885	0.01966531	Col4a3bp
ENSMUSG00000045008.1	-4.6916255	-8.7068999	-0.6763511	0.02142419	9030612E09l
ENSMUSG00000097275.1	-1.8953401	-3.7260942	-0.0645861	0.04189438	Gm26648
ENSMUSG00000020069.16	-4.3016357	-8.3277031	-0.2755683	0.0354584	Hnrnph3
ENSMUSG00000025008.15	-5.8019724	-10.909408	-0.6945365	0.02523041	Tctn3
ENSMUSG00000083282.2	-2.2555934	-4.2853149	-0.2258719	0.02857578	Ctsf
ENSMUSG00000051065.8	-4.1221809	-7.7552626	-0.4890992	0.02540414	Mb21d2
ENSMUSG00000048264.15	-1.9554092	-3.8289236	-0.0818947	0.04015631	Dip2c
ENSMUSG00000028955.3	3.9115275	0.21100631	7.6120487	0.03755689	Vamp3
ENSMUSG00000043468.4	-6.2866092	-11.253932	-1.3192859	0.01315551	Adam30
ENSMUSG00000040414.7	3.14101544	0.03132653	6.25070434	0.04754077	Slc25a28
ENSMUSG00000091957.3	-1.6704949	-2.485995	-0.8549948	0.00034954	Rps2-ps10
ENSMUSG00000095325.1	-5.3208277	-9.3340263	-1.3076291	0.00974491	Zfp870
ENSMUSG00000067199.4	-1.3577152	-2.3742067	-0.3412236	0.00928007	Frat1
ENSMUSG00000028871.7	-4.4498252	-8.5159347	-0.3837158	0.03111824	Rspo1
ENSMUSG00000033763.14	-0.8984816	-1.7177994	-0.0791639	0.03076705	Mtss1l

ENSMUSG00000035620.14	-4.4477694	-8.0926755	-0.8028633	0.01650916	Ric8b
ENSMUSG00000016194.14	-5.1707881	-10.278805	-0.0627713	0.0470161	Hsd11b1
ENSMUSG00000033152.13	-2.3929766	-4.3138372	-0.4721161	0.01452645	Podxl2
ENSMUSG00000092248.1	-5.4713425	-10.501843	-0.4408426	0.03219235	Vmn1r-ps63
ENSMUSG00000025362.5	0.53112002	0.0224863	1.03975374	0.04005604	Rps26
ENSMUSG00000030374.15	-1.8210254	-3.5339514	-0.1080995	0.03642398	Strn4
ENSMUSG00000026788.13	-4.8712453	-9.4512027	-0.2912879	0.03633382	Zbtb43
ENSMUSG00000037003.15	-6.6710084	-12.279908	-1.0621085	0.01928343	Tns2
ENSMUSG00000079658.9	-1.7993306	-3.5857226	-0.0129387	0.04821968	Eloc
ENSMUSG00000054863.8	-2.6550993	-4.7630641	-0.5471345	0.01355874	Fam19a5
ENSMUSG00000024639.5	-1.1416828	-2.2332504	-0.0501152	0.03971483	Gnaq
ENSMUSG00000010358.13	-5.8285038	-10.910043	-0.7469647	0.02386861	Ifi35
ENSMUSG00000039787.13	-5.2725337	-9.7896751	-0.7553923	0.02155585	Cercam
ENSMUSG00000004631.15	-5.49593	-10.092581	-0.8992791	0.0186842	Sgce
ENSMUSG00000079598.3	-2.1160793	-4.0225651	-0.2095936	0.02877017	Clec2l
ENSMUSG00000044933.2	2.05469507	0.0323225	4.07706765	0.04615372	Sstr3
ENSMUSG00000040659.3	-1.2755158	-2.315366	-0.2356655	0.01599019	Efhd2
ENSMUSG00000020919.11	-2.9960451	-5.5785589	-0.4135313	0.02234064	Stat5b
ENSMUSG00000097206.1	5.21034733	0.35963594	10.0610587	0.0344562	Gm26699
ENSMUSG00000000959.6	-1.7366497	-3.2595185	-0.2137808	0.02467772	Oxa1l
ENSMUSG00000049521.1	1.03761169	0.45255355	1.62266983	0.00115837	Cdc42ep1
ENSMUSG00000043448.13	1.91230023	0.01743556	3.80716491	0.04774898	Gjc2
ENSMUSG00000100944.1	-8.50632	-14.103482	-2.9091577	0.00377938	Gm28900
ENSMUSG00000060301.5	-4.7569262	-8.16555	-1.3483024	0.00690681	2610008E11I
ENSMUSG00000104145.1	-4.884333	-8.1420148	-1.6266511	0.00416924	D130019J16F
ENSMUSG00000027324.1	-5.1101833	-9.5436646	-0.6767021	0.02320004	Rpusd2
ENSMUSG00000073514.3	-6.8216928	-12.095934	-1.5474515	0.0114507	Dok6
ENSMUSG00000056919.9	-4.9332432	-9.4318307	-0.4346557	0.03076723	Cep162
ENSMUSG00000027981.14	-1.9398781	-3.8082482	-0.071508	0.04126892	Rnpc3
ENSMUSG00000050390.12	-5.3072465	-10.609066	-0.0054269	0.04974457	C77080
ENSMUSG00000030556.13	-1.6906413	-3.2580917	-0.123191	0.03369225	Lrrc28
ENSMUSG00000030207.15	-2.2049896	-4.3633486	-0.0466305	0.04487071	Fam234b
ENSMUSG00000029148.15	-0.5272461	-0.8500433	-0.2044488	0.00220649	Nrbp1
ENSMUSG00000050730.16	-5.5515931	-10.360475	-0.742711	0.02298931	Arhgap42
ENSMUSG00000031428.11	-0.6806556	-1.3079253	-0.0533859	0.03260455	Zcchc18
ENSMUSG00000050272.9	-2.7019893	-5.2357053	-0.1682732	0.03582303	Dscam
ENSMUSG00000042389.13	-1.769776	-2.9971623	-0.5423898	0.00550603	Tsen2
ENSMUSG00000021193.9	-5.3816662	-10.132527	-0.6308058	0.02564168	Pitrm1
ENSMUSG00000031960.14	-2.3545142	-4.5376096	-0.1714187	0.03370451	Aars
ENSMUSG00000106981.1	-2.2101768	-4.1526268	-0.2677268	0.02499701	Gm45495
ENSMUSG00000022388.14	-6.6442435	-11.953291	-1.3351958	0.01411691	Ttll8
ENSMUSG00000039842.15	-1.7626972	-3.4983774	-0.0270171	0.04625024	Mcph1
ENSMUSG00000030980.17	0.49973599	0.09362031	0.90585167	0.015681	Knop1
ENSMUSG00000033294.11	-5.4414544	-9.8823166	-1.0005921	0.01609639	Noc4l
ENSMUSG00000024856.10	-4.3350057	-8.5336529	-0.1363584	0.04248798	Cdk2ap2
ENSMUSG00000040282.13	-4.6178902	-9.1314707	-0.1043096	0.0445331	BC052040
ENSMUSG00000066829.6	-6.001521	-11.351658	-0.651384	0.02710705	Zfp810
ENSMUSG00000097971.3	-0.8669928	-1.5872286	-0.1467571	0.01793642	Gm26917
ENSMUSG00000046287.7	1.06516695	0.31638783	1.81394607	0.00605166	Pnma3
ENSMUSG00000104625.1	-6.6498539	-11.591145	-1.7085632	0.00882797	Gm42448
ENSMUSG00000064363.1	0.44630236	0.09620261	0.7964021	0.01256485	mt-Nd4
ENSMUSG00000023883.13	-2.9065355	-5.5152145	-0.2978565	0.02816158	Phf10
ENSMUSG00000031578.5	-3.0514058	-5.4996414	-0.6031701	0.0144839	Mak16
ENSMUSG00000020658.9	-1.0905567	-2.1476257	-0.0334877	0.04265834	Efr3b
ENSMUSG00000001729.14	-4.0293869	-7.2131023	-0.8456716	0.01315346	Akt1
ENSMUSG00000024867.14	-4.5590336	-8.9109125	-0.2071548	0.03937883	Pip5k1b
ENSMUSG00000042109.7	-1.8113678	-3.5258344	-0.0969012	0.03765165	Csdc2
ENSMUSG00000046519.15	-5.4880804	-10.287399	-0.6887618	0.02429127	Golph3l
ENSMUSG00000036615.5	-3.7291135	-7.4066321	-0.051595	0.04660766	Rfxap
ENSMUSG00000022150.16	2.56573244	0.40631636	4.72514852	0.01940029	Dab2
ENSMUSG00000033618.6	-2.961484	-5.7391756	-0.1837924	0.03586746	Map3k13
ENSMUSG00000028029.10	0.58748933	0.09632755	1.0786511	0.01863879	Aimp1
ENSMUSG00000032523.10	2.25306103	0.6708605	3.83526156	0.00600845	Hhatl
ENSMUSG00000031870.16	-6.2423714	-11.427788	-1.056955	0.01793014	Pgr
ENSMUSG00000101249.1	2.38304981	0.51165736	4.25444226	0.01265152	Gm29216
ENSMUSG00000038848.14	-2.7460179	-5.2468586	-0.2451773	0.03054825	Ythdf1
ENSMUSG00000037674.15	-1.9300322	-3.3721374	-0.487927	0.00915875	Rfx7
ENSMUSG00000034101.14	-5.9460562	-10.673917	-1.2181955	0.01368773	Ctnnd1
ENSMUSG00000106897.1	-1.3673483	-2.5325962	-0.2021004	0.02089208	Gm43027
ENSMUSG00000074622.4	-6.0335072	-10.628474	-1.4385403	0.0103827	Mafb
ENSMUSG00000037007.17	-1.0355021	-1.9905141	-0.08049	0.03274061	Zfp113
ENSMUSG00000030032.12	-3.0622015	-5.5936421	-0.5307609	0.01741203	Wdr54
ENSMUSG00000024054.13	-1.4054684	-2.5544423	-0.2564945	0.01626504	Smchd1
ENSMUSG00000025821.9	-4.973866	-9.8720342	-0.0756978	0.04627608	Zfp282
ENSMUSG00000021939.7	-2.4790425	-4.7395544	-0.2185305	0.03075909	Ctsb
ENSMUSG00000028644.16	-4.9114336	-9.2041444	-0.6187227	0.02421538	Ermap
ENSMUSG00000005907.14	1.02001394	0.00450382	2.03552406	0.0489024	Pex1
ENSMUSG00000097311.7	-4.2308753	-8.4180014	-0.0437491	0.04745163	Gm26871
ENSMUSG00000094832.1	-4.5751535	-8.9374799	-0.2128272	0.03914466	Gm21846
ENSMUSG00000020484.18	-3.1429471	-5.7830296	-0.5028647	0.01917589	Xbp1
ENSMUSG00000052593.15	3.97021454	0.15201848	7.7884106	0.04095058	Adam17
ENSMUSG00000019948.3	-5.2658919	-9.8707179	-0.6610659	0.02428552	Actr6
ENSMUSG00000087968.1	-5.4583836	-10.571642	-0.3451253	0.03562835	Gm25395
ENSMUSG00000024712.9	-0.9659617	-1.8352083	-0.0967152	0.02857852	Rfk
ENSMUSG00000087437.7	-4.6453289	-8.9663747	-0.3242831	0.03429928	Gm13112
ENSMUSG00000072915.3	-6.1069553	-11.131908	-1.0820023	0.01692412	Gm12258
ENSMUSG00000052605.12	-5.9661873	-11.472753	-0.4596221	0.03287508	Isoc2b
ENSMUSG00000033985.17	-5.5503377	-10.072037	-1.0286386	0.01592172	Tesk2
ENSMUSG00000033499.13	-0.9922258	-1.7896112	-0.1948404	0.01463122	Larp4b
ENSMUSG00000105285.1	-9.3827915	-15.389936	-3.3756474	0.00308997	Gm43238
ENSMUSG00000077450.12	-0.6845288	-1.3065466	-0.062511	0.03017201	Rab11b
ENSMUSG00000024732.7	-3.9868558	-7.9084777	-0.0652339	0.04600312	Ccdc86
ENSMUSG00000064901.1	-2.0078605	-3.7700564	-0.2456647	0.0247989	Snora21
ENSMUSG00000078441.10	-1.8135457	-3.4405806	-0.1865108	0.02809732	NA
ENSMUSG00000029433.14	-1.7748382	-3.5359893	-0.013687	0.04809217	Diablo
ENSMUSG00000071669.14	-4.7562173	-9.3516142	-0.1608203	0.04195385	Snx29
ENSMUSG00000108826.1	-8.3288097	-13.19597	-3.4616492	0.0015383	4931412I15R
ENSMUSG00000034042.16	-1.9492189	-3.2497438	-0.648694	0.00417997	Gpbp1l1
ENSMUSG00000030286.6	0.46909518	0.01569562	0.92249474	0.04203364	Emc3
ENSMUSG00000038593.18	-2.3923294	-4.7646398	-0.0200191	0.04793177	Tctn1
ENSMUSG00000026664.7	0.7143112	0.18728099	1.24134142	0.00841955	Phyh
ENSMUSG00000003378.9	-4.60175	-8.9599838	-0.2435162	0.03777397	Grik5
ENSMUSG00000037805.14	-3.5476724	-6.1355772	-0.9597676	0.00779887	Rpl10a
ENSMUSG00000059482.15	-2.8032464	-5.3403454	-0.2661473	0.02950958	2610301B20I
ENSMUSG00000021115.14	-4.2643668	-7.6767879	-0.8519458	0.01424715	Vrk1

ENSMUSG00000033047.4	-2.4523186	-4.5972101	-0.3074271	0.02431362	Eif3l
ENSMUSG00000107750.1	-8.6073014	-14.627203	-2.5873994	0.00584058	Gm44013
ENSMUSG00000093989.1	-0.9503842	-1.7034788	-0.1972895	0.01339588	Rnasek
ENSMUSG00000053536.6	-2.4998836	-4.4714286	-0.5283387	0.01299934	Cstf2t
ENSMUSG00000045455.7	-5.0523013	-10.008459	-0.0961437	0.04536987	Gm9797
ENSMUSG00000032589.14	-0.7668907	-1.3737049	-0.1600766	0.01327407	Bsn
ENSMUSG00000046192.4	-5.8640311	-10.913638	-0.8144243	0.0222108	Iqub
ENSMUSG00000040896.16	-2.2620018	-4.2595525	-0.2644512	0.02569205	Kcnd3
ENSMUSG00000066677.11	-6.7510114	-12.507685	-0.994338	0.0209671	Ifi208
ENSMUSG00000051343.11	-2.1669958	-4.2635397	-0.070452	0.04224818	Rab11fip5
ENSMUSG00000041168.9	-0.5898125	-1.0172026	-0.1624225	0.00745453	Lonp1
ENSMUSG00000002297.15	-5.250747	-10.256942	-0.2445524	0.03913238	Dbf4
ENSMUSG00000109781.1	5.02205624	0.47032622	9.57378627	0.02974446	Gm45509
ENSMUSG00000074811.2	-4.4739229	-7.7017594	-1.2460863	0.00723731	Hps6
ENSMUSG00000048285.8	2.10145905	0.04434814	4.15856997	0.0448811	Frmd6
ENSMUSG00000018567.14	-0.7082602	-1.3729626	-0.0435578	0.03598275	Gabarap
ENSMUSG00000081342.1	-9.2494103	-14.777539	-3.7212819	0.00183349	Gm11434
ENSMUSG00000026728.9	-2.1582653	-4.1094914	-0.2070392	0.0293309	Vim
ENSMUSG00000056665.2	-4.5284257	-7.7578859	-1.2989655	0.00668448	Them6
ENSMUSG00000039115.13	-5.0302827	-9.5731016	-0.4874638	0.02915449	Itga9
ENSMUSG00000079157.4	-2.8852505	-5.5569846	-0.2135164	0.0334684	Fam155a
ENSMUSG00000043843.16	-5.2612592	-9.9931446	-0.5293738	0.02849071	Tmem145
ENSMUSG00000106841.1	-5.4882369	-10.791568	-0.1849056	0.04198125	Gm42656
ENSMUSG00000050229.3	-7.8064892	-13.362405	-2.2505734	0.00659162	Pigm
ENSMUSG00000102690.1	-7.8138651	-14.170098	-1.4576321	0.01577591	Gm37779
ENSMUSG00000106101.1	5.97285188	0.69400237	11.2517014	0.02581136	Gm43438
ENSMUSG00000083253.1	-2.2453733	-4.1989807	-0.2917659	0.02358747	Gm7108
ENSMUSG00000038594.8	-5.414722	-10.537577	-0.2918667	0.03756582	Cep85l
ENSMUSG00000032567.14	-7.6245094	-13.687189	-1.5618302	0.0136911	Aste1
ENSMUSG00000024260.13	-4.3725586	-8.1003273	-0.64479	0.02094162	Sap130
ENSMUSG00000097189.1	5.69582408	0.05949254	11.3321556	0.04742627	Gm26594
ENSMUSG00000027552.14	5.38953343	0.43741244	10.3416544	0.03207993	E2f5
ENSMUSG00000031728.10	1.19631671	0.00844357	2.38418985	0.04825223	Zfp821
ENSMUSG00000081046.1	-6.0027511	-10.918247	-1.0872548	0.01643315	Gm12846
ENSMUSG00000036285.10	-2.3817072	-4.3420976	-0.4213169	0.01695909	Noa1
ENSMUSG00000035764.5	-2.1529757	-4.2872448	-0.0187066	0.04785352	Fbxo45
ENSMUSG00000048833.8	-5.4512725	-10.405164	-0.4973809	0.03018647	Slc39a9
ENSMUSG00000020935.8	-5.3595168	-10.311139	-0.4078944	0.03305642	Dcakd
ENSMUSG00000033720.12	0.83608878	0.00792229	1.66425527	0.04766186	Sfxn5
ENSMUSG00000086040.8	-2.1553679	-4.222657	-0.0880788	0.04038012	Wipf3
ENSMUSG00000087598.9	-2.1196326	-4.1994593	-0.039806	0.045429	Zfp111
ENSMUSG00000036398.13	-0.7716543	-1.5055324	-0.0377762	0.03861928	Ppp1r11
ENSMUSG00000025894.11	-5.4103592	-8.6172508	-2.2034676	0.00171894	Aasdhppt
ENSMUSG00000046324.12	-5.7428111	-11.11035	-0.3752718	0.03519715	Ermp1
ENSMUSG00000022802.2	-2.0130725	-3.7453707	-0.2807743	0.02212179	Lmln
ENSMUSG00000022350.6	-6.4981049	-11.493718	-1.5024918	0.01103825	Washc5
ENSMUSG00000024451.8	-5.4339544	-10.790623	-0.0772862	0.04651474	Arap3
ENSMUSG00000025348.8	-7.0129073	-12.400653	-1.6251613	0.0109901	Itga7
ENSMUSG00000019774.8	-5.0293971	-8.8052128	-1.2535814	0.00945114	Mtrf1l
ENSMUSG00000048814.10	-4.6470335	-8.2934792	-1.0005879	0.01258906	Lonrf2
ENSMUSG00000008305.18	-4.4497612	-8.1343521	-0.7651703	0.01758786	Tle1
ENSMUSG00000037013.15	7.37680661	1.16047757	13.5931357	0.0195451	Ss18
ENSMUSG00000026385.16	0.63492837	0.00963329	1.26022344	0.04628729	Dbi
ENSMUSG00000003269.16	-2.6187021	-5.0338439	-0.2035604	0.03274005	Cyth2
ENSMUSG00000071359.13	-5.2747048	-10.430661	-0.1187484	0.04455072	Tbpl1
ENSMUSG00000026433.13	-6.0385556	-11.370577	-0.7065341	0.02567652	Rab29
ENSMUSG00000002307.15	-2.9966452	-5.8130608	-0.1802296	0.03626221	Daxx
ENSMUSG00000079083.2	1.33390451	0.00718127	2.66062775	0.0486636	Jrkl
ENSMUSG00000021189.11	-2.4862034	-4.9391703	-0.0332365	0.04672	Atxn3
ENSMUSG00000026077.15	-3.7703151	-6.56933	-0.9713001	0.00877387	Npas2
ENSMUSG00000039801.6	-0.8943603	-1.7101155	-0.0786052	0.03080783	2410089E03I
ENSMUSG00000024395.7	-6.1283511	-11.553765	-0.7029376	0.02606033	Lims2
ENSMUSG00000034055.16	-7.9209372	-14.25468	-1.5871943	0.01418073	Phka1
ENSMUSG00000029787.10	-5.3999394	-10.357219	-0.4426594	0.03192411	Avil9
ENSMUSG00000038002.8	-7.2692248	-13.232624	-1.3058255	0.01661698	Cramp1l
ENSMUSG00000036902.10	-5.4301033	-10.129852	-0.730354	0.02287872	Neto2
ENSMUSG00000034675.17	-0.5871191	-1.1417705	-0.0324678	0.03727142	Dbn1
ENSMUSG00000041439.15	-1.3042191	-2.4569748	-0.1514634	0.02582126	Mfsd6
ENSMUSG00000022132.15	-6.5855795	-11.315064	-1.856095	0.00701292	Cldn10
ENSMUSG00000088185.1	-7.4600894	-13.421664	-1.4985149	0.01412625	Scarna2
ENSMUSG00000016262.14	-6.4632653	-12.703873	-0.222658	0.04181019	Sertad4
ENSMUSG00000039840.7	-5.7821396	-11.17656	-0.3877196	0.03485169	Epg5
ENSMUSG00000030084.11	-3.465299	-6.3689325	-0.5616654	0.0188923	Plxna1
ENSMUSG00000003429.11	-0.4734104	-0.9287102	-0.0181107	0.04095814	Rps11
ENSMUSG00000106032.1	5.03489845	0.2923335	9.77746341	0.036694	Gm42463
ENSMUSG00000024424.14	-2.365177	-4.4479827	-0.2823713	0.02528295	Ttc39c
ENSMUSG00000020086.6	-3.7684037	-7.4022174	-0.13459	0.04152569	H2afy2
ENSMUSG00000085196.1	-2.3052631	-4.1774093	-0.4331169	0.01561651	Gm14963
ENSMUSG00000024404.6	-2.4177073	-4.7805545	-0.0548601	0.04450906	Riok3
ENSMUSG00000083378.3	-1.3754871	-2.4940922	-0.256882	0.01575047	Gm13196
ENSMUSG00000045672.15	-5.9807237	-11.71897	-0.2424771	0.04045113	Col27a1
ENSMUSG00000020900.15	0.49908374	0.11845752	0.87970996	0.0104787	Myh10
ENSMUSG00000015305.6	-0.9995818	-1.9274772	-0.0716864	0.03391973	Sash1
ENSMUSG00000047379.6	-0.6129259	-1.0891676	-0.1366842	0.01182147	B4galt1
ENSMUSG00000018849.6	0.57439892	0.08064771	1.06815013	0.02198243	Wwc1
ENSMUSG00000074505.4	-1.1200651	-2.0486158	-0.1915143	0.01771353	Fat3
ENSMUSG00000020705.6	-0.5830574	-1.1219769	-0.044138	0.0331356	Ddx42
ENSMUSG00000066952.11	-4.8679459	-9.0664924	-0.6693994	0.02241859	Myo1h
ENSMUSG00000025128.7	-2.704584	-5.2309545	-0.1782134	0.03508636	Bhlhe22
ENSMUSG00000051238.5	-5.8898199	-11.059681	-0.7199592	0.02481733	Swsap1
ENSMUSG00000016349.10	-0.9991248	-1.5551316	-0.443118	0.00104227	Eef1a2
ENSMUSG00000020420.8	-7.6603294	-14.275359	-1.0452995	0.02257919	Zfp607a
ENSMUSG00000096956.2	4.60757413	0.36643487	8.84871339	0.03239307	Snhg18
ENSMUSG00000026792.16	-5.6663714	-10.415207	-0.9175356	0.01891347	Lrsam1
ENSMUSG00000031529.5	-1.4067623	-2.5788114	-0.2347132	0.0182551	Tnks
ENSMUSG00000005370.3	-5.4207668	-10.499285	-0.3422489	0.03564713	Msh6
ENSMUSG00000042831.13	-5.8420278	-11.144495	-0.5395608	0.02998112	Alkbh6
ENSMUSG00000029777.10	0.42530487	0.02366294	0.8269468	0.03720057	Gars
ENSMUSG00000041703.7	-1.6859767	-3.3592137	-0.0127397	0.04813019	Zic5
ENSMUSG00000024944.5	-1.1681505	-2.2458869	-0.090414	0.03280485	Arl2
ENSMUSG00000091264.2	1.17139426	0.07390677	2.26888174	0.03565605	Smim13
ENSMUSG00000078630.8	6.93993914	0.69147278	13.1884055	0.02866513	Tomt
ENSMUSG00000028049.15	6.85033922	1.99669917	11.7039793	0.00639112	Scamp3
ENSMUSG00000063767.4	-5.8899655	-10.471188	-1.3087429	0.01190018	S100a7a
ENSMUSG00000014980.14	-6.7111131	-11.359452	-2.0627744	0.0054564	Tsen15

ENSMUSG00000029486.13	-4.521116	-8.8999756	-0.1422564	0.04248577	Mrpl1
ENSMUSG00000069814.6	-5.8572303	-11.421988	-0.2924729	0.03840945	Ccdc92b
ENSMUSG00000019851.7	-6.1972406	-11.703995	-0.690486	0.02661453	Perp
ENSMUSG00000071723.7	-0.9555511	-1.6883687	-0.2227335	0.01086495	Gspt2
ENSMUSG00000038822.15	-5.6706134	-11.028448	-0.312779	0.03730133	Hace1
ENSMUSG00000012609.18	0.68763274	0.07049612	1.30476936	0.02815421	Ttll5
ENSMUSG00000036435.13	-3.9961746	-7.7663917	-0.2259576	0.03701075	Exoc1
ENSMUSG00000044067.6	-6.9341847	-12.100222	-1.7681477	0.00898264	Gpr22
ENSMUSG00000035834.11	-6.8986297	-12.925769	-0.8714909	0.02415918	Polr3g
ENSMUSG00000023345.15	3.96432096	0.11372406	7.81491787	0.04312034	Poc1a
ENSMUSG00000022829.14	-6.0636584	-11.811947	-0.3153699	0.0379667	Stxbp5l
ENSMUSG00000023186.14	5.50097791	0.95869151	10.0432643	0.01729071	Vwa5a
ENSMUSG00000031835.16	0.65711193	0.02976633	1.28445754	0.03940917	Mbtps1
ENSMUSG00000008035.12	-2.7041438	-4.3582449	-1.0500427	0.00219162	Mid1ip1
ENSMUSG00000090624.1	-6.64375	-12.64664	-0.6408602	0.02923477	Gm17060
ENSMUSG00000029797.13	-8.6823508	-16.306246	-1.0584553	0.02487079	Sspo
ENSMUSG00000015488.14	1.14344004	0.5132572	1.77362288	0.0009637	Cacfd1
ENSMUSG00000032199.12	-1.4795773	-2.6552391	-0.3039154	0.01363014	Polr2m
ENSMUSG00000021591.7	5.28784282	0.47362597	10.1020597	0.03049554	Glrx
ENSMUSG00000027184.14	-1.0711282	-2.1220103	-0.0202462	0.04540012	Caprin1
ENSMUSG00000028926.15	-0.4738608	-0.8997019	-0.0480196	0.02836313	Cdk14
ENSMUSG00000025486.17	-5.8814198	-11.066663	-0.6961764	0.02545062	Sirt3
ENSMUSG00000058267.13	-4.201339	-7.9540468	-0.4486313	0.02740962	Mrps14
ENSMUSG00000097482.2	6.0055582	0.22895971	11.7821567	0.04098732	Gm17634
ENSMUSG00000022528.7	6.25460331	1.31909825	11.1901084	0.01304587	Hes1
ENSMUSG00000054855.13	-6.3794486	-11.91072	-0.8481771	0.02311747	Rnd1
ENSMUSG00000022865.13	7.50018923	1.382872	13.6175065	0.01603643	Cxadr
ENSMUSG00000033676.13	-4.6124882	-8.5426611	-0.6823152	0.02087425	Gabrb3
ENSMUSG00000035133.8	1.08354766	0.50101229	1.66608304	0.00078693	Arhgap5
ENSMUSG00000055720.9	-8.6165132	-15.385124	-1.8479025	0.01267679	Ubl7
ENSMUSG00000079069.1	-5.8828277	-11.050177	-0.7154788	0.02491751	8430423G03
ENSMUSG00000020261.15	6.51927568	0.32227855	12.7162728	0.03851632	Slc36a1
ENSMUSG00000025058.4	-2.0180548	-3.9038648	-0.1322448	0.03515974	5430427O19
ENSMUSG00000024030.6	-1.201445	-2.2126547	-0.1902353	0.01940359	Abcg1
ENSMUSG00000093858.1	-6.5244294	-12.890376	-0.1584831	0.04413599	Gm19967
ENSMUSG00000096950.2	3.43681563	1.3827654	5.49086586	0.00183318	Gm9530
ENSMUSG00000106734.3	-6.9768768	-13.584205	-0.3695485	0.0377635	Gm20559
ENSMUSG00000022523.9	-6.2227242	-11.590711	-0.8547373	0.02244201	Fgf12
ENSMUSG00000021867.16	-8.2416765	-14.651163	-1.8321904	0.01188946	Tmem254b
ENSMUSG00000072676.11	-8.2416765	-14.651163	-1.8321904	0.01188946	Tmem254a
ENSMUSG00000003458.12	5.23192178	0.20030843	10.2635351	0.04095145	Ncstn
ENSMUSG00000004698.10	1.50355772	0.3528026	2.65431283	0.01072302	Hdac9
ENSMUSG00000087574.1	-4.3310966	-8.2826218	-0.3795714	0.03085473	C030037D09I
ENSMUSG00000095440.1	-6.6622377	-12.848948	-0.4755279	0.03398714	Fignl2
ENSMUSG00000053929.16	0.52666505	0.05494264	0.99838745	0.02783793	Cyhr1
ENSMUSG00000085492.7	-6.2077007	-11.714526	-0.7008754	0.02636286	Trmt61b
ENSMUSG00000032932.14	-2.168006	-4.2610133	-0.0749987	0.04177784	Hspa13
ENSMUSG00000090048.1	7.1413239	0.8063706	13.4762772	0.02636084	Runx2os3
ENSMUSG00000025738.7	-1.43442	-2.4150841	-0.4537559	0.00497668	Fbxl16
ENSMUSG00000064127.13	-1.9152043	-3.4469759	-0.3834328	0.01420017	Med14
ENSMUSG00000031955.10	-5.1829788	-9.6581882	-0.7077694	0.0225639	Bcar1
ENSMUSG00000006675.10	-0.960669	-1.8916749	-0.029663	0.04261949	P4htm
ENSMUSG00000091475.2	-7.0904402	-14.034972	-0.145908	0.04500463	2810468N07
ENSMUSG00000018821.3	1.14788654	0.18456454	2.11120855	0.01906829	Avpi1
ENSMUSG00000078117.2	-8.902689	-16.410142	-1.3952364	0.01962741	Gm16485
ENSMUSG00000027079.15	-7.0115151	-13.98897	-0.0340605	0.04879322	Clp1
ENSMUSG00000096370.8	4.7326429	0.37494864	9.09033715	0.03245142	Gm21992
ENSMUSG00000025318.13	-0.8292547	-1.5414852	-0.1170242	0.02187532	Jph3
ENSMUSG00000021238.10	-7.5039021	-13.712087	-1.2957176	0.01749589	Aldh6a1
ENSMUSG00000066158.7	8.20701539	2.05097869	14.3630521	0.00939682	AY512931
ENSMUSG00000044505.5	-6.4960526	-12.964944	-0.0271609	0.04896029	Lingo4
ENSMUSG00000087543.1	-9.3904356	-16.16517	-2.6157008	0.00723544	Gm16576
ENSMUSG00000030583.16	-4.3616778	-8.3173055	-0.4060501	0.02984624	Sipa1l3
ENSMUSG00000054693.14	-4.339326	-8.3766654	-0.3019866	0.0343423	Adam10
ENSMUSG00000015837.15	-0.5428963	-1.0043057	-0.0814869	0.02056189	Sqstm1
ENSMUSG00000070544.6	0.59408429	0.0167265	1.17144207	0.04324246	Top1
ENSMUSG00000085326.1	-4.0763953	-8.1126888	-0.0401018	0.04757378	Gm15642
ENSMUSG00000108402.1	-1.1328107	-1.9707879	-0.2948335	0.00856699	9430064I24R
ENSMUSG00000089682.9	6.86304381	0.84281747	12.8832702	0.02472536	Bcl2l2
ENSMUSG00000030534.13	-2.0421668	-3.8693498	-0.2149837	0.027672	Vps33b
ENSMUSG00000029063.16	-6.9288085	-13.697366	-0.1602512	0.0444069	Nadk
ENSMUSG00000022160.17	4.8416586	0.00085354	9.68246366	0.04995591	Mettl3
ENSMUSG00000107091.1	-9.2109899	-17.176219	-1.2457606	0.0227641	Gm43343
ENSMUSG00000052609.8	0.71872368	0.00586889	1.43157846	0.04798118	Plekhg3
ENSMUSG00000030539.13	-2.5319559	-4.9848396	-0.0790722	0.04253928	Sema4b
ENSMUSG00000025903.14	1.48439594	0.04488726	2.92390462	0.04276502	Lypla1
ENSMUSG00000027878.11	-1.112008	-2.0108759	-0.2131402	0.01517094	Notch2
ENSMUSG00000034235.16	-3.9963141	-7.9873486	-0.0052796	0.04967013	Usp54
ENSMUSG00000024798.15	-7.2554215	-13.40914	-1.1017026	0.02031235	Htr7
ENSMUSG00000056260.15	4.95907319	0.6857664	9.23237999	0.02230137	Lrif1
ENSMUSG00000038415.9	5.3223856	0.31384877	10.3309224	0.0365057	Foxq1
ENSMUSG00000050121.8	-7.033153	-13.223637	-0.8426693	0.02521287	Opalin
ENSMUSG00000092837.1	-3.9120553	-7.4920399	-0.3320706	0.03137197	Rpph1
ENSMUSG00000024851.13	-0.3966432	-0.7409467	-0.0523397	0.02327241	Pitpnm1
ENSMUSG00000067219.9	-1.4831792	-2.7166314	-0.2497269	0.01805408	Nipal1
ENSMUSG00000053931.11	0.73229529	0.05823661	1.40635396	0.03239359	Cnn3
ENSMUSG00000102266.1	-1.3478402	-2.6561197	-0.0395607	0.04296809	Gm38106
ENSMUSG00000051149.15	-1.4480774	-2.8772255	-0.0189292	0.04679133	Adnp
ENSMUSG00000015133.17	-8.2826669	-16.265962	-0.299372	0.04142951	Lrrk1
ENSMUSG00000034403.16	-1.1153311	-2.164743	-0.0659193	0.03647766	Pja1
ENSMUSG00000032127.8	-2.3609675	-4.5561841	-0.1657508	0.03422025	Vps11
ENSMUSG00000032905.4	-1.230565	-2.3264147	-0.1347153	0.02694613	Atg12
ENSMUSG00000087502.1	-1.7866367	-3.474873	-0.0984004	0.03731859	Gm16091
ENSMUSG00000042428.6	-1.1276621	-2.211204	-0.0441201	0.04076495	Mgat3
ENSMUSG00000046607.6	1.1658717	0.2011424	2.130601	0.01751479	Hrk
ENSMUSG00000011096.17	-1.2279876	-2.4197439	-0.0362313	0.04293297	Akt1s1
ENSMUSG00000086844.1	-6.865018	-13.610763	-0.119273	0.04576232	B230206H07
ENSMUSG00000022676.6	3.64383738	0.16371532	7.12395943	0.03948951	Snai2
ENSMUSG00000039137.18	-6.4333489	-12.468969	-0.3977284	0.03591632	Whrn
ENSMUSG00000030649.18	-8.7104152	-16.76453	-0.6563003	0.03320487	Anapc15